International Journal of Polymer Science

The Frontier of Biobased Polymers: Synthesis, Characterization, Application, and Sustainability Assessment

Lead Guest Editor: Shida Miao
Guest Editors: Raffaele Cucciniello, Vinay Sharma, and Daniela Saviello

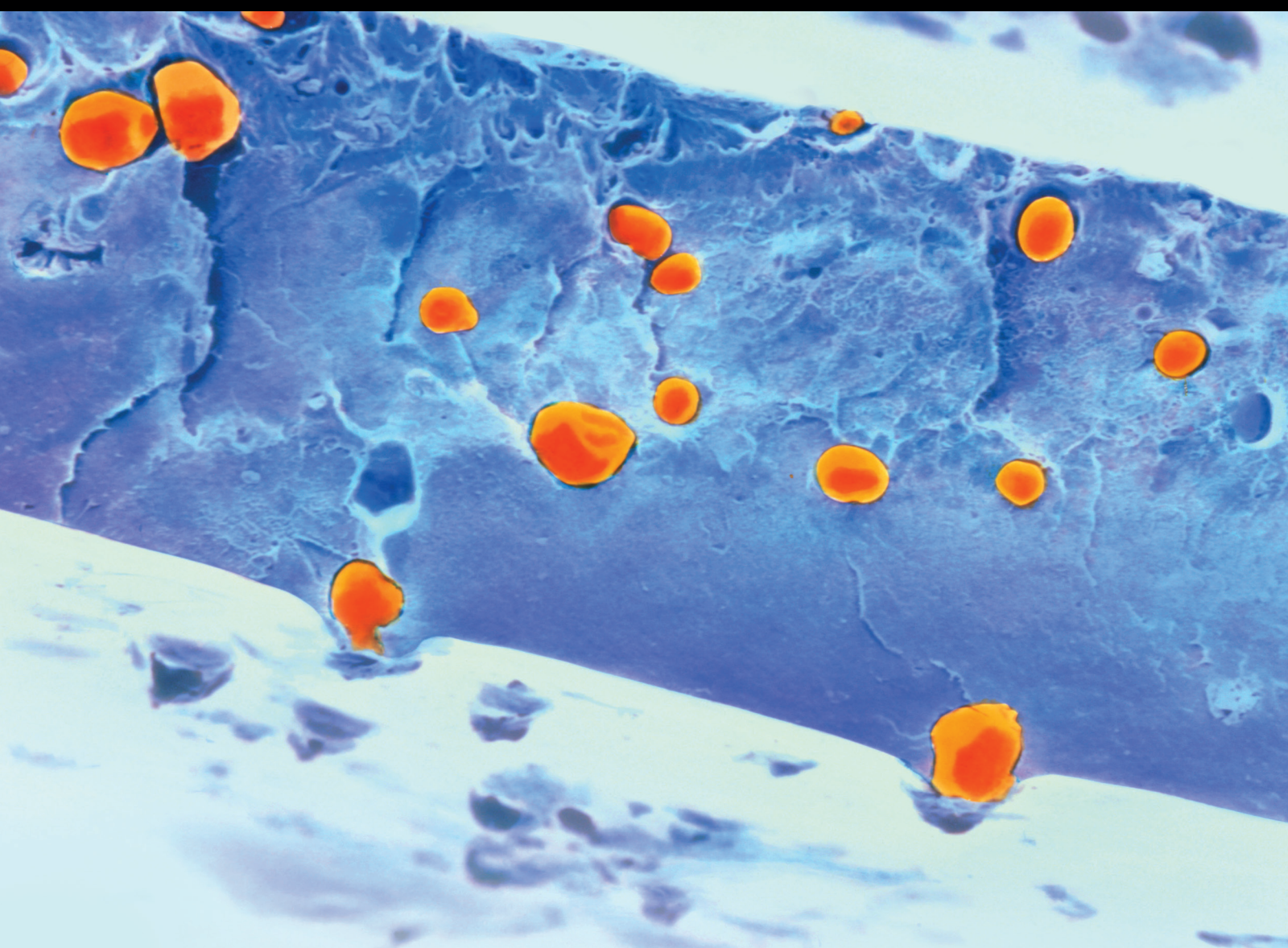

The Frontier of Biobased Polymers: Synthesis, Characterization, Application, and Sustainability Assessment

International Journal of Polymer Science

The Frontier of Biobased Polymers: Synthesis, Characterization, Application, and Sustainability Assessment

Lead Guest Editor: Shida Miao
Guest Editors: Raffaele Cucciniello, Vinay Sharma, and Daniela Saviello

Editorial Board

Contents

Hindawi
International Journal of Polymer Science
Volume 2017, Article ID 5638598, 2 pages
https://doi.org/10.1155/2017/5638598

Editorial

The Frontier of Biobased Polymers: Synthesis, Characterization, Application, and Sustainability Assessment

Daniela Saviello,[1] Daniele Cespi,[2] Vinay Sharma,[3] Shida Miao,[4] and Raffaele Cucciniello[5]

[1] *Tyndall National Institute, University College Cork, Dyke Parade, Cork, Ireland*
[2] *Environmental Management and Consulting (EMC) Innovation Lab S.r.l., Viale Italia 29, 47921 Rimini, Italy*
[3] *Apollo Tyres Ltd., Chennai, India*
[4] *School of Engineering and Applied Science, The George Washington University, Washington, DC 20052, USA*
[5] *Dipartimento di Chimica e Biologia "Adolfo Zambelli", Università di Salerno, Via Giovanni Paolo II, 132-84084 Fisciano, Italy*

Correspondence should be addressed to Raffaele Cucciniello; rcucciniello@unisa.it

Received 29 August 2017; Accepted 29 August 2017; Published 24 October 2017

In the last years, research perspectives in the field of biobased polymers have attracted increasing interest both in industrial and in academic environments forward to a future based on renewable resources. Relevant papers and exhaustive reviews have been published concerning synthesis, extraction, and preparation of biobased monomers and characterization and applications of new biobased polymers.

The importance of biobased feedstocks in the chemical industry is continuously growing and their use is predicted to surpass that of products obtained by nonrenewable fossil sources in the near future.

As a matter of fact, recent statistics have shown that the production of biobased polymers is not intended to recess, but it rather will triple those that the manufacture achieved in 2013. Predictions for 2020 expect production of over 17 million tons. The market in Asia is expected to explode, taking the lion's share of capital investment, while in Europe the bioplastics market will be over 6.7 Mt (+400% compared to 2013) by 2018. More than 74% of the production (5 Mt) will be represented by bio-polyethylene terephthalate (bio-PET). Figure 1 describes the EU breakdown. As stated, bio-PET is dominant (+37% compared to the 2013 value). The other interesting portion is the green one, representing biodegradable polymers: around 17% in 2018 (PLA and polyesters constitute the majority).

The substitution of fossil-based resources with molecules extracted from biomass represents one of the main goals of Green Chemistry (see 7th principle). The importance behind this replacement is associated with two main reasons: the usage of renewable sources rather than limited ones and the development of a low-carbon economy, reducing wastes and minimizing the amount of resources. For example, the replacement of 20% of the carbon content related to the whole PET current production (around 37.5 billion tons) with biobased sources could contribute to the reduction of CO_2 emission by 17 million tons. Moreover, another reason should be also taken into consideration: biobased industry will drive the economy by creating new opportunities and jobs. In general, the environmental sustainability of these biobased plastics is usually related to the embodied loads of the building block monomers used in the manufacture.

In this special issue, there are original research articles that uncover the development of new biobased polymers, including their synthesis, processing, characterization, and applications. The topics in this special issue specially include the following: (I) synthesis, modification, and characterization of biobased polymers; (II) new processes for the preparation of biobased monomers from natural feedstock; (III) the application of biobased polymers in biomedicine and tissue engineering; (IV) the application of biobased polymers in multiresponsive materials; (V) the application of biobased polymers in nanotechnology and in advanced 3D printing; (VI) the durability of biobased polymers; (VII) the degradation of biobased polymers; and (VIII) the life-cycle assessment analysis (LCA) on biobased polymers.

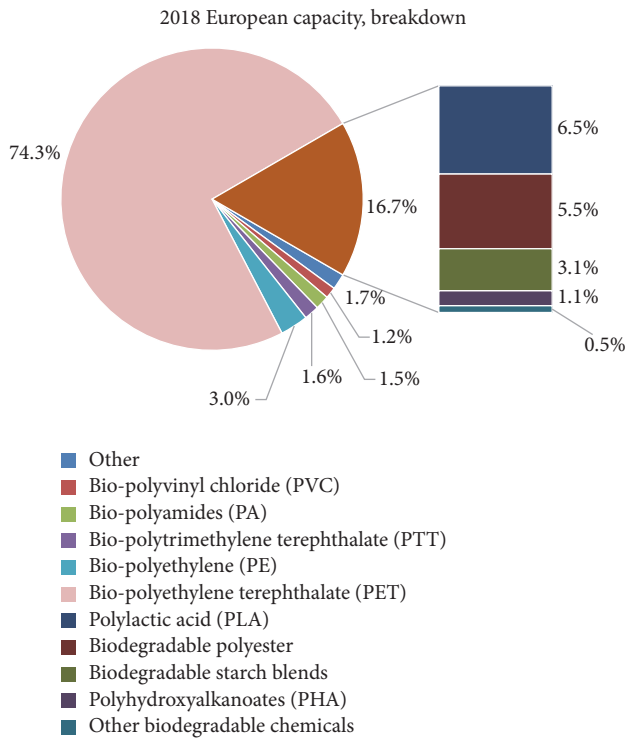

Figure 1: Bioplastics capacity: European breakdown.

We hope readers will benefit for their own research from this special issue.

Acknowledgments

We would like to express our appreciation to all the authors for their informative contributions and the reviewers for their support and constructive critiques in making this special issue possible.

Daniela Saviello
Daniele Cespi
Vinay Sharma
Shida Miao
Raffaele Cucciniello

Hindawi
International Journal of Polymer Science
Volume 2017, Article ID 5147482, 9 pages
https://doi.org/10.1155/2017/5147482

Research Article

UV Dose Governs UV-Polymerized Polyacrylamide Hydrogel Modulus

Saahil Sheth, Era Jain, Amin Karadaghy, Sana Syed, Hunter Stevenson, and Silviya P. Zustiak

Department of Biomedical Engineering, Parks College of Engineering, Aviation and Technology, Saint Louis University, 3507 Lindell Blvd., St. Louis, MO 63103, USA

Correspondence should be addressed to Silviya P. Zustiak; szustiak@slu.edu

Received 19 April 2017; Accepted 24 August 2017; Published 10 October 2017

Academic Editor: Shida Miao

Polyacrylamide (PAA) hydrogels have become a widely used tool whose easily tunable mechanical properties, biocompatibility, thermostability, and chemical inertness make them invaluable in many biological applications, such as cell mechanosensitivity studies. Currently, preparation of PAA gels involves mixtures of acrylamide, bisacrylamide, a source of free radicals, and a chemical stabilizer. This method, while generally well accepted, has its drawbacks: long polymerization times, unstable and toxic reagents, and tedious preparation. Alternatively, PAA gels could be made by free radical polymerization (FRP) using ultraviolet (UV) photopolymerization, a method which is quicker, less tedious, and less toxic. Here, we describe a simple strategy based on total UV energy for determining the optimal UV crosslinking conditions that lead to optimal hydrogel modulus.

1. Introduction

In recent years, polyacrylamide (PAA) hydrogels have gained popularity as substrates for cell culture due to their biocompatibility, hydrophilicity, low cost, and ease of preparation, as well as their attractive mechanical properties [1, 2]. Another advantage of PAA hydrogels is the ability to vary the ratio of monomer (acrylamide) to crosslinker (bisacrylamide) and total monomer concentration; these strategies lead to hydrogels with Young's modulus anywhere between 0.1 and 300 kPa and emulate any physiological soft tissue [3]. PAA hydrogels are commonly implemented as cell substrates to assess stiffness-dependent cell behavior due to their tunable compliance. For example, in the seminal paper by Lo et al. [4], the authors used PAA hydrogels of two different moduli to demonstrate that cells preferentially move from a softer substrate to a stiffer substrate, a phenomenon known as durotaxis. Since then, PAA hydrogels of different moduli have been used to demonstrate the role of substrate stiffness on cell morphology and the cytoskeleton [5], cancer cell metastasis and invasiveness [6, 7], cellular responses to drugs and toxins [8, 9], and directing cell phenotype [10].

Currently, when used as cell culture substrates, PAA gels are mainly polymerized with catalysts such as tetramethylenediamine (TEMED) and ammonium persulfate (APS), which are highly toxic and also lead to slow polymerization times—on the order of 45 min to 1 h for lower gel precursor concentrations [1, 11]. Photocrosslinking with various photoinitiators, such as Irgacure 2959, has been more recently employed for the fabrication of PAA hydrogels with a stiffness gradient [1, 10, 12], or for the quick preparation of large PAA hydrogel arrays for applications such as drug screening [8]. Photocrosslinking circumvents the use of toxic catalysts and is typically much faster—on the order of 1–5 min [8]. Final properties of UV-polymerized gels depend on the UV wavelength, uniformity, light intensity, and exposure times [1].

In this study, we present a method for preparing UV-polymerized PAA hydrogels with a focus on UV dose, rather than UV intensity or UV exposure time independently. We demonstrated that, for UV-polymerized hydrogels, rather than independently varying UV exposure time and intensity, one should consider the UV dose: interestingly, for all PAA hydrogels as well as UV parameter combinations tested here,

Table 1: Concentrations and volumes of acrylamide and bisacrylamide required to prepare polyacrylamide hydrogels of various moduli.

Nomenclature	Acrylamide concentration (%)	Bisacrylamide concentration (%)	Acrylamide from 40% stock solution (mL)	Bisacrylamide from 2% stock solution (mL)	DI water (mL)
A5-B.025	5	0.025	0.625	0.063	4.31
A5-B.10	5	0.100	0.625	0.250	4.13
A8-B.10	8	0.100	1.000	0.250	3.75
A8-B.25	8	0.250	1.000	1.000	0.63
A12-B.25	12	0.250	1.500	0.625	2.88

the optimal UV dose was ~5×10^3 mJ/cm^2. The optimal dose was defined as the lowest dose required to reach hydrogel modulus saturation, above which the modulus did not change appreciably.

2. Materials and Methods

2.1. Materials. Acrylamide (A) (40% w/v), bisacrylamide (B) (2% w/v), and Irgacure 2959 were purchased from BASF Corporation (Florham Park, NJ); phosphate-buffered saline (PBS) and Repel Silane® were purchased from GE Healthcare Life Sciences (Logan, UT); and silicone spacers were purchased from Grace Bio-Labs (Bend, OR). RPMI media and fetal bovine serum (FBS) were purchased from GE Healthcare Hyclone (Little Chalfont, UK). Trypsin was purchased from Sigma-Aldrich (St. Louis, MO). MDA-MB-231 breast cancer cells were obtained from NCI DCTD Repository (NCI, Frederick, MD). Type I collagen and sulfosuccinimidyl-6-(4′-azido-2′-nitrophenylamino)hexanoate (Sulfo-SANPAH) were purchased from Thermo Fisher (Waltham, MA), and penicillin-streptomycin (pen/strep) was purchased from MP Biomedicals (Santa Ana, CA).

2.2. Hydrogel Preparation

2.2.1. UV-Polymerized Hydrogels. To prepare the PAA gel precursor solution, A, B, and deionized (DI) water were added at specific ratios (Table 1) to prepare 5 mL working solutions. The gel precursor solution was degassed for 30 min at which point the photoinitiator, Irgacure 2959 for UV-crosslinked gels, was added to the solution at 0.1% w/v final concentration and mixed gently. Irgacure 2959 was chosen because it has been shown to be UV sensitive (at UV wavelength of 365 nm) and also nontoxic to cells at low concentrations [13]. The solution was then pipetted on the center of a glass slide that was pretreated with Repel Silane to provide a hydrophobic surface. Silicone spacers (0.5 mm thick) were placed at the ends of the glass slide and a second hydrophobic-treated slide was placed on top; hence, the resulting uncured material had a uniform thickness of 0.5 mm to ensure uniform cure throughout the depth of the material. The slides were exposed to UV light (365 nm; IntelliRay 600W, Uvitron International, Inc.) of various intensities for various amounts of time to initiate crosslinking. Intensity was varied by placing the gels at a predetermined distance from the light source, where values for light intensity as a function of distance were measured and provided by the manufacturer.

2.2.2. Free Radical-Polymerized Hydrogels. TEMED-crosslinked gels were prepared in a similar way as described in the previous subsection with several notable differences. Briefly, to prepare 5 ml of gel precursor solution, A, B, and deionized water were mixed at a desired ratio to give 4,972.5 μl total volume. Upon degassing the precursor solution for 30 min, 25 μl APS (10% w/v stock solution in deionized water; Bio-Rad, Hercules, CA) and 2.5 μl of TEMED (Bio-Rad, Hercules, CA) were added. The solution was then again sandwiched between two hydrophobic-treated glass slides separated by spacers and left in a degassing chamber under vacuum for 45 min to polymerize.

2.3. Rheological Testing. Hydrogel slabs (0.5 mm thick) were swollen in PBS overnight and cut into circular slabs 20 mm in diameter for rheological testing. Residual buffer from the hydrogel surface was carefully blotted with a KimWipe® prior to measurement to avoid slipping. The storage modulus (G') and loss modulus (G'') were measured with an AR 2000ex rheometer (TA Instruments, New Castle, DE) in a parallel plate geometry with a 20 mm diameter, flat upper plate, at 22°C, a frequency of 1–10 rad/s, a constant 2% strain, and a normal force of 0.20–0.25 N [14]. Young's modulus was related to G' by the following equation:

$$E = G'2\,(1 + \nu)\,, \tag{1}$$

where E is Young's modulus and ν is Poisson's ratio which was approximated to 0.5 for PAA gels [15, 16].

2.4. Sample Preparation for Testing the Effect of Polymerization Conditions on Hydrogel Stiffness

2.4.1. Effect of UV Intensity. A8-B.10 and A12-B.25 hydrogel precursor solutions were prepared in 50 ml conical vials. To degas the hydrogel precursor solution, the conical vials were left uncapped and placed in a degassing chamber under vacuum for 30 min. Next, 350 μL samples of each of the solutions were placed between two hydrophobic-treated glass slides. The slides were then placed in a UV oven with the following settings: exposure time of 300 s and/or 100 s and UV intensity of 15, 26, 67, and 131 mW/cm^2.

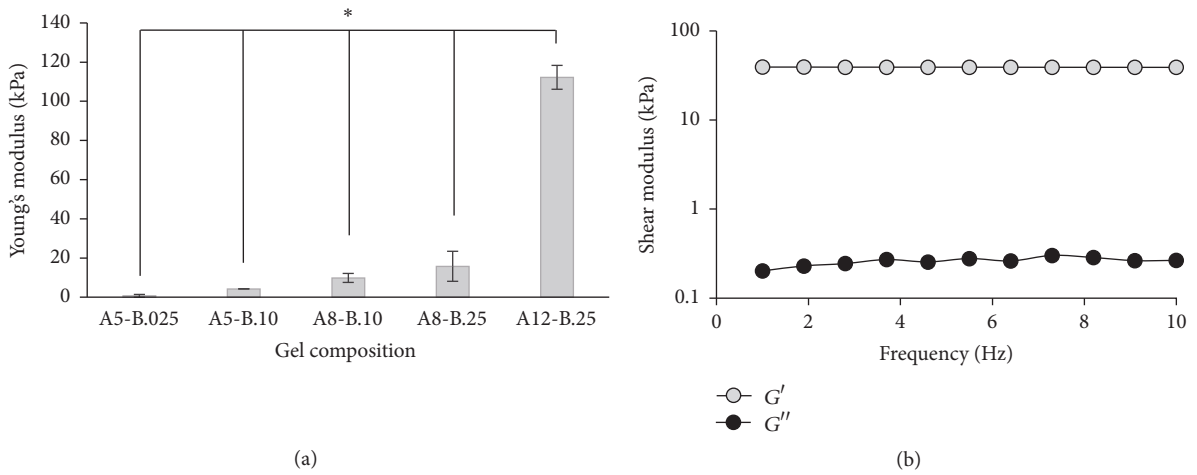

Figure 1: (a) Young's modulus as a function of gel composition for TEMED-crosslinked PAA hydrogels. (b) Representative shear stress as a function of frequency plot for A12-B0.25 PA hydrogel. Asterisks designate significant differences for $p < 0.05$, $n = 3$.

2.4.2. Effect of Exposure Time. A8-B.10 and A12-B.25 hydrogel precursor solutions were prepared in a 50 ml conical vial and degassed for 30 min, and 350 μL samples of each were placed between two hydrophobic-treated glass slides. The slides were then placed in a UV oven with the following settings: exposure time of 50 s, 75 s, 100 s, 125 s, and 300 s and UV intensity of 15 mW/cm^2.

2.4.3. Effect of Irgacure Concentration. UV-crosslinked gels were prepared with various amounts of Irgacure 2959: 0.01%, 0.10%, and 0.50%. Precursor solutions of A8-B.10 gels were prepared, degassed for 30 min, and placed between two hydrophobic-treated glass slides. The slides were placed in the UV oven to polymerize at an intensity of 15 mW/cm^2 for 300 s.

2.4.4. Effect of UV Dose. PAA hydrogels were fabricated at different doses (i.e., total energy) calculated as follows:

$$\text{Dose} = \text{intensity} \times \text{time}, \quad (2)$$

where the dose is in mJ/cm^2, intensity is in mW/cm^2, and time is in s. UV-crosslinked gels were prepared at various doses ranging from ~1 mJ/cm^2 to ~40 mJ/cm^2. Two types of PAA gels were prepared for this experiment to compare the effects of dose on gels with different moduli: a stiff gel (A12-B.25) and a soft gel (A8-B.10). For the stiff gel, three different UV intensities were used (15, 26, and 67 mW/cm^2), while the exposure time was steadily increased to obtain increasing dose values. For the soft gel, the intensity was held at 15 mW/cm^2, while the exposure time was again increased to obtain an increasing dose.

2.5. Collagen Coating of PAA Gels and Cell Culture. The PAA gels of desired moduli were prepared using UV-initiated polymerization. The PAA gels were coated with 0.1 mg/mL Type I collagen using a Sulfo-SANPAH crosslinker (50 mg/ml) as described by us previously [17]. Gel plates were then sterilized under UV light (302 nm) for 2 h. The coated gels were then washed 2 times in PBS and equilibrated with 1x RPMI medium supplemented with 10% v/v FBS and 1% v/v pen/strep overnight. MDA-MB-231 human breast cancer cells were cultured on the hydrogels and maintained using regular cell culture techniques in RPMI medium supplemented with 10% v/v FBS and 1% v/v pen/strep. Cells were harvested through exposure to 0.5% v/v trypsin/EDTA for 5 min and seeded onto the PAA gels at a concentration of 1 $\times 10^5$ cells/cm^2. After supplementing with complete medium, cells were placed in a humidified incubator at 37°C and 5% CO_2 and cultured for 24 h.

2.6. Cell Imaging and Morphology. Cells were stained with acridine orange (green fluorescence, membrane permeable dye) at 24 h of culture on the PAA gels. Bright field and fluorescent images were captured using an inverted fluorescent microscope (Axiovert 200, Zeiss, Germany) with a 20x objective. Images were analyzed for cell spreading using the line plug-in on ImageJ (NIH free software).

2.7. Statistical Analysis. The results of all experiments are reported as the mean values (±SD) of triplicate samples performed in a minimum of three independent experiments. For measuring cell elongation, a total of ~75–100 cells were analyzed from 9 images taken from three independent sample sets used for each condition. Comparisons between multiple groups were performed with single factor analysis of variance (ANOVA) followed by Tukey's post hoc test. Comparisons between two samples were performed with two-tailed Student's t-tests with post hoc analysis. Differences between two data sets were considered significant when $p < 0.05$.

3. Results and Discussion

While the use of TEMED-polymerized PAA hydrogels is common practice, UV-polymerized PAA gels for use as cell substrates are now gaining momentum. Although TEMED-polymerized gels offer a range of elastic moduli (Figure 1),

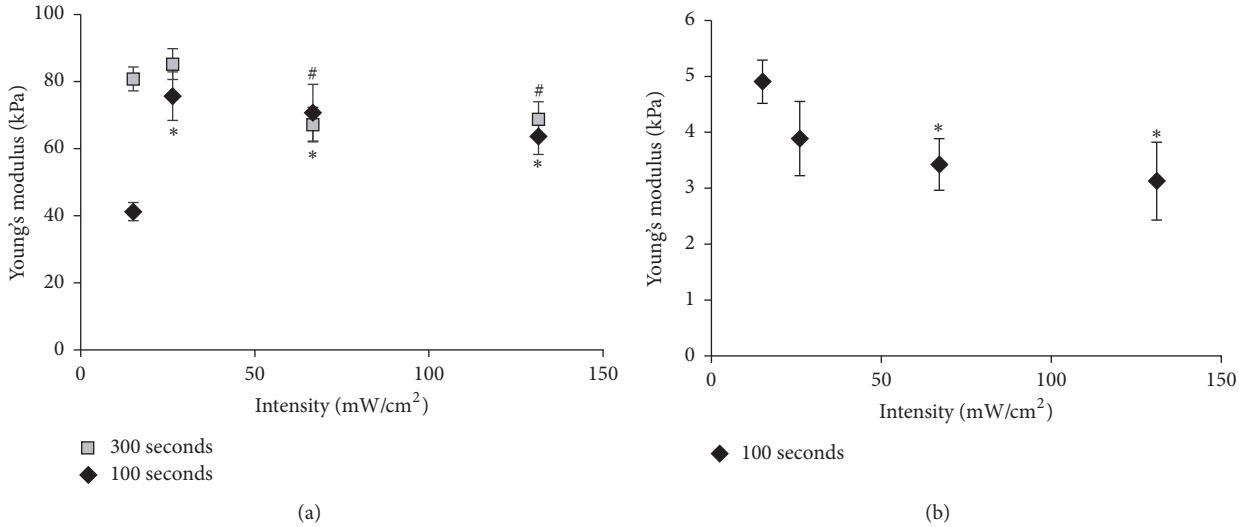

Figure 2: Young's modulus as a function of UV light intensity for (a) A12-B.25 and (b) A8-B.10, PAA hydrogels. Asterisks and pound symbols designate significant differences from Young's modulus for gels polymerized at 15 mW/cm^2 ($p < 0.05$, $n = 3$).

there are several distinct advantages to using UV polymerization. First, it allows for the formation of gradient gels which are excellent platforms for the investigation of cell motility, durotaxis, or differentiation [1, 10, 12]. Second, UV polymerization also allows for gel and surface patterning, providing a tool for evaluating cell behavior as a function of surface topography or composition [18, 19]. From a practical standpoint, UV crosslinking is faster; a typical gelation time for TEMED-based gels would be ~30–45 min, while the gelation time for UV-polymerized gels is ~1–5 min [1]. Lastly, the chemicals typically needed for UV polymerization (e.g., photoinitiators such as Irgacure) are less hazardous as opposed to the ones required for standard free radical polymerization, such as the toxic TEMED catalyst [8]. However, while both reactions are based on free radical polymerization, different parameters govern the polymerization kinetics and the resultant Young's modulus. Rather than trying to manipulate multiple parameters (UV exposure time and intensity) independently to obtain desired stiffness, we aimed to streamline the process, while simultaneously increasing reproducibility. Additionally, rather than using multiple gel compositions for subsequent experiments, we chose a soft hydrogel of lower acrylamide and bisacrylamide concentration (A8-B.10) and a stiff hydrogel of higher acrylamide and bisacrylamide concentration (A12-B.25). The A8-B.10 gel was chosen over the other soft hydrogels (A5-B.025 and A5-B.10), because it was easier to handle. Two different hydrogels were selected to ensure that the observed trends in modulus as a function of UV-polymerization parameters would hold for hydrogels of significantly different monomer and crosslinker concentration (i.e., resultant modulus).

3.1. Effect of UV Intensity. Here, we first examined the effect of light intensity on the final PAA hydrogel modulus(Figure 2). We specifically examined a soft (A8-B.10) and a stiff (A12-B.25) PAA hydrogel at two different exposure times: 100 s and 300 s. We observed a bimodal dependence of gel modulus on UV light intensity. There was ~83% increase in gel stiffness with a 74% increase in light intensity (from 15 to 26 mW/cm^2) for the stiff gel at a short exposure time of 100 s. However, rather than a further increase in modulus with an increase in intensity, we observed a slight, yet not statistically significant decrease in modulus. While not as significant, a similar trend was observed for the stiff gel at an exposure time of 300 s. There was a slight, but insignificant, increase of 6% in Young's modulus with an increase in UV intensity from 15 to 26 mW/cm^2, followed by a statistically significant 20% decrease in modulus for the higher UV intensities of 67 and 131 mW/cm^2. For the softer A8-B.10 gel at an exposure time of 300 s, the highest modulus was achieved at the lowest 15 mW/cm^2 UV light intensity; there was a 37% drop in modulus between gels made at 15 mW/cm^2 versus 131 mW/cm^2 intensity.

An increase in photopolymerized hydrogel modulus with increased light intensity was an anticipated result and can be explained by an improved crosslinking reaction and a greater number of functional crosslinks formed [20]. The second trend, which showed no further increase in modulus above a certain threshold UV light intensity, is not as well documented. For the free radical UV polymerization studied here, we postulate that the phenomena can be explained by overall faster polymerization kinetics and faster radical transfer, resulting in shorter polymer chains. Also, it is possible that complete photoinitiator consumption, leading to reaction completion past a threshold UV light intensity, can explain the lack of modulus increase. The rate of UV polymerization is directly proportional to the UV light intensity and photoinitiator concentration [21]. Thus, we note that, for a predetermined photoinitiator concentration, there was an optimal UV light intensity for achieving a higher modulus

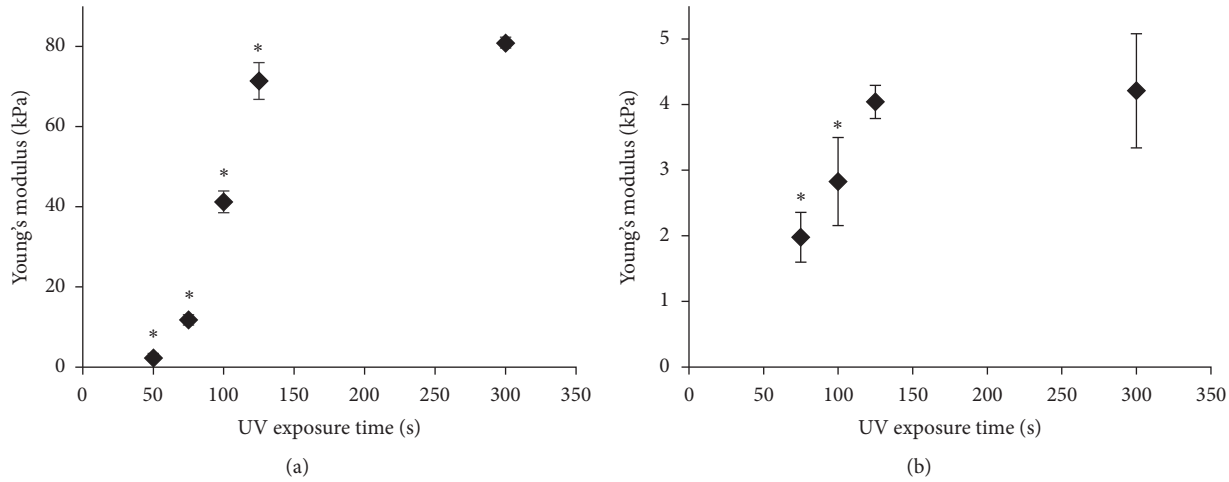

Figure 3: Young's modulus as a function of UV exposure time for (a) A12-B.25 and (b) A8-B.10, PAA hydrogels. Asterisks designate significant differences from Young's modulus for gels polymerized at an exposure time of 300 s ($p < 0.05$, $n = 3$).

from a given gel precursor solution, which was dependent on the total acrylamide and bisacrylamide concentration.

3.2. Effect of UV Exposure Time. For photopolymerized PAA hydrogels, UV exposure time has been utilized as the most effective strategy to achieve varying Young's moduli from the same hydrogel precursor solution [1, 10, 12]. As polymerization is a kinetic process, the longer exposure times allow for the reaction to proceed to completion. For this reason, longer polymerization times, up to a certain threshold, are expected to lead to a larger number of functional crosslinks, resulting in a higher Young's modulus. Further, it is possible that UV exposure time, by altering reaction rate, has an effect on the resultant hydrogel network defects, which have been shown to occur for PAA hydrogels, especially at higher acrylamide and bisacrylamide concentrations [22]. Increase in network defects (i.e., hydrogel heterogeneity) with an increase in reaction rate has been shown previously [21]. Network defects, on the other hand, have a pronounced effect on hydrogel modulus [23]. For example, chain entanglements cause an increase in crosslink density within the polymer network, which in turn results in a higher modulus [24, 25]. Alternatively, intramolecular cycles (chain loops) decrease crosslink density, thus negatively affecting hydrogel modulus [21]. Furthermore, since the polymerization rate depends on the concentrations of the acrylamide monomer and bisacrylamide crosslinker, they are expected to change for each precursor solution. Here, we again tested a soft gel (A8-B.10) and a stiff gel (A12-B.25). As expected, the polymerization rate was dependent on the total acrylamide and bisacrylamide concentration (Figure 3).

We noted that longer polymerization times were needed to reach the gelation point for precursor solutions of lower total acrylamide and bisacrylamide concentration. For example, while only a 50 s exposure time was required to form the stiff gel (Figure 3(a)), a minimum exposure time of 75 s was needed to achieve gelation for the soft gel (Figure 3(b)). However, for both gels, we noted a significant increase in Young's modulus for higher exposure times. For example, for the A12-B.25 gel, we saw a 97% increase in Young's modulus for gels with an exposure time of 50 s versus gels with an exposure time of 300 s. For the A8-B.10 gel, we saw a similarly large increase of 53% for gels with an exposure time of 75 s versus gels with an exposure time of 300 s. Hence, by simply changing exposure time, we were able to achieve a large variation in stiffness in gels from the same gel precursor solution.

3.3. Effect of Photoinitiator Concentration on PAA Hydrogel Modulus. For UV-polymerized PAA gels, the photoinitiator Irgacure absorbs UV light to generate free radicals causing a chain reaction that leads to polymerization. The resulting polymer chain length affects the hydrogel modulus—the higher the chain length, the stiffer the resultant gel. One way to affect the polymer chain length is by altering the photoinitiator concentration. Increasing the photoinitiator concentration has been shown to result in multiple shorter polymer chains and hence a lower modulus [26]. Decreasing the photoinitiator concentration has been shown to result in a lower number, but higher molecular weight polymer chains leading to a higher modulus [26]. Our data corroborates previous findings: we observed a 1.3-fold increase in modulus when the Irgacure concentration was decreased from 0.5% to 0.1% and another 1.2-fold increase in modulus when the Irgacure concentration was decreased from 0.1% to 0.01% (Figure 4).

3.4. Effect of UV Dose. While above we demonstrated that both UV exposure time and UV light intensity could be used to control PAA hydrogel modulus, it is often impractical to test multiple samples to determine the optimal UV condition that would lead to an optimal hydrogel modulus. Along with manipulating intensity and time independently, we followed the evolution of hydrogel modulus as a function of total UV energy, that is, UV dose (see (1)). We again considered a soft gel (A8-B.10) and a stiff gel (A12-B.25). The data in Figure 5

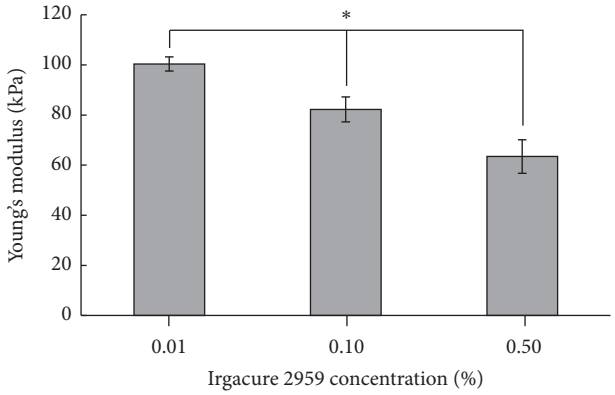

Figure 4: Young's modulus as a function of photoinitiator Irgacure 2959 concentration for A12-B.25 PAA hydrogel for a fixed UV intensity of 15 mW/cm^2 and fixed exposure time of 300 s. Asterisks designate significant differences for $p < 0.05$, $n = 3$.

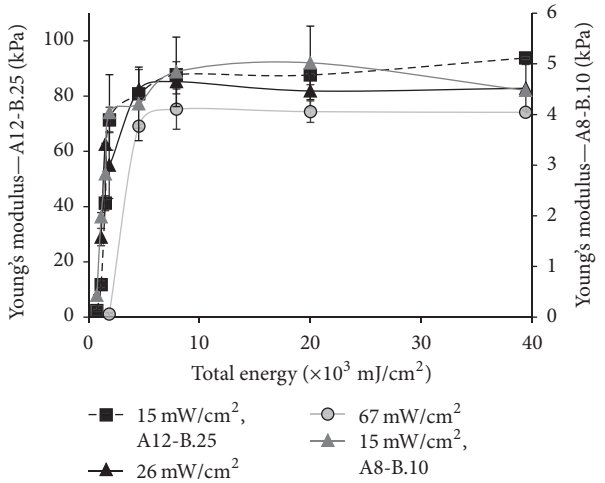

Figure 5: Young's modulus of two PAA hydrogel compositions as a function of UV dose calculated as UV intensity multiplied by UV exposure time.

represents the change in Young's modulus as a function of UV dose, where dose was varied by a change in UV exposure time for a fixed light intensity. When presented in this fashion, we saw an important trend emerge: there was a threshold dose of ~5 × 10^3 mJ/cm^2 at which no further increase in Young's modulus was observed for any hydrogel tested. It is important to note that this threshold value was achieved by manipulating either the UV intensity or the UV exposure time and was independent of the total acrylamide and bisacrylamide concentrations tested in this study. However, it is conceivable that using a significantly lower acrylamide or bisacrylamide concentration would affect the threshold modulus; the concentrations here were chosen to simulate the modulus range of most soft tissues in the body [3]. To the best of our knowledge, this trend has not been previously reported for UV-polymerized PAA hydrogels.

Furthermore, we saw a steep increase in Young's modulus for minimal changes in dose in the range of 0.8 × 10^3 to 5 × 10^3 mJ/cm^2 and leveling off in the modulus for changes in dose in the range of 5 × 10^3 to 40 × 10^3 mJ/cm^2. Overall, the observed dose, as well as total time needed to fully polymerize the PAA hydrogel, aligned closely with data reported in the literature [12]. The above described trends along with the individual intensities and exposure times used are summarized in Table S1 (in the Supplementary Material available online at https://doi.org/10.1155/2017/5147482). Lastly, the moduli achieved via UV polymerization are similar to those measured when fabricating PAA hydrogels using traditional AP/TEMED polymerization (Figure 1). For example, for A12-B.25 UV-polymerized gel using UV intensity of 15 mW/cm2 and 0.10% Irgacure concentration, Young's modulus was 93.8 ± 0.27 kPa, while the same gel made using AP/TEMED polymerization had Young's modulus of 112.3 ± 8.0 kPa. It is important to note that further optimization of UV-polymerization conditions to achieve a higher modulus is possible. For example, decreasing the Irgacure concentration ten times (from 0.1% to 0.01% w/v) increased Young's modulus of the A8-B.10 PAA and the A12-B.25 PAA gels, making them of the same modulus as the AP/TEMED-polymerized hydrogels of the same composition (Table S2). Note that the exposure time was also increased for the lower Irgacure concentration to allow for complete polymerization to occur. This increase in modulus with the decrease in photoinitiator concentration could be attributed to higher molecular weight polymer chains (see Figure 4).

3.5. Cell Morphology on UV-Polymerized PAA Hydrogels. We also evaluated cell spreading on PAA hydrogels fabricated using UV polymerization. Our goal was to show that, regardless of the method with which the dose for PAA polymerization was obtained (i.e., high intensity but short exposure time versus low intensity by long exposure time), cell behavior would be identical on gels of identical stiffness. For this experiment, we maintained a constant dose of 8 mJ/cm^2 but altered the UV intensity and the exposure time. For one set of gels, the intensity was low (15 mW/cm^2) and the exposure time was high (524 s). Consequently, for another set of gels, the intensity was high (67 mW/cm^2) and the exposure time was low (119 s). We used tissue culture polystyrene (TCP) as control. We found that the cell spreading area on all three samples was ~600 μm^2 and that there were no significant differences (Figure 6). This result corroborates the cell spreading area observed on the TEMED-polymerized gels of similar stiffness (Figure 7), indicating that UV polymerization can be utilized to fabricate PAA hydrogels for the use of substrates to assess cellular behavior.

4. Conclusions

In conclusion, we present a comprehensive analysis on the effect of various crosslinking parameters on the final PAA hydrogels' Young's modulus. Manipulating PAA hydrogels modulus is becoming increasingly important in the fields of basic cell biology, biophysics, tissue engineering, and regenerative medicine, where PAA gels are widely used as cell culture substrates. Importantly, for UV-polymerized hydrogels, we

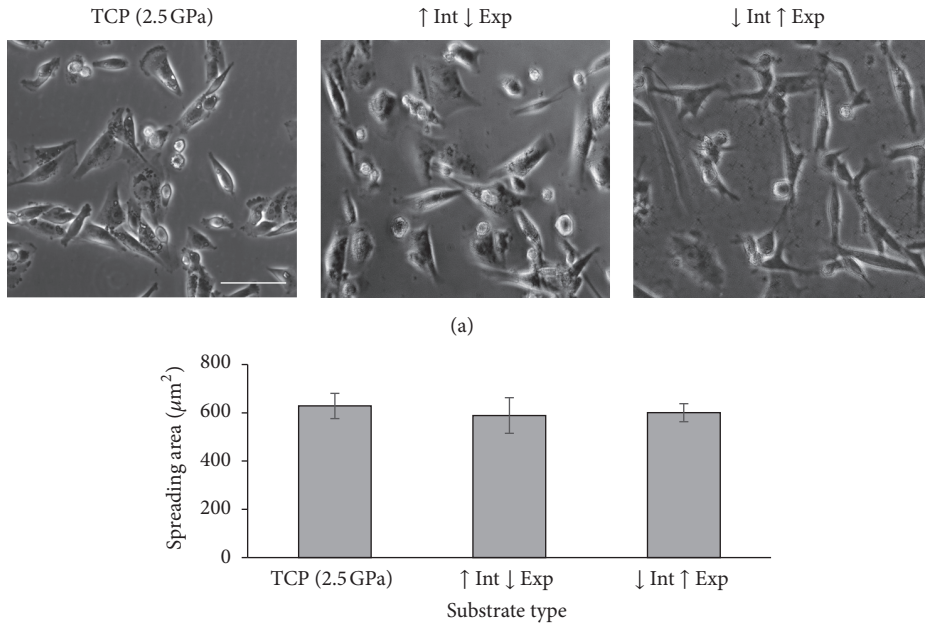

Figure 6: Cell morphology after 24 h of culture on collagen-coated UV-polymerized A12-B.25 PAA hydrogels. (a) Phase contrast images of MDA-MB-231 cells seeded onto PAA gels of equal dose, but with different exposure times and UV intensity. The "↑ Int ↓ Exp" condition had an intensity of 67 mW/cm^2 and exposure time of 119 s. The "↓ Int ↑ Exp" condition had an intensity of 15 mW/cm^2 and exposure time of 524 s. (b) No significant differences were found in the spreading area of MDA-MB-231 cells seeded onto PAA gels of equal dose (8 mJ/cm^2), but with different exposure time and UV intensity (same as in (a)). Scale bar represents 100 μm.

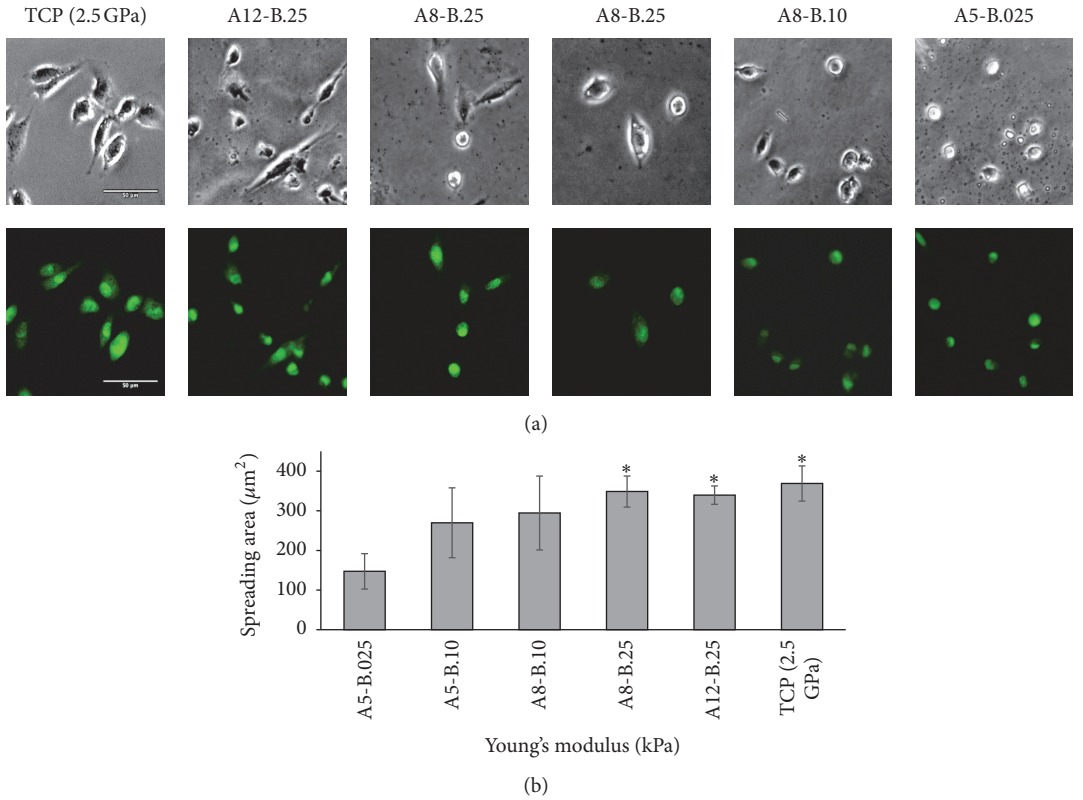

Figure 7: Cell morphology after 24 h of culture on collagen-coated PAA gels of varying stiffness. (a) Phase contrast (upper panel) and fluorescent (lower panel, acridine orange staining) images of MDA-MB-231 cells seeded on PAA gels of different stiffness. (b) Spreading area of MDA-MB-231 cells seeded on PAA gels of different stiffness. Asterisks designate significant differences from the 1 kPa hydrogel ($p < 0.05$, $n = 3$).

demonstrated that, rather than tuning the hydrogel modulus via UV intensity or exposure time independently, one should consider the UV dose for the system. For our system, which utilized 0.1% w/v of Irgacure photoinitiator, the threshold dose was found to be 5×10^3 mJ/cm^2; below this energy, we saw an abrupt increase in compliance for incremental changes in energy, while we did not observe any significant changes in hydrogel compliance for any changes in UV dose above the threshold value. The cell spreading observed in PAA gels prepared using UV polymerization corroborated results seen in the TEMED-polymerized PAA gels. Our comprehensive analysis on the effect of implementing UV dose could serve as a useful guide to increase the reproducibility and ease of use for the fabrication of UV-polymerized PAA hydrogels for many research applications.

Disclosure

Hunter Stevenson's current affiliation is Department of Bioengineering, University of Texas at Dallas, 2850 Rutford Ave., Richardson, TX 75080, USA. Era Jain's current affiliation is Department of Biomedical Engineering, Washington University in St. Louis, 6201 Forsyth Blvd., St. Louis, MO 63105, USA.

Conflicts of Interest

The authors declare that there are no conflicts of interest regarding this paper.

Acknowledgments

Funding was provided by start-up funds awarded to Dr. Silviya Zustiak from Saint Louis University.

References

[1] J. R. Tse and A. J. Engler, *Current Protocols in Cell Biology*, 2010, 10.16. 11-10.16. 16.

[2] R. J. Pelham Jr. and Y.-L. Wang, "Cell locomotion and focal adhesions are regulated by substrate flexibility," *Proceedings of the National Academy of Sciences of the United States of America*, vol. 94, no. 25, pp. 13661–13665, 1997.

[3] I. Levental, P. C. Georges, and P. A. Janmey, "Soft biological materials and their impact on cell function," *Soft Matter*, vol. 3, no. 3, pp. 299–306, 2007.

[4] C.-M. Lo, H.-B. Wang, M. Dembo, and Y.-L. Wang, "Cell movement is guided by the rigidity of the substrate," *Biophysical Journal*, vol. 79, no. 1, pp. 144–152, 2000.

[5] T. Yeung, P. C. Georges, L. A. Flanagan et al., "Effects of substrate stiffness on cell morphology, cytoskeletal structure, and adhesion," *Cell Motility and the Cytoskeleton*, vol. 60, no. 1, pp. 24–34, 2005.

[6] R. W. Tilghman, C. R. Cowan, J. D. Mih et al., "Matrix rigidity regulates cancer cell growth and cellular phenotype," *PLoS ONE*, vol. 5, no. 9, Article ID e12905, 2010.

[7] R. W. Tilghman, E. M. Blais, C. R. Cowan et al., "Matrix rigidity regulates cancer cell growth by modulating cellular metabolism and protein synthesis," *PLoS ONE*, vol. 7, no. 5, Article ID e37231, 2012.

[8] S. Zustiak, R. Nossal, and D. L. Sackett, "Multiwell stiffness assay for the study of cell responsiveness to cytotoxic drugs," *Biotechnology and Bioengineering*, vol. 111, no. 2, pp. 396–403, 2014.

[9] J. D. Mih, A. S. Sharif, F. Liu, A. Marinkovic, M. M. Symer, and D. J. Tschumperlin, "A multiwell platform for studying stiffness-dependent cell biology," *PLoS ONE*, vol. 6, no. 5, Article ID e19929, 2011.

[10] A. M. Kloxin, J. A. Benton, and K. S. Anseth, "In situ elasticity modulation with dynamic substrates to direct cell phenotype," *Biomaterials*, vol. 31, no. 1, pp. 1–8, 2010.

[11] Y. Aratyn-Schaus, P. W. Oakes, J. Stricker, S. P. Winter, and M. L. Gardel, "Preparation of Complaint Matrices for Quantifying Cellular Contraction," *Journal of Visualized Experiments*, no. 46, 2010.

[12] R. Sunyer, A. J. Jin, R. Nossal, and D. L. Sackett, "Fabrication of Hydrogels with Steep Stiffness Gradients for Studying Cell Mechanical Response," *PLoS ONE*, vol. 7, no. 10, Article ID e46107, 2012.

[13] C. G. Williams, A. N. Malik, T. K. Kim, P. N. Manson, and J. H. Elisseeff, "Variable cytocompatibility of six cell lines with photoinitiators used for polymerizing hydrogels and cell encapsulation," *Biomaterials*, vol. 26, no. 11, pp. 1211–1218, 2005.

[14] B. K. Mann, A. S. Gobin, A. T. Tsai, R. H. Schmedlen, and J. L. West, "Smooth muscle cell growth in photopolymerized hydrogels with cell adhesive and proteolytically degradable domains: Synthetic ECM analogs for tissue engineering," *Biomaterials*, vol. 22, no. 22, pp. 3045–3051, 2001.

[15] S. P. Zustiak and J. B. Leach, "Hydrolytically degradable poly(ethylene glycol) hydrogel scaffolds with tunable degradation and mechanical properties," *Biomacromolecules*, vol. 11, no. 5, pp. 1348–1357, 2010.

[16] T. Boudou, J. Ohayon, C. Picart, and P. Tracqui, "An extended relationship for the characterization of Young's modulus and Poisson's ratio of tunable polyacrylamide gels," *Biorheology*, vol. 43, no. 6, pp. 721–728, 2006.

[17] S. Syed, A. Karadaghy, and S. Zustiak, "Simple polyacrylamide-based multiwell stiffness assay for the study of stiffness-dependent cell responses," *Journal of Visualized Experiments*, vol. 2015, no. 97, Article ID e52643, 2015.

[18] M. J. Poellmann, P. A. Harrell, W. P. King, and A. J. W. Johnson, "Geometric microenvironment directs cell morphology on topographically patterned hydrogel substrates," *Acta Biomaterialia*, vol. 6, no. 9, pp. 3514–3523, 2010.

[19] H. Shin, "Fabrication methods of an engineered microenvironment for analysis of cell-biomaterial interactions," *Biomaterials*, vol. 28, no. 2, pp. 126–133, 2007.

[20] S. Seiffert, W. Oppermann, and K. Saalwächter, "Hydrogel formation by photocrosslinking of dimethylmaleimide functionalized polyacrylamide," *Polymer*, vol. 48, no. 19, pp. 5599–5611, 2007.

[21] B. D. Fairbanks, M. P. Schwartz, C. N. Bowman, and K. S. Anseth, "Photoinitiated polymerization of PEG-diacrylate with lithium phenyl-2,4,6-trimethylbenzoylphosphinate: polymerization rate and cytocompatibility," *Biomaterials*, vol. 30, no. 35, pp. 6702–6707, 2009.

[22] J. Baselga, M. A. Llorente, I. Hernández-Fuentes, and I. F. Piérola, "Network defects in polyacrylamide gels," *European Polymer Journal*, vol. 25, no. 5, pp. 471–475, 1989.

[23] A. S. Hoffman, "Hydrogels for biomedical applications," *Advanced Drug Delivery Reviews*, vol. 64, pp. 18–23, 2012.

[24] W. Chassé, M. Lang, J. Sommer, and K. Saalwächter, "Cross-Link Density Estimation of PDMS Networks with Precise Consideration of Networks Defects," *Macromolecules*, vol. 45, no. 2, pp. 899–912, 2012.

[25] O. Okay and S. Durmaz, "Charge density dependence of elastic modulus of strong polyelectrolyte hydrogels," *Polymer*, vol. 43, no. 4, pp. 1215–1221, 2001.

[26] N. S. Allen, J. Segurola, M. Edge, E. Santamari, A. McMahon, and S. Wilson, "A comparative kinetic study of commercial photoinitiators for UV/visible curable acrylate clear coatings," *Surface Coatings International Part B: Coatings International*, vol. 82, no. 2, pp. 67–76, 1999.

Hindawi
International Journal of Polymer Science
Volume 2017, Article ID 8632072, 10 pages
https://doi.org/10.1155/2017/8632072

Research Article

(Bio)degradable Ionomeric Polyurethanes Based on Xanthan: Synthesis, Properties, and Structure

T. V. Travinskaya, A. N. Brykova, Yu. V. Savelyev, N. V. Babkina, and V. I. Shtompel

Institute of Macromolecular Chemistry, NAS of Ukraine, Kharkovskoe Shosse 48, Kiev 02160, Ukraine

Correspondence should be addressed to T. V. Travinskaya; travinskaya-tamara@rambler.ru

Received 1 June 2017; Revised 21 July 2017; Accepted 9 August 2017; Published 24 September 2017

Academic Editor: Shida Miao

New (bio)degradable environmentally friendly film-forming ionomeric polyurethanes (IPU) based on renewable biotechnological polysaccharide xanthan (Xa) have been obtained. The influence of the component composition on the colloidal-chemical and physic-mechanical properties of IPU/Xa and based films, as well as the change of their properties under the influence of environmental factors, have been studied. The results of IR-, PMS-, DMA-, and X-ray scattering study indicate that incorporation of Xa into the polyurethane chain initiates the formation of a new polymer structure different from the structure of the pure IPU (matrix): an amorphous polymer-polymer microdomain has occurred as a result of the chemical interaction of Xa and IPU. It predetermines the degradation of the IPU/Xa films as a whole, unlike the mixed polymer systems, and plays a key role in the improvement of material performance. The results of acid, alkaline hydrolysis, and incubation into the soil indicate the increase of the intensity of degradation processes occurring in the IPU/Xa in comparison with the pure IPU. It has been shown that the introduction of Xa not only imparts the biodegradability property to polyurethane, but also improves the mechanical properties.

1. Introduction

Problem of environmental pollution with polymeric waste has shown a clear need for ecologically friendly materials based on renewable resources: vegetable oils and natural polymers, in particular, polysaccharides, which results in the development of a new trend in polymer chemistry, creation of sustainable biodegradable polymers having a wide range of applications [1–4]. Several methods of incorporating polysaccharides into the polyurethanes are discussed depending on the desired final properties of the polyurethane [5]. Due to the success of biotechnologies, a particular attention in modern chemistry of biodegradable polymers is paid to microbial polysaccharides (exopolysaccharides), which are climate and season independent. One of the leading places in this line belongs to xanthan, an extracellular polysaccharide of the bacteria *Xanthomonas campestris*. Xanthan molecules are prone to the self-association in aqueous solutions; a rise of solution ionic strength or polysaccharide concentration results in gel formation [6, 7]. Xanthan provides the synthetic polymers, in particular, polyurethanes, with ability to degrade under the influence of natural factors. It was shown that the chemical bond between synthetic and natural components played a crucial role in giving to the synthetic polymer biodegradability, opposed to mechanical mixtures, where only the natural component decomposed with time [8, 9]. Aqueous film-forming polyurethane dispersions have found diverse applications as finishing, impregnating, stiffener, protective materials, and adhesives in leather, textile, and furniture industry [10, 11]. The synthesis and characterization of novel aqueous polyurethane dispersions derived from plant oil and starch with the use of dimethylolpropionic acid as internal emulsifier which allows us to incorporate hydrophilic groups into the polymer chain and achieve stable self-emulsifying dispersions are discussed in [12–14]. It should be noted that the synthesis of degradable polyurethanes based on renewable feedstock is one of developing branches of green polyurethane chemistry. Such materials may be used as packaging, finishing, impregnating, stiffener, protective materials, and adhesives in leather, textile, and furniture industry, biologically active substances in agriculture. A distinctive feature of degradable polymers is to preserve

the necessary operational parameters during the time of their use in combination with accelerated degradation under the influence of various natural factors after the expiration. Microorganisms are the main biological systems which destroy the polymeric compounds. The ability of polymers to degrade and be assimilated by microorganisms depends on a number of their characteristics: the chemical structure of the polymer, molecular weight, branching of macrochain, and supramolecular structure [15]. The aim of the latest developments in the field of degradable polymers is to establish the common principles in selecting the components for synthesis of polymer which combine a high level of performance with the (bio)degradation ability and knack of adjusting the (bio)degradation processes to ensure fast and safe (bio)degradation of polymer materials at the expiration of their working time. The paper considers the synthesis and complex study of "composition, structure, properties, and (bio)degradation ability" relationship of structurally modified polymeric materials based on polyurethane ionomer and microbial exopolysaccharide xanthan.

2. Experimental

2.1. Materials. Hexamethylene diisocyanate (HMDI) (Merck), polyoxytetramethylene glycol (POTMG 1000), dimethylolpropionic acid (DMPA), triethylamine (TEA), and Xa in the form of powder (Brookfield viscosity of 1% solution, according to Certificate of analysis, amounts 959 cps) were purchased from Aldrich and used as received; acetone was purchased from Fluka.

2.2. Preparation of Xanthan Containing Ionomer Polyurethane. Xanthan containing ionomer polyurethanes (IPU/Xa) in the form of aqueous dispersions was prepared by the reaction of an isocyanate precursor based on POTMG and HMDI with DMPA as ion centers carrier, taken in a molar ratio of 1 : 2 : 0.6. The reaction time for the isocyanate precursor formation was 2 h at 80°C until the NCO content reached the theoretical value to produce NCO-terminated prepolymer. The content of NCO groups was controlled according to [16]. Then, DMPA was added and reacted with prepolymer at 80°C for 1 h. Suitable amount of acetone was added to the system to decrease the viscosity of reaction mixture. Xa $(C_{35}H_{49}O_{29})_n$, was added to the reaction mixture in a form of dry powder (the reaction time was 1 h at 56°C). Neutralization of the DMPA fragments' carboxyl groups of obtained IPU/Xa hard block was performed with TEA (the molar ratio of TEA : DMPA = 1 : 1). Next, a simultaneous elongation and water dispersion were carried out, followed by removal of acetone. Film-forming opalescent dispersions were then obtained by phase inversion. Polymer films were formed at room temperature on a Teflon disk, followed by drying in an oven at 65°C and in a vacuum oven at 55°C to constant weight.

IPU/Xa systems with different Xa weight concentrations, 5%, 10%, and 30% (IPU/5Xa, IPU/10Xa IPU/30Xa), were prepared. IPU matrix was synthesized similar to IPU/Xa (using water as chain extender, without addition of Xa) and has been selected as an object of comparison.

2.3. Characterization

2.3.1. pH Values. pH values were determined using pH-meter "pH-150 M" (Russia).

2.3.2. Particle Size. Particle size measurements were determined from the turbidity spectrum using FEK-56M, according to [17].

2.3.3. Mechanical Properties. Measurements were performed using a tensile testing machine FU-1000 (VEB MWK "Fritz Heckert," Germany) at a tensile speed of 100 mm/min and temperature 25°C. The number of samples used in each measurement was three. Samples were prepared in a form of strips (width: 4 mm, operating length: 2 mm). Measurements were carried out in accordance with standard 14236-81; allowed error is 3%.

2.3.4. Water Absorption. Preliminary weighed dry films of IPU matrix, IPU/Xa, were immersed in water for 24 h, whereupon the excess water was removed with filter paper and samples were weighed. Water absorption (W_{H2O}, wt.%) was calculated according to $W_{H2O}(\%) = [(W_w - W_d)/W_d] \cdot 100\%$, where W_w and W_d are weight of the films in a wet and dry state, correspondingly.

2.3.5. Degree of Hydrolysis in Acid and Alkali Medium. Degree of hydrolysis in acid and alkali medium was determined by evaluation of the weight change and physic-mechanical characteristics of the samples after hydrolysis. Preweighed samples were immersed in 0.1 N solution of KOH and HCl and kept in a thermostat for 30 days at $T = 25$°C; afterwards the films were dried to constant weight with following weight control and tensile test.

2.3.6. IR Measurements. IR measurements were performed on Bruker "Tensor-37" Fourier transform infrared spectrometer in the region of wave numbers of 4500 cm^{-1}–500 cm^{-1}. Samples' surfaces were studied by attenuated total internal reflection infrared spectroscopy.

2.3.7. Thermodestruction of Xa-Containing IPU. Thermodestruction of Xa-containing IPU was studied by pyrolytic mass spectrometry (PMS). A device consisting of a mass spectrometer MX-1321 for determination of the components of gas mixtures in the range of mass numbers of 1–4000 and of cells for linearly programmable pyrolysis in the temperature range 25–400°C was used. The sample was placed into the cell which was evacuated ($1.33 \cdot 10^{-4}$ Pa) for 30 minutes at 25°C. The same pressure was maintained during the experiment. The heating rate was (6 ± 1)°C/min. The accuracy of determining the temperature of the sample was ±1°C. The ionization energy in the chamber of the mass spectrometer was 70 eV.

2.3.8. The X-Ray Diffraction Patterns. The wide-angle X-ray diffraction patterns (WAXS) were recorded with

Table 1: Properties of aqueous IPU/Xa dispersions and based films.

Xa content, %	Dispersion properties		Film characteristics			
	r_{av^*}, nm	pH	Water absorption, 24 hours, %	Contact angle, degree	Tensile strength σ, MPa	Elongation at a break point ε, %
0	71	7,84	2,6	68	7,3	1100
5,0	176	7,55	23	50	8,1	742
10,0	272	7,17	65	45	16,9	530
30,0	504	6,82	405	29	36,4	360
100,0	—	—	The film was dissolved	—	**	**

r_{av^*}: average particle radius, ** not applicable (the film is brittle).

X-ray diffractometer DRON-4-07 with roentgen schema made according to Debye-Scherrer method (transmission). Supramolecular structure was studied by small-angle X-ray diffraction (SAXS), using small-angle camera KRM-1 with flat-filled collimator, made according to Kratky method. All X-ray measurements were carried out in CuK_α radiation, monochromatic with Ni-filter at $T = 22 \pm 2^\circ C$.

2.3.9. Dynamic Mechanical Analysis (DMA). Dynamic mechanical measurements were carried out on a dynamic mechanical analyzer Q 800, TA Instruments in the tension mode at frequency of 10 Hz and heating rate of 2.0°C/min. The samples for DMA study were cut from the polymer films and had the following dimensions: length: 12.75 mm, width: 4 mm, and thickness: 0.3 mm. The viscoelastic properties, that is, mechanical loss factor ($\tan\delta$) and storage modulus (E'), were recorded as function of temperature. The glass transition temperature (T_g) was determined by the position of the loss factor maximum.

3. Results and Discussion

3.1. Colloid-Chemical Properties. The composition, colloid-chemical, and physic-mechanical properties of synthesized IPU/Xa dispersions and films are presented in Table 1.

The average particle size reports the degree of physical interaction of the constituent macromolecules and the dispersion medium. The introduction of Xa results in increasing of r_{av} owing to growth of the specific content of three-dimensional Xa fragments in macromolecules (as previously was shown using the small Xa concentrations [18]), which, however, does not lead to a loss of dispersions' stability [19]. With increase of Xa content, the pH of dispersions is systematically reduced as a result of the presence in Xa of a large number of acid pyruvic cycles.

3.2. Water Absorption. The degree of swelling of polymer components and their affinity to water is one of the indices of decomposition rate of polymeric materials under the influence of environmental factors. The investigation of the hydrolytic stability of IPU/Xa has shown the increase of the water absorption up to a maximum value of 405% at 30% Xa content. Such increase may be due to the presence of free polar fragments (carboxyl and OH groups), which determine the hydrophilic properties of the polymer. Probably, a part of Xa hydrophilic hydroxyls involved in the formation of intermolecular bonds with the polar groups of IPUs remains unengaged, following an increase of their concentration in the surface layers and contributing to the elevation of the hydrophilicity degree and, normally, to decreasing of contact angle values (Table 1).

3.3. Physic-Mechanical Properties. The tensile strength of IPU/Xa films significantly increases as the Xa content increases and exceeds this index of the IPU matrix in 1–5 times (Table 1). The increase of tensile strength for the IPU/Xa films indicates the occurrence of the intermolecular interaction between IPU and Xa. The loss of elasticity is specified by decrease of the specific weight of the flexible IPU segments in polymer composition, which is in agreement with the IR spectroscopic data indicating the hydrogen association of ether oxygen of POTMG with OH groups of Xa and steric hinders effected by volume molecules of Xa.

3.4. IR Spectroscopy. IR spectra of IPU matrix (1), IPU/10Xa (2), and Xa (3) are presented in Figure 1(a). The IR spectrum of the initial Xa is characterized by intense absorption bands of stretching vibrations of O-H bonds in the region of 3236–3613 cm^{-1}, 1031 cm^{-1}, by peak of medium intensity of stretching vibrations of C-H bonds (2926 cm^{-1}), an intense band with a frequency of 1736 cm^{-1}, apparently corresponding to the vibrations of ester groups. IPU matrix shows all characteristic bands of polyurethanes: $\nu(NH)_{assoc}$: 3314 cm^{-1}; $\nu(CH_2)$ and $\nu(CH_3)$ intermolecular hydrogen bonds: 2939 cm^{-1} and 2850 cm^{-1}, respectively; $\nu(C{=}O)_{free.}$: 1720 cm^{-1} and $\nu(C{=}O)_{assoc.}$: 1705 cm^{-1} of urethane groups; $\delta(NH)_{free}$: 1540 cm^{-1}; ν(CO-N): 1415 cm^{-1}; ν(COO) (ester fragments of urethane group) 1250 cm^{-1}; and ν(C-O-C) (of flexible segments of the matrix): 1105 cm^{-1}. The high-frequency shoulder at the peak of the stretching vibrations of NH groups in the IPU spectrum (3375 cm^{-1}) indicates the presence of free NH groups. In the spectrum of IPU/10Xa (Figure 1(a)), this shoulder disappears, and the intensity of hydrogen-bonded NH groups (3314 cm^{-1}) increases. A redistribution of the intensities of free 1720 cm^{-1} and bonded 1705 cm^{-1} CO groups is observed. The appearance of low-frequency shoulder (1031 cm^{-1}), which refers to the stretching

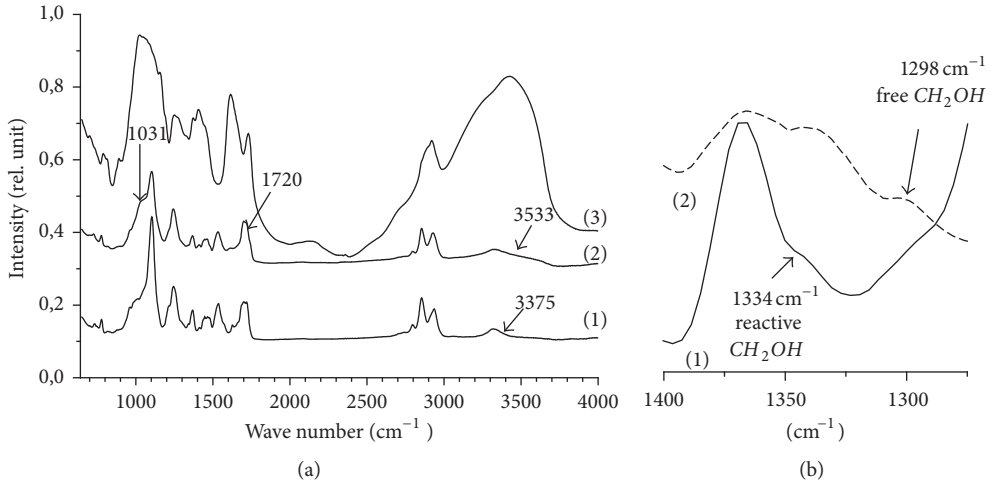

Figure 1: IR spectra: (a) IPU (1), IPU/10Xa (2), and Xa (3); (b) IPU /10Xa (1) and Xa (2).

vibrations of C-O and decrease of intensity of the valence symmetric vibrations of C-O-C 1105 cm^{-1} (Figures 1(a) and 2), indicates the hydrogen association of ether oxygen of polyurethane with OH -groups of Xa. The appearance of a broad weak band at 3533 cm^{-1} is associated with the presence of free OH groups of Xa.

At the same time, the appearance in the spectrum of the IPU/Xa (Figure 1(b), curve (1)) of the band at 1334 cm^{-1}, assigned to the C-H bond of CH_2OH group, with intensity lower than that for the native Xa and absence of the band 1298 cm^{-1} (Figure 1(b), curve (2)), indicates the participation of these groups in the formation of a chemical bond with the NCO groups of ionomeric oligourethane.

3.5. DMA Results. The temperature dependencies of tan δ и E' and viscoelastic characteristics for the IPU and IPU/Xa films are shown in Figure 2 and Table 2. The dependence tan δ-T (Figure 2(a)) for the IPU is typical for segmented polyurethanes: there are two relaxation processes, corresponding to the soft and hard blocks. The maximum in the temperature range of −70 to 10°C (T_g = −30°C) corresponds to the IPU soft blocks' relaxation transition. In the same temperature range, a sharp drop of E' (Figure 2(b)) is observed. Sharp peak of tan δ at 90°C and sharp drop of E' higher that 70°C indicate the existence of hard block in IPU.

Such viscoelastic behavior is inherent to many segmented IPU. This is due to the segmental mobility in the hard blocks' microregions (hard domains) and their destruction. The relaxation transition typical for the soft block of IPU is also observed for all IPU/Xa films along with the fixed beginning of the relaxation transition for the hard block (Figure 2(a)). However, the viscoelastic behavior of the IPU/Xa is significantly affected by incorporation of Xa. The increase of Xa content results in significant lowering of the relaxation peak corresponding to the soft block and in T_g reduction (Table 2). Thus, 30% of Xa content (IPU/30Xa) leads to lowering of T_g by 20°C in regard to T_g of IPU.

Table 2: Viscoelastic characteristics of xanthan containing IPU.

Xa content, %	T_g, °C (according to tan δ_{max})	tan δ_{max}	E', MPa (25°C)
0	−30	0,54	6,5
5	−42	0,21	136
10	−45	0,18	247
30	−50	0,09	1230

Such changes in relaxation behavior may be caused by three-dimensional Xa molecules which form steric hindrances during the IPU/Xa soft block formation. It leads to its partial destruction and T_g lowering. At the same time, the decrease of specific weight of IPU/Xa soft-segmented part and interaction between the polar groups of the IPU and the OH groups of Xa results in the blocking of flexible polymer chains mobility and, consequently, decreasing tan δ_{max}. The relaxation transition corresponding to the hard block of IPU/Xa begins at higher temperatures compared to IPU matrix and is characterized by a smoother increase of mechanical loss factor (Figure 2(a)). Possibly the destruction of hard domains in IPU/Xa is preceded by the gradual destruction of intermolecular hydrogen bonds between the OH groups of Xa and urethane and urea groups of IPU. When Xa content amounts to 30%, the growth of mechanical loss factor is not observed up to 240°C. Perhaps a significant increase in the proportion of bound urethane groups at such Xa concentration leads to a sharp restriction or complete blocking of segmental mobility in the hard block. The low-intensity relaxation maxima on the temperature dependence of tan δ indicate the heterogeneity of the IPU/Xa systems and the presence of amorphous microregions with different compositions. Incorporation of Xa results in substantial increase of storage modulus (Figure 2(b)). Thus, at T = 25°C, the value of the storage modulus for IPU/5Xa is more than 20 times higher than that for the pure IPU. When the content of Xa reaches 30% (IPU/30Xa), the value of storage modulus increases almost in 200 times (Table 2). Such significant

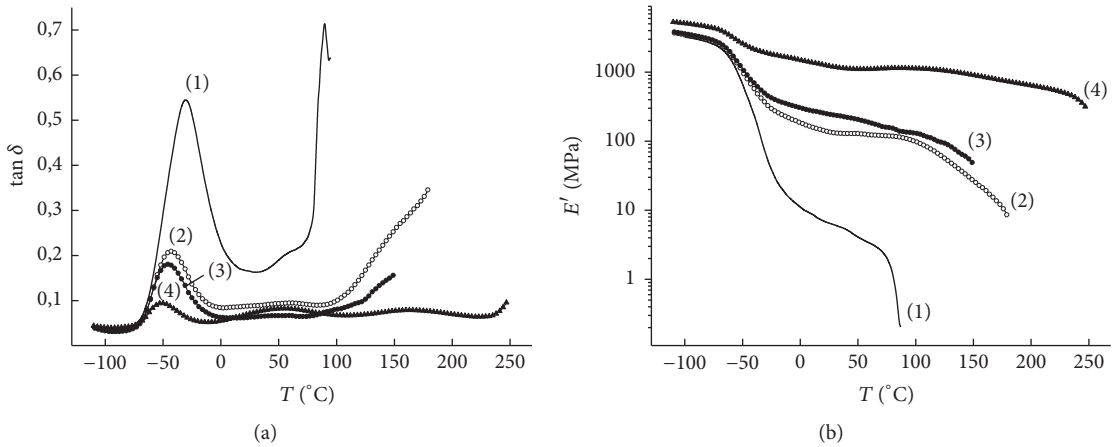

Figure 2: Temperature dependence of tan δ (a) and E' (b) of IPU matrix (1), IPU/5Xa (2), IPU/10Xa (3), and IPU/30Xa (4).

increase of the storage modulus of Xa-comprising IPUs confirms the presence of chemical and hydrogen bonding between the components.

Thus, viscoelastic properties of IPU/30Xa are determined by Xa content and intermolecular interactions between the components.

3.6. Acid and Alkaline Hydrolysis. The presence of Xa in the IPU chain determines the nature of hydrolysis, one of the main factors of the materials' degradation under environmental conditions. The higher the Xa content, the greater the mass loss and the lower the strength and elasticity of the films after hydrolysis (Table 3); that is, IPU/Xa films are more susceptible to hydrolytic destruction in comparison with the IPU matrix.

The IPU/Xa (bio)degradation ability was studied by a technique that allows us to simulate the processes taking place under the natural conditions [20]. Samples were incubated in containers with soil of medium biological activity (pH = 6.82, relative humidity: 60%, T = 14–25°C) for a period of 1–4 months [21]. The analysis of the soil's bacterial population has shown the presence of fungi of the following genera: *Rhizopus, Aspergillus,* and *Penicillium*.

The rate of degradation was controlled by weight loss of incubated samples through regular intervals. The higher the Xa content, the greater the mass loss of the samples (Table 4), and within 4 months it reaches 10.2% (IPU/5Xa) and 38% (IPU/30X a), which exceeds the actual Xa content and the specified matrix characteristic. This indicates the possibility of control of destruction rate by changing the component composition.

Soil-born microorganisms (MO) affect the films' properties. They provoke a decrease of physic-mechanical parameters (σ/ε) after remaining 4 months in the soil: for IPU matrix by 2.8/1.4%, for IPU/5Xa by 50.1/18, 0%, respectively, and for IPU/10Xa and IPU/30Xa; these indices are not available, because the films have lost their integrity. Thus, the presence of Xa promotes biodegradation of polymer materials. Visual assessment of the films after testing in the soil also indicates a sufficiently high degree of samples' damage with MO.

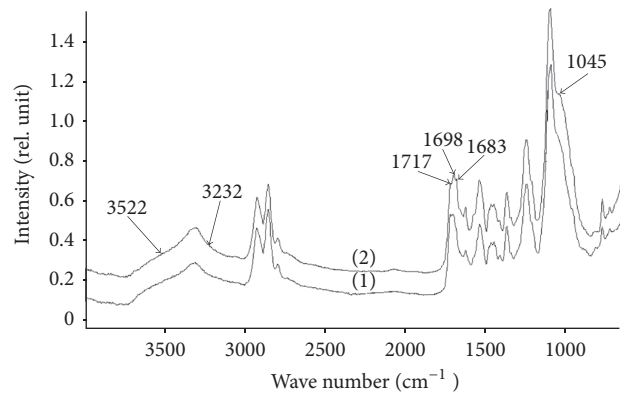

Figure 3: IR spectra of IPU/10Xa before (1) and after (2) incubation into the soil for 4 months.

The degradation of the samples was confirmed by IR spectroscopy on the example of IPU/10Xa. Figure 3 shows IR spectra of IPU/10Xa before (1) and after (2) incubation into the soil. In the absorption region (1000–1800) cm^{-1} of the after-ground sample (spectrum 2), a redistribution of the intensities of the bonded 1698 cm^{-1} and free 1717 cm^{-1} C=O groups is observed. The appearance of a new band 1683 cm^{-1} is associated with the decomposition of COOH groups: the ester group turns into an ether one. In addition, the expanse of the OH- groups' band to the more (3522 cm^{-1}) and less (3232 cm^{-1}) frequency region is observed. The appearance of a new band 1045 cm^{-1} is a result of the ether bonds decomposition after sample incubation in the soil.

3.7. Thermodestruction. The processes of thermal destruction of IPU and IPU/Xa, a comparative analysis of their structure, and the depth of (bio)degradation in the soil were estimated by the PMS method.

Analysis of the temperature dependence of the total ion current of the emission of volatile degradation products of the IPU (Figure 4(a)) has shown its complete thermal decomposition in two stages with maximum decomposition rates at the

Table 3: Physic-mechanical characteristics of the IPU, IPU/Xa films after acid and alkaline hydrolysis.

Xa content, %	0,1 N solution of KOH			0,1 N solution of HCl		
	Weight loss, %	Tensile strength σ, MPa	Elongation at a break point, ε, %	Weight loss, %	Tensile strength σ, MPa	Elongation at a break point, ε, %
0	0,1	5,7	970	0,22	6,7	860
5,0	1,8	1,3	442	1,7	1,7	402
10	3,3	*	*	3,4	*	*
30	10,6	*	*	11	*	*

* Fragmentation of the film.

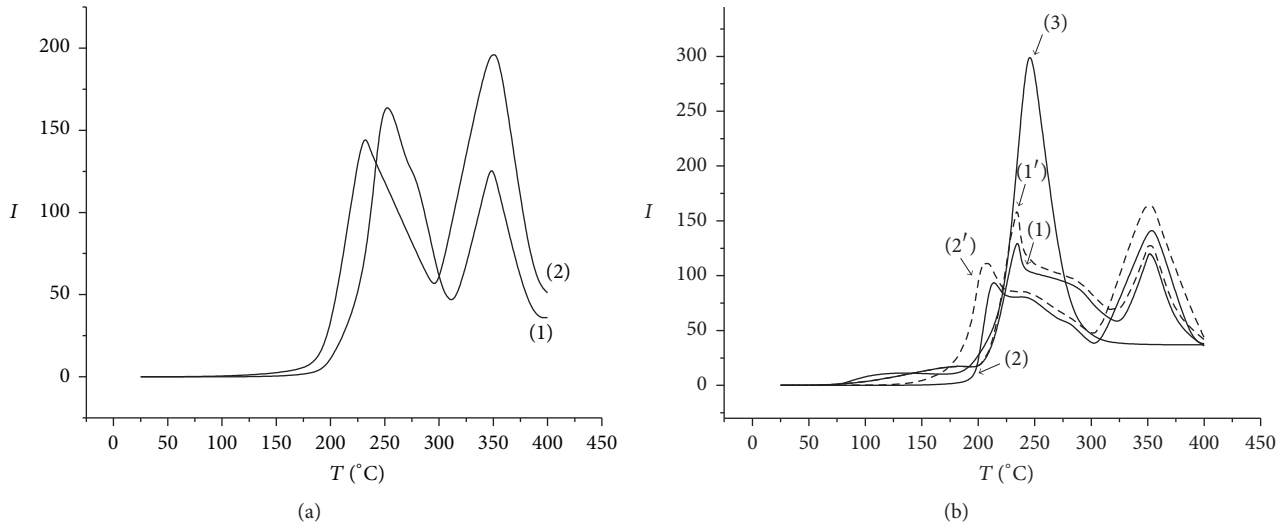

Figure 4: The temperature dependence of the ion current intensity for IPU (a), IPU/10Xa (1, 2), and IPU/30Xa (1′, 2′) (b): (1, 1′) initial sample; (2, 2′) sample after incubation in the soil (4 months); (3) initial Xa.

Table 4: Results of of IPU/Xa incubation in the soil.

Characteristic (4 months)	Xa content, %			
	0	5,0	10,0	30,0
Weight loss, %	1,3	10,2	13	38
Changing of physic-mechanical indices after the test (σ/ε), %	2,8/1,4	50,1/18,0	*	*

* Fragmentation of the film.

temperatures of 250°C and 350°C, which corresponds to the decomposition temperatures of hard and soft blocks. The first stage corresponds to the pyrolysis of urethane and urea bonds and the second to the pyrolysis of oligoether fragments [22]. The maximum of the peak of IPU kept in the soil shifts to the lower temperature (220°C) and is supplemented by a decrease of the intensity of the decomposition peak of hard blocks. The maximum decomposition peak of soft blocks remains at the same temperature of 350°C; however, the intensity of the total ion current of volatile products is significantly increased. Thus, keeping the IPU films in the soil results in the primary degradation of oligoether component, since it is known [23] that the oligoether fragments are predominantly situated in the IPU surface layers. In the initial IPU/10Xa (Figure 4(b)), the high intensity of the volatile products' release is observed at the hard blocks' decomposition and is accompanied by the release of water, as well as the following fragments: (m/z: 28 (CO, C_2H_4, N_2, CHNH), 31 (CH_3O, CH_2OH), 43 (C_2H_5N), C_3H_7), CH_3CO), 55 (C_4H_7), CH_2CHCO), 71 (CH_2CHCH_2CHO), and 73 ($OHCCH_2CHOH$)), which are the pyrolysis products of urethane and urea groups. With the increase of Xa content (sample IPU/30Xa), the intensity of release of the volatile products of the hard block decomposition increases (Figure 4(b) (1′)). After the incubation into the soil, similar to IPU, a greater intensity of volatile products' release is observed at the decomposition of the soft blocks for both IPU/10Xa and IPU/30Xa. The shift of the maximum (350°C) is not observed. For the incubated IPU/10Xa and IPU/30Xa samples, the temperature of the maximum intensity of the release of volatile decomposition products of the hard block is shifted towards the lower temperatures, from 230 to 210°C for IPU/10Xa and from 230 to 200°C for IPU/30Xa.

The dependence of the ion current on temperature for Xa has only one maximum at 250°C (Figure 4(b)). The fragments with m/z 18 and 44, corresponding to water and carbon dioxide, have the maximum specific content. It should be noted that there are practically no fragments typical for the degradation of native Xa (m/z 15 (CH_3), 17 (OH), 32 (O_2),

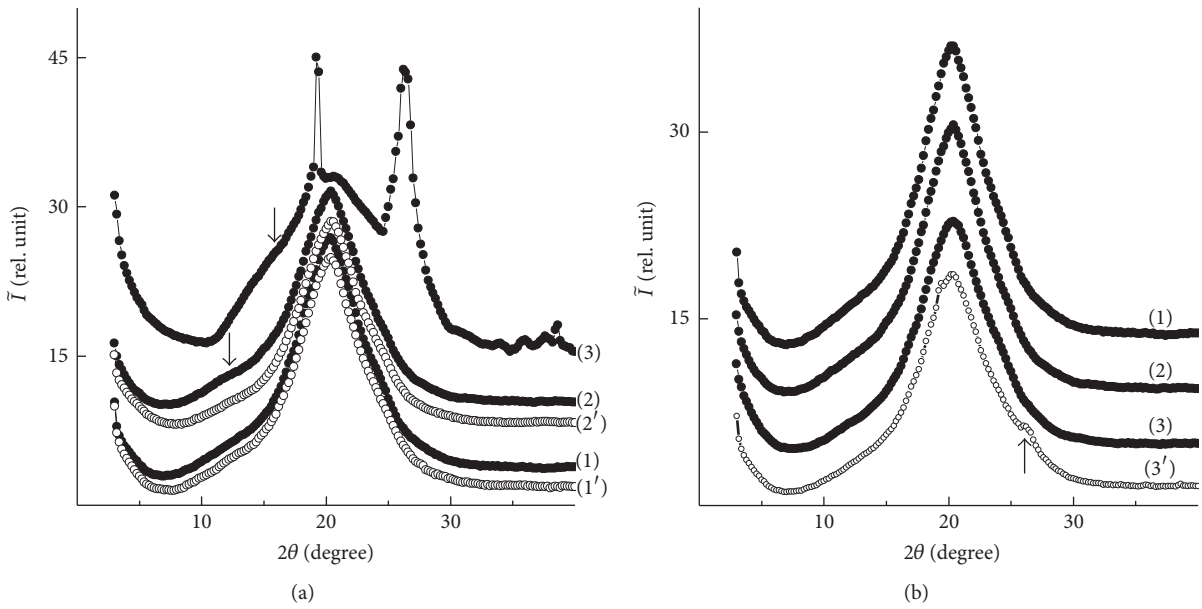

Figure 5: WAXS patterns of IPU and Xa-containing IPU: (a) initial IPU (1), IPU/5Xa (2), Xa (3), and being exposed in a soil for 4 months: IPU (1′) and IPU/5Xa (2′); (b) initial IPU (1), IPU/5Xa (2), and IPU/10Xa (3, 3′): (3) experimental and (3′) additive.

and 60 (CH_2CO_2H)) among the degradation products of IPU/10Xa and IPU/30Xa, which indicates the chemical binding of Xa. As it follows from the temperature dependence, the destruction of the IPU hard block occurs with higher intensity in comparison with the IPU/10Xa and IPU/30Xa, which may be a result of intra- and intermolecular hydrogen bonding between OH groups of Xa and urethane and urea groups of IPU. Therefore, the destruction of intermolecular hydrogen bonds precedes the destruction of the hard blocks and results in the decrease of the IPU/Xa hard blocks' decomposition intensity. However, the higher the Xa content, the lower the degradation temperature.

3.8. X-Ray Analysis. The presence of a single diffuse diffraction maximum with angular position $2\theta_m = 20{,}3^\circ$ in WAXS patterns of IPU and IPU/5Xa (Figure 5(a), curves (1, 2)) shows that these polymers are characterized by short-range order at the translation in expanse of their macrochain fragments.

The average distance (d) between the centers of macromolecular chain layers of IPU and IPU/5Xa, according to the Bragg equation $d = \lambda\,(2\sin\theta) - 1$ (where λ is the wavelength of the CuK_α radiation $\lambda = 0{,}154$ nm), amounts to 0.437 nm.

Two discrete diffraction maxima, singlet and multiplet at $2\theta_m = 19{,}3^\circ$ and $26{,}2^\circ$, respectively, appeared against a background of evident asymmetric diffraction peak $2\theta_m \approx 20{,}6^\circ$ in WAXS pattern of Xa (Figure 5(a), curve (3)), testifying to the amorphous-crystalline structure of Xa.

Nonlinear change of scattering intensity in the range of $2\theta \sim 11.2^\circ$–17.0° is indicated by poorly detected diffraction maximum at $2\theta_m \sim 15{,}8^\circ$ (arrow). This maximum describes the short-range order at the translation in the Xa volume of its side branch fragments.

We evaluated the relative level of crystallinity X_{cr} of polysaccharide Xa in accordance with Matthews's method [24], $X_{cr} \approx 20\%$, and determined effective size L of Xa crystallites using Scherer method [25], $L \approx 18$ nm.

The amorphous-crystalline structure of Xa was not detected on the X-ray diffraction pattern of IPU/5Xa and IPU/10Xa (Figure 5(b), curve (2, 3)), due to intermolecular interaction between components. Comparison of experimental and calculated additive (when interaction between components is absent) X-ray diffraction patterns of IPU/10Xa (Figure 5(b), curves (3, 3′)) has served as evidence that the absence of Xa crystalline structure phenomenon in IPU/Xa composition is caused by intermolecular interactions between IPU and Xa components.

Calculated additive X-ray diffraction pattern of IPU/10Xa (Figure 5(b), curve (3′)) has shown that in case of the absence of components' interaction there is a weak expression of the most intense diffraction peaks (at $2\theta_m = 19{,}3^\circ$ and $26{,}2^\circ$) that characterize the crystalline structure of Xa. This is a conformation of intermolecular interactions between IPU and Xa which results in suppression of Xa capacity for crystallization.

The invariable intensity and angular position of the amorphous halo ($2\theta_m \approx 20{,}3^\circ$) of the initial and aged in the soil IPU and IPU/5Xa samples (Figure 5(a), curves (1, 1′) and (2, 2′)) indicate that there is no change in their amorphous structure.

For more complete structural characterization of the initial 13 and aged for 4 months in the soil IPU and IPU/5Xa samples, we study their microheterogeneous structure. SAXS results (Figures 6(a) and 6(b)) have shown that all studied polymers have microheterogeneous structure. There are the areas of microheterogenity in their volume, the electron density ($\Delta\rho$) between which is different from zero, $\Delta\rho =$

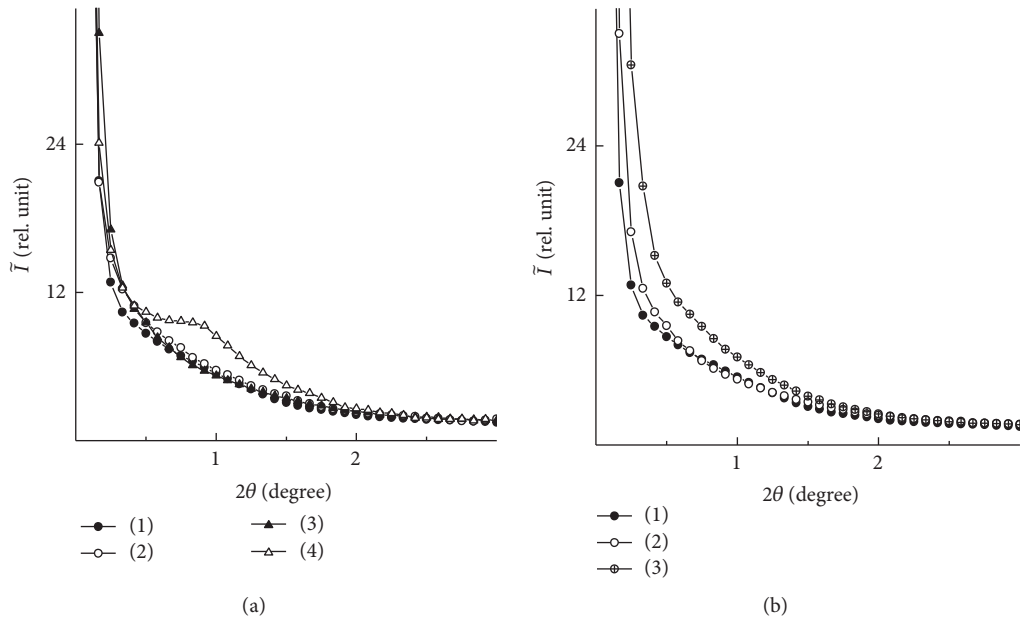

Figure 6: SAXS patterns of IPU and Xa-containing IPU: (a) initial IPU (1) and IPU/5Xa (2), and being exposed in soil for 4 months: IPU (3) and IPU/5Xa (4); and (b) initial IPU (1), IPU/5Xa (2), and IPU/10Xa (3).

$\rho - \langle\rho\rangle$, where ρ and $\langle\rho\rangle$ are the local and average value of the electron density in two-phase system.

The comparison of the profiles of the initial and aged for 4 months in soil IPU and IPU/5Xa samples has shown that the initial IPU has the lowest scattering intensity as a result of thermodynamic incompatibility between soft and hard IPU units [26]. The sample IPU/5Xa has a slightly higher scattering intensity than the IPU. Even higher scattering intensity and, correspondingly, the value of the electron density contrast have the sample IPU/10Xa. At that the lack of interference maximum on the intensity profiles indicates a disordered placement of microareas of heterogeneity in polymer volume (Figure 6(b)). Attention is drawn to the fact that exposure of samples to soil for 4 months results in a growth of scattering intensity of both IPU and, particularly, IPU/5Xa. The appearance of the interference maximum $2\theta_m \approx 0{,}92^\circ$ in a form of "shoulder" (Figure 6(a), curves (3, 4)) indicates the existence of periodicity in distribution of microareas of heterogeneity with different size of local electron density in IPU/5Xa volume. According to the above Bragg equation, the value of period D of alternation in the volume of monotype ρ-sized microareas of heterogeneity is 9.6 nm. It should be noted that the increase of the SAXS intensity at the transition from IPU to IPU/5Xa and IPU/10Xa, as well as the result of exposure of the first two samples for 4 months in soil, characterizes the variations of the level of heterogeneity of their structure. To quantify the relative level of heterogeneity of the structure, we calculated the structural parameter "Porod invariant" Q' [27], the value of which is independent (invariant) of the form of microareas of heterogeneity:

$$Q' = \int_0^\infty q\tilde{I}(q)\,dq, \tag{1}$$

where q is directed magnitude of wave vector s ($q = 2\pi s$).

Table 5: Parameters of microheterogeneous structure of initial IPU, IPU/5Xa, IPU/10Xa and IPU, IPU/5Xa after 4 months of exposure in soil.

Sample	Q', rel. unit	l_p, nm
IPU	5,9	6,5
IPU/5Xa	6,4	5,4
IPU/10Xa	7,8	6,1
IPU, 4 months in soil	6,5	5,8
IPU/5Xa, 4 months in soil	7,8	5,3

This parameter characterizes the integral intensity of X-ray scattering by two-phase system and has a direct connection with the quadratic fluctuation of electron density in its volume.

According to calculated values of Q' (Table 5), IPU possesses the least level of structure heterogeneity, while IPU/10Xa and IPU//5Xa, which are kept for 4 months in soil, have the largest level of structure heterogeneity.

Another characteristic of microheterogeneous structure of studied systems is the average size of microareas of heterogeneity existing in their volume. The range of heterogeneity l_p was determined by the Ruland method [28]. This parameter is directly related to the average diameter of the microareas of heterogeneity in the two-phase system. It was determined that presence of Xa results in a decrease of the effective size of microareas of heterogeneity both in the initial samples and after 4 months of exposure in soil (Table 4). Unlike the level of heterogeneity Q', the transition from IPU to IPU/5Xa and IPU/10Xa causes, in general, the reduction of the range of heterogeneity l_p (Table 4).

Thus, as a result of X-ray study, Xa has been found to miss its ability to crystallization due to the intermolecular

interactions between components in IPU/Xa systems. The increase of Xa content in IPU/Xa systems reduces the size of microareas of heterogeneity. The disappearance of the diffraction maximum ($2\theta_m \approx 12{,}2^\circ$) after exposure of the sample IPU/5Xa in the soil indicates a change of its amorphous structure as a result of (bio)degradation following a consecutive increase of structure heterogeneity on nanosized level.

4. Conclusions

New ecologically friendly IPUs were prepared on the basis of the renewable exopolysaccharide Xa. Introduction of Xa allows partially replacing exhaustible oil row materials and improving the strength properties of pure IPU matrix: the tensile strength of IPU/Xa systems is 1–5 times higher compared with IPU. Along with retention of other functional characteristics of the IPU, Xa imparts it a property of (bio)degradation after the end of lifetime that leads to the deep chemical transformations occurring in the IPU/Xa systems. The proven covalent and hydrogen bonding between components ensures the occurrence of destructive processes of the entire system as a whole. With an increase of Xa content, the mass loss of IPU/Xa systems as a result of hydrolytic splitting and degradation in the soil increases and exceeds the actual content of Xa and the value of mass loss of the IPU matrix. The results of PMS, DMA, and X-ray scattering indicate that the presence of Xa in polymer macrochain leads to the formation of a new structural organization different from the structure of the IPU matrix due to the chemical bonding between the exopolysaccharide and diisocyanate. The structural and operational properties and degradability of studied polymers are determined by the structure and content of the natural component. Film-forming aqueous polyurethane dispersions on the basis of exopolysaccharide Xa are perspective as biologically active substances in agriculture: immunostimulants and protective coating for seeds and plants; antitranspirants for reducing water scarcity and optimization of the production process of crops in drought conditions; and binders for biologically active substances granulation. The advantages of such material lie in environmentally friendly production technology due to the absence of organic solvent, economy through the use of cheap renewable raw materials, and reducing the harmful impact on the environment through the regulated level of (bio)degradation after the expiration of life time.

Conflicts of Interest

The authors declare that there are no conflicts of interest.

References

[1] S. Rogovina, K. Aleksanyan, E. Prut, and A. Gorenberg, "Biodegradable blends of cellulose with synthetic polymers and some other polysaccharides," *European Polymer Journal*, vol. 49, no. 1, pp. 194–202, 2013.

[2] S. A. Ashter, "Overview of biodegradable polymers," in *Introduction to Bioplastics Engineering*, pp. 19–30, Elsevier, Amsterdam, Netherlands, 2016.

[3] T. Travinskaya and Y. Savelyev, "Aqueous polyurethane dispersions—sodium alginate based blends and hydrogels," *Frontiers in Heterocyclic Chemistry*, vol. 2, no. 1, pp. 20–25, 2016.

[4] P. Alagi, Y. J. Choi, and S. C. Hong, "Preparation of vegetable oil-based polyols with controlled hydroxyl functionalities for thermoplastic polyurethane," *European Polymer Journal*, vol. 78, pp. 46–60, 2016.

[5] M. J. Donnelly, J. L. Stanford, and R. H. Still, "The conversion of polysaccharides into polyurethanes: A review," *Carbohydrate Polymers*, vol. 14, no. 3, pp. 221–240, 1991.

[6] J. G. Southwick, H. Lee, A. M. Jamieson, and J. Blackwell, "Self-association of xanthan in aqueous solvent-systems," *Carbohydrate Research*, vol. 84, no. 2, pp. 287–295, 1980.

[7] S. C. Moldovenau, *Analytical Pyrolysis of Natural Organic Polymers*, vol. 20, Brown & Williamson Tobacco Corp., Macon, Ga, USA, 1998, p. 510.

[8] T. V. Travinskaya, A. N. Brykova, I. K. Kurdish, A. V. Chevychalova, and Y. V. Savelyev, "Degradable ionomer polyurethane on the basis of xanthan," *Reports of the Academy of Sciences*, vol. 7, pp. 132–139, 2014.

[9] Y. V. Savelyev, T. V. Travinskaya, L. A. Markovskaya, and A. N. Brykova, "The method of obtain of degradable polymer composition," Pat. No 93372 Ukraine, Publ. 25.09.2014. Bull. no. 18, 2014.

[10] Q. B. Meng, S.-I. Lee, C. Nah, and Y.-S. Lee, "Preparation of waterborne polyurethanes using an amphiphilic diol for breathable waterproof textile coatings," *Progress in Organic Coatings*, vol. 66, no. 4, pp. 382–386, 2009.

[11] V. Sriram, S. Sundar, A. Dattathereyan, and G. Radhakrishnan, "Synthesis and characterization of cationomeric AB crosslinked polyurethane polymers based on different chain extenders," *Reactive and Functional Polymers*, vol. 64, no. 1, pp. 25–34, 2005.

[12] J. Bullermann, S. Friebel, T. Salthammer, and R. Spohnholz, "Novel polyurethane dispersions based on renewable raw materials—Stability studies by variations of DMPA content and degree of neutralisation," *Progress in Organic Coatings*, vol. 76, no. 4, pp. 609–615, 2013.

[13] T. Travinskaya, Y. Savelyev, and E. Mishchuk, "Waterborne polyurethane based starch containing materials: preparation, properties and study of degradability," *Polymer Degradation and Stability*, vol. 101, no. 1, pp. 102–108, 2014.

[14] S. J. Lee and B. K. Kim, "Covalent incorporation of starch derivative into waterborne polyurethane for biodegradability," *Carbohydrate Polymers*, vol. 87, no. 2, pp. 1803–1809, 2012.

[15] Y. V. Savelyev, T. V. Travinskaya, L. P. Robota et al., "Biodegradable polyurethane materials of different origin based on natural components," *Austin Journal of Biomedical Engineering*, vol. 2, no. 1, article 1030, 2015, http://www.austinpublishinggroup.com/.

[16] ASTM D2572-03, "Standard test method for isocyanate groups in urethane materials or prepolymers," ASTM, West Conshohocken, Pa, USA, 2003.

[17] S. Y. Shegolev and V. I. Klenin, "Determination of parameters of complicated disperse polymer system from turbidity spectrum," *Vysokomolekulyarnye Soedineniya B*, vol. 13, no. 12, pp. 2809–2815, 1971.

[18] T. V. Travinskaya, A. N. Brykova, V. I. Bortnitskiy, and Yu. V. Savelyev, "Preparation and Properties of (bio)degradable

ionomer polyurethanes based on xanthan," *Polymernyj Journal*, vol. 36, no. 4, pp. 393–400, 2014.

[19] N. I. Levchenko, S. A. Sukhorukova, and T. V. Travinskaya, "Aqueous anionactive polyurethanes for high—quality coatings," in *Proceedings of the Partnership in Polymers, the Cambridge Polymer Conference*, pp. 195–200, Cambridge, UK, 1996, Special conference issue of full papers.

[20] B. S. Lee, M. Vert, and E. Holler, *Water-Soluble Aliphatic Polyesters: Poly(malic acid)s*, Wiley-VCH Verlag Gmbh, Weinheim, Germany, Polyester, 1st edition, 2002.

[21] I. P. Babaeva and G. M. Zenova, *Biology of Soils*, Moscow University, Moscow, Russia, 1989.

[22] V. A. Zaikin, *Mass Spectroscopy of Synthetic Polymers*, All-Russian Mass Spectrometric Society, Moscow, Russia, 2009.

[23] V. V Boyko, L. V. Kobrina, S. V. Riabov, and R. L. Gaiduk, "Investigation of biodegradable properties of polyurethane compositions filled by chitosan," *Polymernyj Journal*, vol. 26, no. 4, pp. 235–238, 2004.

[24] J. L. Matthews, H. S. Peiser, and R. B. Richards, "The X-ray measurement of the amorphous content of polythene samples," *Acta Crystallographica*, vol. 2, no. 2, pp. 85–90, 1949.

[25] A. Guiner, *Radiography of Crystals. Theory And Practice*, Nauka, Moscow, Russia, 1961, p. 604.

[26] V. I. Shtompel and Y. Y. Kercha, *Structure of Linear Polyurethanes*, Nauka, Moscow, Russia, 2008, Kiev, p. 248.

[27] G. Porod, in *General Theory, Small-Angle X-Ray Scattering*, O. Glatter and O. Kratky, Eds., pp. 17–51, Academic Press, Cambridge, Mass, USA, 1982, London.

[28] R. Perret and W. Ruland, "Eine verbesserte Auswertungsmethode für die Röntgenkleinwinkelstreuung von Hochpolymeren," *Kolloid-Zeitschrift & Zeitschrift für Polymere*, vol. 247, no. 1-2, pp. 835–843, 1971.

Hindawi
International Journal of Polymer Science
Volume 2017, Article ID 4308687, 6 pages
https://doi.org/10.1155/2017/4308687

Research Article

Structural Foams of Biobased Isosorbide-Containing Copolycarbonate

Stefan Zepnik,[1] Daniel Sander,[2] Stephan Kabasci,[1] and Christian Hopmann[2]

[1] *Fraunhofer Institute for Environmental, Safety and Energy Technology (Fraunhofer UMSICHT), Oberhausen, Germany*
[2] *Institute of Plastics Processing (IKV) in Industry and the Skilled Crafts, RWTH Aachen University, Aachen, Germany*

Correspondence should be addressed to Stephan Kabasci; stephan.kabasci@umsicht.fraunhofer.de

Received 8 May 2017; Accepted 17 August 2017; Published 20 September 2017

Academic Editor: Vinay Sharma

Isosorbide-containing copolycarbonate (Bio-PC) is a partly biobased alternative to conventional bisphenol A (BPA) based polycarbonate (PC). Conventional PC is widely used in polymer processing technologies including thermoplastic foaming such as foam injection molding. At present, no detailed data is available concerning the foam injection molding behavior and foam properties of Bio-PC. This contribution provides first results on injection-molded foams based on isosorbide-containing PC. The structural foams were produced by using an endothermic chemical blowing agent (CBA) masterbatch and the low pressure foam injection molding method. The influence of weight reduction and blowing agent concentration on general foam properties such as density, morphology, and mechanical properties was studied. The test specimens consist of a foam core in the center and compact symmetrical shell layers on the sides. The thickness of the foam core increases with increasing weight reduction irrespective of the CBA concentration. The specific (mechanical) bending properties are significantly improved and the specific tensile properties can almost be maintained while reducing the density of the injection-molded parts.

1. Introduction

Polycarbonates (PC) are widely used in injection molding and extrusion including foaming technologies. However, conventional PC is based on nonrenewable resources and bisphenol A (BPA), which is still in discussion due to its toxicological effects [1–5]. Isosorbide-containing PC is a copolymer obtained by polymerization of isosorbide in presence of diphenyl carbonate and other dihydroxy components as comonomers. Figure 1 shows the molecular structures of conventional PC with bisphenol A as diol monomer component (Figure 1(a)) and of a polycarbonate composed of solely isosorbide as monomeric diol (Figure 1(b)).

Isosorbide-containing copolycarbonate is partly biobased and nondegradable with main mechanical and optical properties comparable to conventional PC (Table 1).

Because isosorbide-containing Bio-PC has been on the market for less than five years, most available literature and patents are focused on chemical aspects such as the synthesis of Bio-PC as well as on structural analysis of the polymer [6–11]. Only few patents and no detailed scientific investigations concerning foaming and foam properties of Bio-PC were published [12].

Thermoplastic foam injection molding (FIM) is a special injection molding process being practiced for many decades. The thermoplastic melt is loaded with a blowing agent which results in foaming of the plastics material after being injected into the cavity of the mold. The cavity is filled only partially in order to allow the melt to expand. Diffusion of the blowing agent and gas bubble formation lead to the formation of a structural foam and the complete volume of the mold is filled out. This structural foam is characterized in general by a compact skin layer and a foamed core. While the foam structure can be influenced directly by process parameters, the mechanical properties depend on the resulting foam structure, the thermoplastic material used and the part design [13–16].

This contribution characterizes basic properties of structural Bio-PC foams in a nutshell. The foams were produced by foam injection molding using an endothermic chemical blowing agent (CBA). Physical foam properties, morphology,

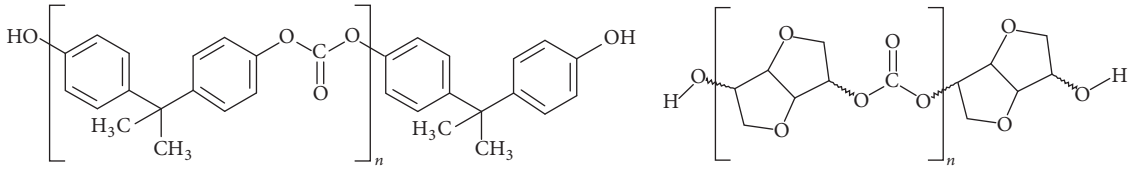

(a) (b)

Figure 1: Molecular structures of conventional PC with bisphenol A as diol monomer component (a) and of a polycarbonate composed of solely isosorbide as monomeric diol (b).

Table 1: Comparison of properties of Bio-PC and a conventional bisphenol A based PC (for both types supplier data from Mitsubishi Chemical Company).

	Bio-PC Durabio D 7340 R	Conv. PC Xantar 24 R
Tensile modulus (MPa)	2700	2300
Tensile strength (MPa)	79	60
Elongation at break (%)	72	>50
Flexural modulus (MPa)	2700	2400
Flexural strength (MPa)	116	90
HDT @ 1,80 MPa (°C)	106	130
Light transmission (%)	92	89
Refractive index (-)	1.50	1.58
Density (g/cm^3)	1.37	1.20
Biobased carbon content	60%	0%

and mechanical properties obtained from tensile test and bending test were analyzed. Specific mechanical properties were also calculated and discussed in conjunction with the CBA concentration, shell layer thickness, and morphology.

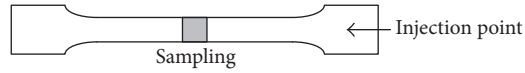

Figure 2: Sample position for morphology analysis and density measurement.

2. Materials and Methods

2.1. Materials. Isosorbide-containing PC was obtained as granules from Mitsubishi Chemical Holdings, formerly Mitsubishi Chemical Corporation, Tokyo (Japan), under the trade name Durabio D 7340 R. The melt flow rate at 230°C and 5 kg load is 19 g/10 min. The neat density is 1366 kg m^{-3} and the heat deflection temperature according to ISO 75 method B is 114°C [17, 18].

Palmarole MB.BA.16 from Adeka Palmarole SAS, Mulhouse (France), was used as an endothermic CBA masterbatch for the thermoplastic foam injection molding tests. The carrier polymer of the CBA masterbatch is a low-density polyethylene (LDPE). The active gas concentration of MB.BA.16 is 20% and the decomposition starts at 180°C [19]. Two concentrations of MB.BA.16 were used, namely, 2 wt.% and 3 wt.%. Bio-PC and CBA masterbatch resins were dry-blended in an internal mixer and this mixture was fed into the injection molding machine.

2.2. Foam Injection Molding. Multipurpose test specimens of type 1B were produced as foam parts according to DIN EN ISO 3167 by using an injection molding machine IntElect 100–340 from Sumitomo Demag Plastics Machinery GmbH, Schwaig, Germany. Low pressure foam injection molding technology, wherein the cavity is only partially filled, was applied to achieve two different weight reductions of the specimens, namely, 5% and 10%. The injection molding processing temperature was set to 220°C and the mold temperature was fixed at 50°C. The injection speed and maximum injection pressure were kept constant at about 35 cm^3 s^{-1} (screw diameter: 30 mm, volume flow rate 25 cm^3 s^{-1}) and 2000 bar, respectively. The back pressure was set to 120 bar which is high enough to prevent formation of gas bubbles in the screw vestibule.

2.3. Foam Characterization. Foam morphology was investigated in transverse direction to the melt flow by means of scanning electron microscopy (SEM). The samples were taken from the middle part of the multipurpose test specimen as shown in Figure 2 by cryogenic fracturing. Shell layer thickness and foam core thickness were measured.

The foam density was calculated from the specific volume and weight of five different samples. Tensile properties according to ISO 527 and bending properties according to

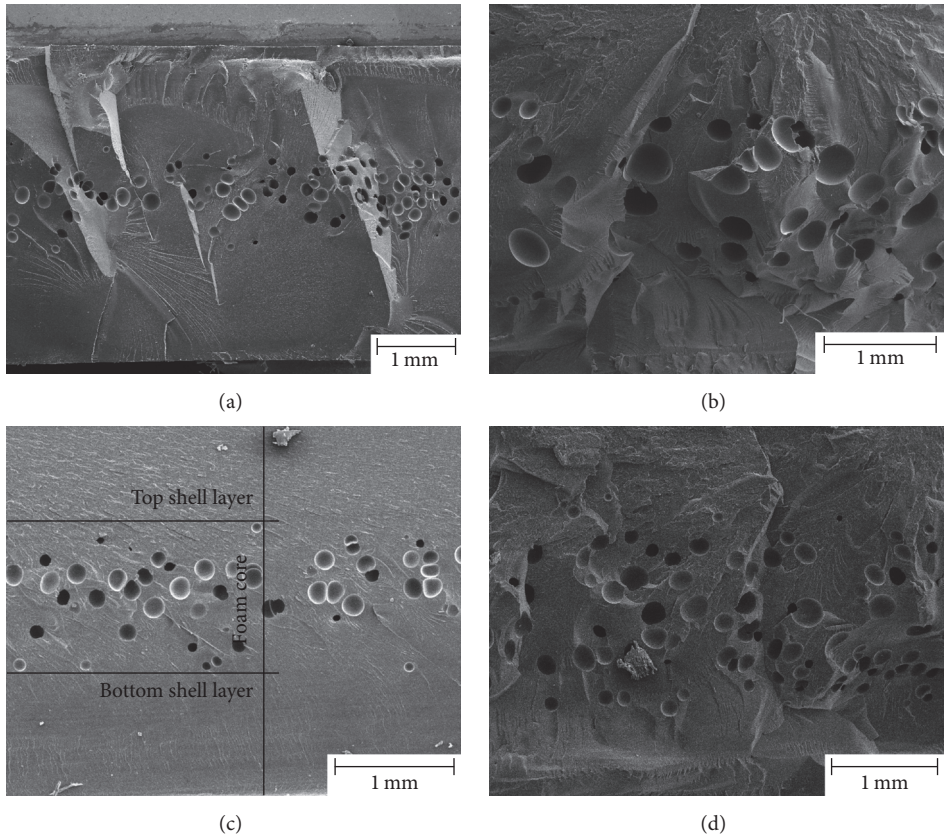

Figure 3: Morphology of injection-molded Bio-PC foams (cryogenically fractured surfaces transverse to melt flow): (a) 2 wt.% MB.BA.16, 5% weight reduction; (b) 2 wt.% MB.BA.16, 10% weight reduction; (c) 3 wt.% MB.BA.16, 5% weight reduction; (d) 3 wt.% MB.BA.16, 10% weight reduction.

ISO 178 (three-point bending test) were determined each using five samples.

3. Results and Discussion

Both CBA concentrations, 2 wt.% and 3 wt.%, proved to be suitable for achieving the desired weight reductions of 5% and 10% without any loss in specimen quality, that is, a fully filled specimen without sink marks, evaluated by visual inspection of the parts. The nonfoamed specimens are transparent due to the amorphous character of Bio-PC. The foamed parts are nontransparent and white caused by light scattering at the gas bubble polymer interfaces. The density of the nonfoamed Bio-PC specimens was measured at 1363 kg m^{-3} ± 1 kg m^{-3}, well matching the supplier data. From this, the density of the foamed Bio-PC specimens can be calculated taking the partial filling of the mold into account to 1295 kg m^{-3} for 5% weight reduction and 1227 kg m^{-3} for 10% weight reduction. These values should be independent from the CBA content in case that sufficient gas is produced for filling the mold completely.

Figure 3 shows representative morphologies of the cryogenically fractured surfaces of the injection-molded Bio-PC foams.

No significant differences with respect to the morphologies of the structural foam due to a compact shell layer and foamed core can be observed between 2 wt.% and 3 wt.% CBA concentration. The foam core is homogeneous, irrespective of the CBA concentration. The determination of the nonfoamed shell layer thicknesses and foam core thickness is shown exemplarily in Figure 3(c). The ratio between the top and bottom shell layer thicknesses (mean values for five specimen) ranges from 0.97 to 1.07 for the different experimental conditions. This indicates that the top and bottom shell layers have nearly identical thicknesses and the cross sections are almost symmetrical showing that the foam core is located right in the center. Contrary to the CBA concentration, significant influence is observed for the desired weight reduction. With increasing weight reduction from 5% to 10%, the shell layer thickness decreases and the foam core thickness increases from around 30% to 60% of the total cross-sectional area. By using the low pressure foaming method, the shot volume and therefore the injected amount of Bio-PC decrease with increasing weight reduction. This leaves more space in the cavity for foaming causing thicker foam cores. Similar results can be found in the literature [20–22].

Mechanical properties were measured in terms of tensile and three-point bending behavior, which is presented in Figure 4. The nonfoamed Bio-PC behaves ductile, similar to conventional BPA-based PC. In Figure 4(a), a strong decrease of the tensile elongation is found for the injection-molded Bio-PC foams in comparison to the nonfoamed Bio-PC.

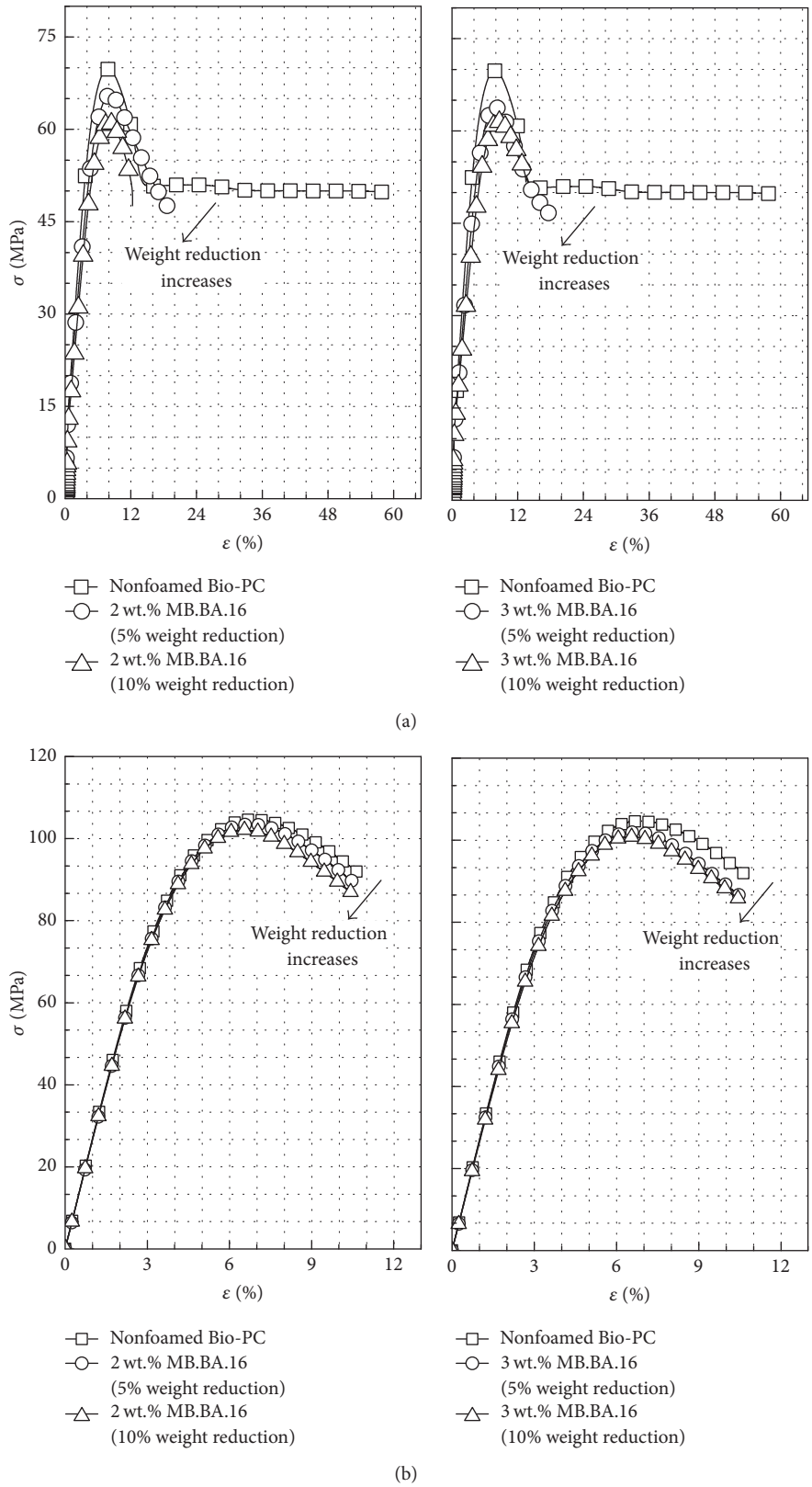

Figure 4: (a) Tensile curves of nonfoamed Bio-PC and foamed Bio-PC and (b) three-point bending curves of nonfoamed Bio-PC and foamed Bio-PC (2 wt.% and 3 wt.% CBA; 5% and 10% weight reduction). Graphs show the mean values recorded from five specimens tested.

Table 2: Specific mechanical tensile and bending properties of nonfoamed and foamed Bio-PC (the weight of the nonfoamed Bio-PC multipurpose test specimen is 13.53 g).

Property		Bio-PC	Bio-PC foams			
CBA concentration	(wt.%)	0	2	2	3	3
Weight reduction	(%)	0	4.9	11.2	5.1	10.6
Density	($kg\,m^{-3}$)	1363 ± 1	1296 ± 3	1211 ± 18	1293 ± 6	1219 ± 10
Specific tensile modulus	($MPa/(kg\,m^{-3})$)	1.98 ± 0.05	1.95 ± 0.07	1.92 ± 0.10	1.97 ± 0.10	1.91 ± 0.05
Specific tensile strength	($kPa/(kg\,m^{-3})$)	52.0 ± 0.4	50.0 ± 0.4	49.1 ± 1.3	49.4 ± 0.3	49.3 ± 0.8
Specific bending modulus	($MPa/(kg\,m^{-3})$)	1.96 ± 0.01	2.03 ± 0.01	2.13 ± 0.03	2.03 ± 0.01	2.12 ± 0.01
Specific bending strength at F_{max}	($kPa/(kg\,m^{-3})$)	77.0 ± 0.0	79.5 ± 0.0	83.1 ± 0.9	78.3 ± 0.4	82.1 ± 0.5
Specific bending strength at 3.5%	($kPa/(kg\,m^{-3})$)	60.1 ± 0.3	62.4 ± 0.2	66.0 ± 0.4	62.2 ± 0.2	64.9 ± 0.3

In addition, tensile strength and tensile stiffness as well as bending strength and bending stiffness decrease slightly. The reduction is less pronounced in case of bending (Figure 4(b)) due to higher resistance of the nonfoamed shell layers against deformation. There is no significant influence of the CBA concentration on the tensile and bending behavior. This is in good agreement with the morphologies observed in Figure 3, which show no significant difference between 2 wt.% and 3 wt.% MB.BA.16.

However, the achieved weight reduction clearly affects the mechanical properties due to the determination of the amount of nonfoamed material in the specimen. With increasing weight reduction from 0% over 5% to 10% the stiffness and strength as well as the ductility decrease continuously. In other words, the higher the degree of foaming, the lower the absolute mechanical properties.

On the other hand, it is well known that structural foams, for example, produced by injection molding, have excellent stiffness to weight and strength to weight ratios. That means the weight-related mechanical properties in terms of stiffness and strength are higher for the structural foam than for the nonfoamed part. Lots of studies have been conducted which confirm the excellent weight-related mechanical performance for many different polymeric structural foams [20, 23–26]. For example, Müller et al. [25] obtained 95% increase in relative flexural stiffness for 30 wt.% glass fiber reinforced PP while decreasing the density by about 28%. In addition, Müller [26] reported an increase in specific flexural stiffness of PP from about 25 $(N/mm^2)/(g/cm^3)$ to 40 $(N/mm^2)/(g/cm^3)$ while the density is reduced by about 49%. This typical result for structural foams also holds true for the Bio-PC foams, as can be seen from the specific tensile properties and specific bending properties summarized in Table 2. The density of the Bio-PC can be reduced by foam injection molding while maintaining or even increasing the specific mechanical properties in comparison to the nonfoamed parts. In particular, the specific bending properties steadily improve along with the density reduction and are noticeably better than the nonfoamed Bio-PC. In case of bending deformation, the nonfoamed shell layers are responsible for stiffness and strength whereas the centered foam core is close to the neutral axis. Therefore, the specific bending properties are significantly improved. In case of tensile load, the whole cross section of the specimen is uniformly deformed. Thus, the relatively large foam cells in the foam core act as voids causing a reduction in the specific tensile properties.

4. Conclusions

This contribution summarizes the first results on foam injection molding of isosorbide-containing copolycarbonate (Bio-PC) as potential long-term alternative to bisphenol A based polycarbonate (PC). The structural foams were produced by using the low pressure foam injection molding method. Two weight reductions, namely, 5% and 10%, and two concentrations of the chemical blowing agent (CBA), namely, 2 wt.% and 3 wt.%, were investigated. The weight reduction has a higher influence on the foam properties than the CBA concentration investigated in this study. All specimens consist of a central foam core with top and bottom shell layers of nearly identical thickness. A higher weight reduction leads to a higher degree of foaming, which is expressed in terms of increasing thickness of the foam core and decreasing thickness of the compact surface layers. The specific tensile and specific bending properties of the injection-molded Bio-PC are on the same level as the nonfoamed Bio-PC parts or even slightly higher. These results are in good agreement with the theory where structural foams provide excellent stiffness to weight and strength to weight ratios.

Further studies will be conducted using state of the art foam injection molding technologies such as the core-back technique or gas counterpressure method to guarantee a constant foam structure in the cross section of the foamed tensile bar over flow length. Impact properties and stress relaxation properties of Bio-PC foams will also be investigated.

Conflicts of Interest

The authors declare that there are no conflicts of interest regarding the publication of this paper.

References

[1] A. Maćczak, M. Cyrkler, B. Bukowska, and J. Michałowicz, "Eryptosis-inducing activity of bisphenol A and its analogs in human red blood cells (in vitro study)," *Journal of Hazardous Materials*, vol. 307, pp. 328–335, 2016.

[2] E. B. Yalcin, S. R. Kulkarni, A. L. Slitt, and R. King, "Bisphenol A sulfonation is impaired in metabolic and liver disease," *Toxicology and Applied Pharmacology*, vol. 292, pp. 75–84, 2016.

[3] H. H. Le, E. M. Carlson, J. P. Chua, and S. M. Belcher, "Bisphenol A is released from polycarbonate drinking bottles and mimics the neurotoxic actions of estrogen in developing cerebellar neurons," *Toxicology Letters*, vol. 176, no. 2, pp. 149–156, 2008.

[4] L. N. Vandenberg, R. Hauser, M. Marcus, N. Olea, and W. V. Welshons, "Human exposure to bisphenol A (BPA)," *Reproductive Toxicology*, vol. 24, no. 2, pp. 139–177, 2007.

[5] J.-H. Kang, F. Kondo, and Y. Katayama, "Human exposure to bisphenol A," *Toxicology*, vol. 226, no. 2-3, pp. 79–89, 2006.

[6] H. Brouwer, R. D. Van de Grampel, and J. H. Kamps, "Isosorbide-based polycarbonates, method of making, and articles formed therefrom," in *Patent WO 2011/ A1*, 2011.

[7] H. Brouwer, R. D. Van de Grampel, and J. H. Kamps, "Blends of isosorbide-based copolycarbonate, method of making, and articles formed therefrom," in *Patent WO 2011/ A1*, 2011.

[8] B. A. J. Noordover, D. Haveman, R. Duchateau, R. A. T. M. Van Benthem, and C. E. Koning, "Chemistry, functionality, and coating performance of biobased copolycarbonates from 1,4:3,6-dianhydrohexitols," *Journal of Applied Polymer Science*, vol. 121, no. 3, pp. 1450–1463, 2011.

[9] C.-H. Lee, M. Kato, and A. Usuki, "Preparation and properties of bio-based polycarbonate/clay nanocomposites," *Journal of Materials Chemistry*, vol. 21, no. 19, pp. 6844–6847, 2011.

[10] C.-H. Lee, H. Takagi, H. Okamoto, and M. Kato, "Improving the mechanical properties of isosorbide copolycarbonates by varying the ratio of comonomers," *Journal of Applied Polymer Science*, vol. 127, no. 1, pp. 530–534, 2013.

[11] Q. Li, W. Zhu, C. Li et al., "A non-phosgene process to homopolycarbonate and copolycarbonates of isosorbide using dimethyl carbonate: Synthesis, characterization, and properties," *Journal of Polymer Science, Part A: Polymer Chemistry*, vol. 51, no. 6, pp. 1387–1397, 2013.

[12] T. Takashima, K. Yamaoka, and T. Ishikawa, Foam molded body. Patent application WO2013031924 A1, 2013.

[13] L. F. Sastre, *Effects of the foam morphology on the mechanical properties of structural polymer foams [Dissertation, thesis]*, RWTH Aachen, 2011.

[14] A. Cramer, *Analysis and optimization of the part properties in thermoplastic foam injection moulding [Dissertation, thesis]*, RWTH Aachen, 2008.

[15] W. Michaeli, C. Hopmann, and D. Obeloer, "Examinations on the influencing factors on the foamability using the profoam process," in *Proceedings of the 69th Annual Technical Conference of the Society of Plastics Engineers 2011, ANTEC 2011*, pp. 1551–1556, Boston, Mass, USA, May 2011.

[16] A. K. Bledzki, H. Kirschling, M. Rohleder, and A. Chate, "Correlation between injection moulding parameters, morphology and properties of microcellular polycarbonate foams," in *Proceedings of the 10th Rapra Blowing Agents and Foaming Processes*, Berlin, Germany, 2008.

[17] Mitsubishi Chemical Corporation: Durabio Material Properties, 2015, http://www.jimshin.com/UploadFiles/DURABIO-20151111v3Eng.pdf.

[18] DIN EN ISO 75-2:2013. Plastics - Determination of temperature of deflection under load - Part 2: Plastics and ebonite.

[19] N.N.: PALMAROLE MB.BA.16. Adeka Palmarole SAS, Mulhouse (France), 2008.

[20] V. Volpe and R. Pantani, "Foam injection molding of poly(lactic) acid: effect of back pressure on morphology and mechanical properties," *Journal of Applied Polymer Science*, vol. 132, pp. 42612–42619, 2015.

[21] F. J. Gómez-Gómez, D. Arencón, M. Á. Sánchez-Soto, and A. B. Martínez, "Influence of the injection moulding parameters on the microstructure and thermal properties of microcellular polyethylene terephthalate glycol foams," *Journal of Cellular Plastics*, vol. 49, no. 1, pp. 47–63, 2013.

[22] J. F. Gómez-Gómez, D. Arencón, M. A. Sánchez-Soto, and A. B. Martínez, "Influence of the injection-molding parameters on the cellular structure and thermo-mechanical properties of ethylene-propylene block copolymer foams," *Advances in Polymer Technology*, vol. 32, no. 1, pp. E692–E704, 2013.

[23] R. Pantani, V. Volpe, and G. Titomanlio, "Foam injection molding of poly(lactic acid) with environmentally friendly physical blowing agents," *Journal of Materials Processing Technology*, vol. 214, no. 12, pp. 3098–3107, 2014.

[24] V. K. Stokes, "Local stiffness-density correlations for polycarbonate structural foams," *Journal of Materials Science*, vol. 35, no. 1, pp. 159–178, 2000.

[25] J. Müller, A. Spörrer, and V. Altstädt, "Overmoulding of plane structural foamed parts with a second thermoplastic component," *Cell Polym*, vol. 31, pp. 223–240, 2012.

[26] N. Müller, *Spritzgegossene Integralschaumstrukturen mit ausgeprägter Dichtereduktion; Universität Erlangen-Nürnberg, [Dissertation, thesis]*, 2006, ISBN: 3-931864-25-1.

Hindawi
International Journal of Polymer Science
Volume 2017, Article ID 6192924, 12 pages
https://doi.org/10.1155/2017/6192924

Research Article

Genome Structure of *Bacillus cereus* tsu1 and Genes Involved in Cellulose Degradation and Poly-3-Hydroxybutyrate Synthesis

Hui Li,[1] Suping Zhou,[1] Terrance Johnson,[1] Koen Vercruysse,[1] Ouyang Lizhi,[1] Parthasarathy Ranganathan,[1] Nsoki Phambu,[1] Alexander J. Ropelewski,[2] and Theodore W. Thannhauser[3]

[1]*College of Agricultural, Human and Natural Sciences, Tennessee State University, Nashville, TN, USA*
[2]*Pittsburgh Supercomputing Center, Pittsburgh, PA, USA*
[3]*R.W. Holley Center for Agriculture and Health, Plant, Soil and Nutrition Research Unit, USDA, ARS, Ithaca, NY, USA*

Correspondence should be addressed to Suping Zhou; zsuping@tnstate.edu

Received 11 April 2017; Accepted 9 July 2017; Published 10 September 2017

Academic Editor: Raffaele Cucciniello

In previous work, we reported on the isolation and genome sequence analysis of *Bacillus cereus* strain tsu1 NCBI accession number JPYN00000000. The 36 scaffolds in the assembled tsu1 genome were all aligned with *B. cereus* B4264 genome with variations. Genes encoding for xylanase and cellulase and the cluster of genes in the poly-3-hydroxybutyrate (PHB) biosynthesis pathway were identified in tsu1 genome. The PHB accumulation in *B. cereus* tsu1 was initially identified using Sudan Black staining and then confirmed using high-performance liquid chromatography. Physical properties of these PHB extracts, when analyzed with Raman spectra and Fourier transform infrared spectroscopy, were found to be comparable to the standard compound. The five PHB genes in tsu1 *(phaA*, *phaB*, *phaR*, *phaC,* and *phaP)* were cloned and expressed with TOPO cloning, and the recombinant proteins were validated using peptide mapping of in-gel trypsin digestion followed by mass spectrometry analysis. The recombinant *E. coli* BL21 (DE3) (over)expressing *phaC* was found to accumulate PHB particles. The cellulolytic activity of tsu1 was detected using carboxymethylcellulose (CMC) plate Congo red assay and the shift towards low-molecular size forms of CMC revealed by gel permeation chromatography in CMC liquid culture and the identification of a cellulase in the secreted proteome.

1. Introduction

Since 1960s, driven by public concerns about environmental pollution by petroleum-derived plastics [1–6] and the escalating crude oil price due to the depletion of fossil oil resources, bioplastics have attracted widespread attention, as eco-friendly, biodegradable, and sustainable alternatives [4, 7]. Among all the biodegradable plastics, the polyhydroxyalkanoates (PHAs) family has unique properties like insolubility in water, biocompatibility, oxygen permeability, and ultraviolet (UV) resistance [8]. Because of these advantageous characteristics, comprehensive applications have been discovered and developed using PHAs-derived materials for packaging plastics, medical materials, chiral monomer, and others [9, 10]. Also stable engineered industrial microbial strains have been developed overexpressing genes in PHAs biosynthesis pathway with additional functions in regulating cellular metabolisms and stress resistance [11, 12]. The main member of the PHAs family is polyhydroxybutyrate (PHB). These polymers are accumulated intracellularly in PHB producing bacteria when cultured under carbon-excess and other nutrients-limited conditions [13].

A large number of microorganisms have been found to accumulate PHA as lipoidic storage materials in the cytosol [14–17]. These microorganisms are mainly divided into four classes (I, II, III, and IV) based on the type of PHA synthases, which are the key enzymes for PHA biosynthesis [18]. While a single subunit PhaC was found in class I (e.g., *Ralstonia eutropha*) and class II (e.g., *Pseudomonas aeruginosa*) synthases, two subunits, PhaE and PhaC, or PhaR and PhaC, were suggested to be used, respectively, in type III (e.g., *Allochromatium vinosum*) and type IV (e.g.,

Bacillus megaterium) synthases [19, 20]. Classes I, III, and IV synthases act on polymerase short-chain monomers (C3–C5) whereas class II synthase acts on medium-chain length (mcl) monomers (C6–C14). The most recently discovered class IV PHA synthase is only present in *Bacillus* sp. There is little information about the capacity of PHAs production and the substrate specificity of class IV PHA synthase.

The higher production cost compared to petroleum-derived plastics is the primary factor limiting practical application of these biodegradable polymer materials. The following two approaches have been taken to make the PHAs mass production economically feasible. Firstly, engineered *E. coli* strains producing higher yield of PHAs [21, 22] have been developed using recombinant DNA technology. The optimization of the intermediate substrates and fermentation conditions is the key step in utilizing this technology in large scale PHAs production. The second approach focuses on looking for cheaper raw materials. Carbon source for PHB production accounts for up to 50% of the total production costs. Agricultural byproducts like soybean cake [23], biogas methane [24], and palm oil [25] as inexpensive carbon feedstock exhibit a high potential to accelerate the commercialization of PHAs. Rapeseed (canola seed) oil is one of the preferred oil stocks for biodiesel production, partly because rapeseed produces more oil per unit of land area compared to other oil sources, such as soybeans [26]. Rapeseed cake is generated as a byproduct during the oil extraction process from rapeseed (canola seed), which will be tested in this study for its potential use as a substrate for PHB production. The physical properties of PHB products produced by the bacteria cultured in aqueous extracts of rapeseed cake were confirmed with Raman spectrum and Fourier transform infrared spectroscopy (FTIR).

Previously, we reported the genome sequence of *B. cereus* tsu1 [27]. This paper reports on the assembly of the genomic structure, and characterization of cellulolytic and PHB producing activities of this strain. PHB biosynthesis pathway genes were cloned and (over)expressed in *E. coli* BL21 (DE3) using TOPO cloning system. The recombinant bacterial clones were confirmed to accumulate PHB granules.

2. Materials and Methods

2.1. Genomic Structure Analysis. In previous research, draft genome of *Bacillus cereus* tsu1 was generated using next generation sequencing analysis [27]. To generate an alignment map of the assembled tsu1 scaffolds (GenBank: KN321896-KN321931) using MUMmer (version 3.0) on the galaxy working station (biou.psc.edu/galaxy) [28], the genome sequence of *B. cereus* B4264 (NCBI GenBank: CP001176.1) with the highest identity similarity clustered by phylogenetic COG (PCOGR) was downloaded from NCBI database and used as the reference (Figure S1 in Supplementary Material, available online at https://doi.org/10.1155/2017/6192924) [29]. Based on the alignment, 20 scaffolds of tsu1 were selected to construct a circular genomic map using DNAPlotter (version 10.2) [30, 31]. Localizations of annotated genes on these scaffolds and on the reconstructed circular map were described in Supplementary Table S1.

2.2. Cloning and Expression of PHB Pathway Genes. Putative genes encoding for enzymes in PHB biosynthesis pathways were identified in the annotated genome. Five genes were amplified from tsu1 genomic DNA using the polymerase chain reaction (PCR) with primers designed against the assembled gene sequences (see Supplementary Table S2). The PCR program was conducted as follows: after a hot start cycle of 94°C for 2 mins, there were 35 cycles of denaturation at 94°C for 30 s, annealing at a melting temperature (T_m) for each individual primer, and extension at 72°C for 1 min, followed by a final cycle of 72°C for 10 mins. PCR products were separated on a 0.7% agarose gel. After staining with ethidium bromide, DNA fragments were isolated from the gel, purified using Qiagen Gel Extraction Kit (Cat. number 28704), and then cloned into TOPO pET101 vector (Invitrogen, CA). Plasmid with gene inserts was sent to GenHunter (624 Grassmere Park Drive, St 17, Nashville, TN 37211) for Sanger sequencing with primers (T7 forward and reverse) that flank the insertion site. Recombinant plasmids carrying full-length gene sequences were transformed into *E. coli* BL21 (DE3) cells and expression of recombinant proteins was induced by the addition of isopropyl β-D-1-thiogalactopyranoside (IPTG) in LB broth to a final concentration of 0.5–0.8 mM. Cells were harvested after 4-hour induction by centrifugation. Cell pellets were frozen in liquid N_2 and stored at −20°C before conducting protein analyses.

For two-dimensional (2D) protein gel electrophoresis of the recombinant proteins, cell pellets were homogenized in 500 μL dissolution buffer consisting of 7 M urea, 2 M thiourea, and 4% (3-((3-cholamidopropyl) dimethylammonio)-1-propanesulfonate) (CHAPS). After centrifugation at 16,000 ×g, 4°C for 20 min, supernatants were collected. Protein concentration was assayed following the Bradford method using BSA as the standard protein (Bio-Rad). Supernatants containing 200 μg protein samples were mixed with 5 μM dithiothreitol (DTT), and 1.25 μL IPG buffer (pH 3–10 NL, GE Healthcare). Upon bringing to a final volume of 250 μl using DeStreak Rehydration Solution (GE), proteins were loaded onto 13 cm pH 3–10 NL Immobiline DryStrips (GE). After an overnight passive rehydration at room temperature, proteins were focused on an Ettan IPGphor II (Amersham Biosciences) until reaching 24,000 total voltage hours (VhT). Prior to second dimensional electrophoresis, IPG strips were reduced with 1% DTT and then neutralized in 2.5% iodoacetic acid (IAA). Both of these steps were performed in a buffer containing 50 mM Tris-HCl, pH 8.8, 6 M urea, 30% glycerol, and 2% SDS. The second dimensional separation was performed on 12.5% sodium dodecyl sulfate polyacrylamide gel electrophoresis (SDS-PAGE) gels (1 mm in thickness) using a SE 600 Ruby Standard Vertical Unit (GE). Gels were run at a constant current (20 mA/strip after an initial run of 10 mA/strip for 30 min) until the bromophenol front reached the bottom of the gel and then stained with Colloidal blue staining kit (Invitrogen, LC6025). Gel images were captured by scanning on a Typhoon 9400 variable mode imager (GE). Recombinant proteins were localized to the spots on 2D gels according to their hypothetical isoelectric point and molecular weight. These protein spots and spots at the same

position on gels loaded with proteins without IPTG induction were picked followed by in-gel tryptic digestion [32].

Tryptic peptide samples were reconstituted in 15 μL of 3% acetonitrile with 0.1% trifluoroacetic acid. Nano-liquid chromatography (LC) separation of tryptic peptides was performed using a nanoAcquity UPLC (Waters, Manchester), equipped with a Symmetry C_{18} 5 μm, 20 mm × 180 μm trapping column and a bonded ethyl hybrid C_{18} 1.7 μm, 15 cm × 75 μm analytical column (Waters). Mobile phase A consisted of water with 0.1% formic acid (FA) in water and mobile phase B acetonitrile with 0.1% FA. Samples, at 5 μL injection volume, were transferred to the trapping column at a flow rate of 7 μL/min 100% mobile phase A for 5 min. Following desalting and concentrating, the trapping column was eluted to the analytical column equilibrated with 2% mobile phase B at 300 nL/min. The eluent from the analytical column was delivered to a Xevo G2 Q-TOF mass spectrometer (MS) via a nanolockspray ion source (Waters). Data dependent acquisition (DDA) mode was used to obtain one 0.25 s MS survey scan. MS survey scans were acquired from m/z 300–1500, while product ion scans were acquired from m/z 50–2000. All data were acquired using MassLynx 4.1 SCN 862 (Waters). ProteinLynx Global Server v.2.5 was used to convert raw spectral data files for each injection into a peak list (.pkl format). To identify the matching sequences, the peak list from each protein spot was compared to theoretical tryptic digestion fragments of recombinant proteins.

2.3. Cellulolytic Activity Assay. Bacteria were cultured on the double-layered carboxymethyl cellulose sodium salt- (CMC-Na-) containing plates of which the bottom M9 minimal salt (11%; wt/vol) medium was overlaid with soft-agar containing 1% (wt/vol) CMC-Na (Sigma, St. Louis, MO). A cellulolytic bacterial strain *Paenibacillus polymyxa* 25A2^T [33–35] was obtained from the Bacillus Genetic Stock Center (Columbus, OH). In these assays, *P. polymyxa* 25A2^T was used as the positive control for testing cellulase activity and *E. coli* was used as the negative control. After incubation at 37 ± 1°C for 2 days, the CMC agar plates were stained with 0.1% Congo red solution following the method described previously [36, 37]. Plates were recorded for the formation of a clear zone around colonies, which indicates extracellular cellulolytic activity of the bacteria.

To further characterize the bacterial strain, a single colony of *B. cereus* tsu1 was inoculated into LB broth and incubated at 37°C under constant agitation at 200 rpm. Aliquots of an overnight culture of *B. cereus* tsu1 (1 mL) were inoculated into 10 mL M9 minimal salt medium supplemented with 1% (wt/vol) CMC-Na, and the control culture used the broth solution only. Cultures were continued under the same conditions. Two culture period treatments of 2 days and 6 days each with three replicates were conducted. At the end of each treatment period, bacterial cultures were centrifuged at 16,000 ×g for 1 min to collect supernatants. For gel permeation chromatography (GPC) assays of cellulose degradation, 2 mL of the supernatant from each sample was filtered through a 0.22 μm sterile filter (EMD Millipore, Massachusetts) and eluted into a clean 2 mL Eppendorf centrifuge tube. Gel permeation chromatography (GPC) analyses were performed on a Varian Prostar chromatography system (Walnut Creek, CA) equipped with a Waters Ultrahydrogel 2000 column (Milford, WA). Each 800 μL sample was diluted in 200 μL GPC solution (25 mM Na-acetate : methanol; 9 : 1). For each sample, 20 μL was injected each time. Analyses were performed at room temperature with a mobile phase consisting of 25 mM Na-acetate : methanol (9 : 1) at a flow rate of 0.75 mL/min and the UV/Vis absorbance was monitored at 210 nm using a photodiode array (PDA) detector. The collected data was used to compare the molecular weight changes between samples.

Supernatant collected for GPC analysis was mixed with acetone (1 : 3; v/v) followed by incubation overnight at −20°C for secreted protein precipitation. After centrifugation at 16,000 ×g for 1 min at 4°C, supernatant was removed. Protein pellets were air-dried, solubilized in a 1x Laemmli protein sample buffer (Biorad), and denatured by boiling for 5 min. Proteins were separated on a SDS-PAGE protein gel [27]. After staining with Coomassie Blue, protein bands were isolated from the gel and digested with trypsin [32], followed by liquid chromatography (LC)/mass spectrometry (MS) as described above. The generated peptides were searched against annotated protein database of *B. cereus* tsu1 (download from https://www.ncbi.nlm.nih.gov/protein/?term=bacillus±cereus±tsu1).

2.4. Poly-3-Hydroxybutyrate (PHB) Producing Activity Assay. The intracellular accumulation of PHB in *B. cereus* tsu1 was determined using the Sudan Black B staining method [38]. Bacterial smears were prepared using a four-day culture in LB broth and stained in a 0.3% Sudan Black stain solution (w/v) in 60% ethanol for 10 min. After rinsing with water, bacterial cells were counter-stained with 0.25% safranin for 1 min. Stained bacterial cells were observed and photographed under a Nikon Eclipse E600 Pol microscope (Japan).

Rapeseed cake samples (25 g) were soaked in 1 L water overnight under constant stirring. The supernatant was filtered through a 0.22 μm filtration system (EMD Millipore), and the rapeseed cake substrate (RCS) was used for bacterial cultures without any supplements. The total protein concentration in RCS was quantified using Bradford protein assay method. Bacterial cultures were incubated overnight in RCS and harvested by centrifugation at 3,220 ×g, 24°C, for 10 min. Cell pellets were oven-dried at 70°C to a constant weight and lysed by dispersing in 6% sodium hyperchlorite. After incubation at 37°C for 1 h, cell pellets were washed in 5 mL alcohol and then in 5 mL acetone. PHB was extracted by bathing the pellet in chloroform at 60°C for 1 h [39–41]. Then, chloroform was evaporated to obtain PHB crystals. PHB extracts were digested in 1 mL concentrated sulfuric acid at 100°C for 30 min, chilled to room temperature, and then diluted in 0.001 N H_2SO_4 to a final concentration of 0.8 mg/mL adipic acid, which are the 250x stock solutions.

The digested PHB-containing mixture was fractionated using high-performance liquid chromatography (HPLC) equipped with an Aminex HPX-87H ion-exclusion resin for organic acid analysis column (300 by 7.8 mm). The poly-(R)-3-hydroxybutyric acid (Sigma, MO) was used as the standard.

The crotonic acid formed from PHB acid digestion was detected by the absorbance peak at 210 nm [42] (Supplementary Table S4). Aliquots of PHB extracts were also analyzed on a spectrophotometer (SpectraMax M5, Molecular Devices, CA). The absorbance of the diluted sample (1 : 250) from acid digestion was measured at 235 nm. A standard curve was constructed using commercial PHB (Sigma) [43]. After confirmation of both methods giving nearly the same results, PHB content from bacterial batch culture was assayed using the spectrophotometric method (Supplementary Table S4).

2.5. Physical Structural Property Analysis of tsu1-PHB. An Xplora Raman spectrometer (LabRAM; HORIBA Jobin Yvon, NJ) was used with a NIR diode laser (λ = 785 nm, power = 2.5 mW) as an excitation source. The instrument settings were 100 μm confocal hole, 100 μm wide entrance slit, 600 gr/mm grating, and Olympus SLM Plan N 10x objective lens. Samples were mounted on a computer-controlled, high-precision x-y stage. An exposure time of 40 s and 5 accumulations were used to collect the spectra. Baseline fitting was performed using a LabSPEC 5 (HORIBA Jobin Yvon).

Samples were placed on the diamond crystal top plate of an attenuated total reflectance (ATR) accessory (Thermo Scientific Nicolet IS10, Thermo Scientific, Waltham, MA). Thumbscrew pressure was used to ensure that samples were in contact with the crystal. Data from sixteen scans were averaged over the spectral range of 4000 to 650 cm^{-1}, with a resolution of 4 cm^{-1}. Ambient air was used as the reference for the background spectrum before each sample. Between samples, the ATR crystal was cleaned using distilled water and dried. All spectra were recorded at room temperature. No data processing was performed on the raw spectra. The PHB standard (Sigma) was used as the reference for these analyses.

3. Results

3.1. Characterization of Microbial Genome of B. cereus tsu1. The 36 assembled scaffolds of *B. cereus* tsu1 were each aligned to a distinct region of the genome from *B. cereus* B4262 [27]. Regions of scaffolds 4, 6, and 15 did not match the reference genome (Figure 1). The circular genome map of *B. cereus* tsu1 (Figure 2) was constructed using the annotation of the assembled scaffolds in reference to *B. cereus* B4264 genome (see Table S1 in Supplementary Material).

3.2. Characterization of the PHB Biosynthesis Pathways. Six PHA synthesis related genes were located on scaffold 9. *phaR* (PHB synthase subunit), *phaB* (acetoacetyl-coA reductase), and *phaC* (PHB synthase subunit) are divergently transcribed as a tricistronic operon; *padR/phaQ* (transcription regulator), *phaP* (Phasin protein), and *phaJ* are transcribed in one direction. The *padR* gene is a PHB-responsive repressor controlling expression of *phaP* and *phaR*. Phasins are proteins that accumulate during PHA synthesis; they bind to PHA granules and promote further PHA synthesis. Gene *phaA* is located on a separate scaffold. The *phaJ* gene encodes for (R)-specific enoyl-CoA hydratase which is involved in fatty acid metabolism (Figure 3(a)). PHB granules were seen inside bacterial cells (Figure 3(b)). The five genes in PHB synthesis pathway *(phaA*, *phaB*, *phaC*, *phaP*, and *phaR)* were cloned. The size and sequences of these genes are identical to the predicted gene sequences in the annotated genome sequences (Figure 3(c)). The recombinant proteins matched the predicted proteins in both molecular size and isoelectric points (pI value). Furthermore, mass spectrometry (MS) analysis of the tryptic digests of recombinant proteins showed that the peptide coverage ratio (identified/predicted) is 70%, 95%, 82%, 78%, and 100% for PhaA, PhaB, PhaC, PhaR, and PhaP, respectively (Figure 3(d); see Table S3 in the Supplementary Material). When the *phaC*-(over)expressing recombinant *E. coli* cells were cultured overnight under the IPTG induction condition, PHB granules were observed in Sudan Black stained cells (Figure 3(e)). These results confirmed that the PHB genes from *B. cereus* tsu1 can drive biosynthesis of the polymer in recombinant *E. coli* clones.

3.3. Characterization of Cellulolytic Pathways. The conversion of cellulose into glucose consists of two steps. During the first step, beta-1,4 glucanase breaks the glucosidic linkage to cellobiose. Subsequently, this beta-1,4 glucosidic linkage of cellobiose is broken down by beta-glucosidase to produce glucose. Both endo-beta-glucanase and beta-glucosidase were found in the tsu1 genome. One xylanase gene for the degradation of hemicellulose was identified in the genome (Figure 4(a)).

The Congo red test showed that the *B. cereus* tsu1 colonies formed a clear distinct yellow halo, which is an indication of extracellular cellulase enzymes produced by the bacterium. The same reaction was observed in *Paenibacillus polymyxa*, but not in *E. coli* colonies (Figure 4(b)). Gel permeation chromatography (GPC), also known as size-exclusion chromatography, is often used to characterize the molar mass distribution of natural and synthetic polymers. Various incubation-period products from CMC-containing substrates after culturing *B. cereus* tsu1 were compared. With longer treatment time (in 6-day sample), a lower intensity of high molecular weight component (between 11.5 and 12.5 min) was observed whereas a higher peak intensity of small molecules (between 13 and 14 min) emerged. The clear shift to longer retention times of the bacterial-treated products relative to the untreated products clearly demonstrates CMC degradation into smaller molecules in the bacterial-treated samples (Figure 4(c)).

The bacterial secreted proteins were separated into five major bands on SDS-PAGE gels (Supplementary Figure S2). Among all the proteins identified by searching the tryptic digestion peptides against the *B. cereus* tsu1 protein dataset annotated by prokaryotic genome annotation pipeline, one endo-glucanase matching (GenBank ID: KGT43479.1) was identified (Table S5 in the Supplementary Material) [27].

Conclusively, the Congo red test, GPC analysis, and secreted proteome analysis all supported the extracellular cellulase activity of *B. cereus* tsu1 which concurs with its genome structure.

3.4. PHB Production Efficiency of Bacillus cereus tsu1 on Rapeseed Cake Substrate (RCS). In this study, bacterial cell cultures were grown in RCS without any additional materials.

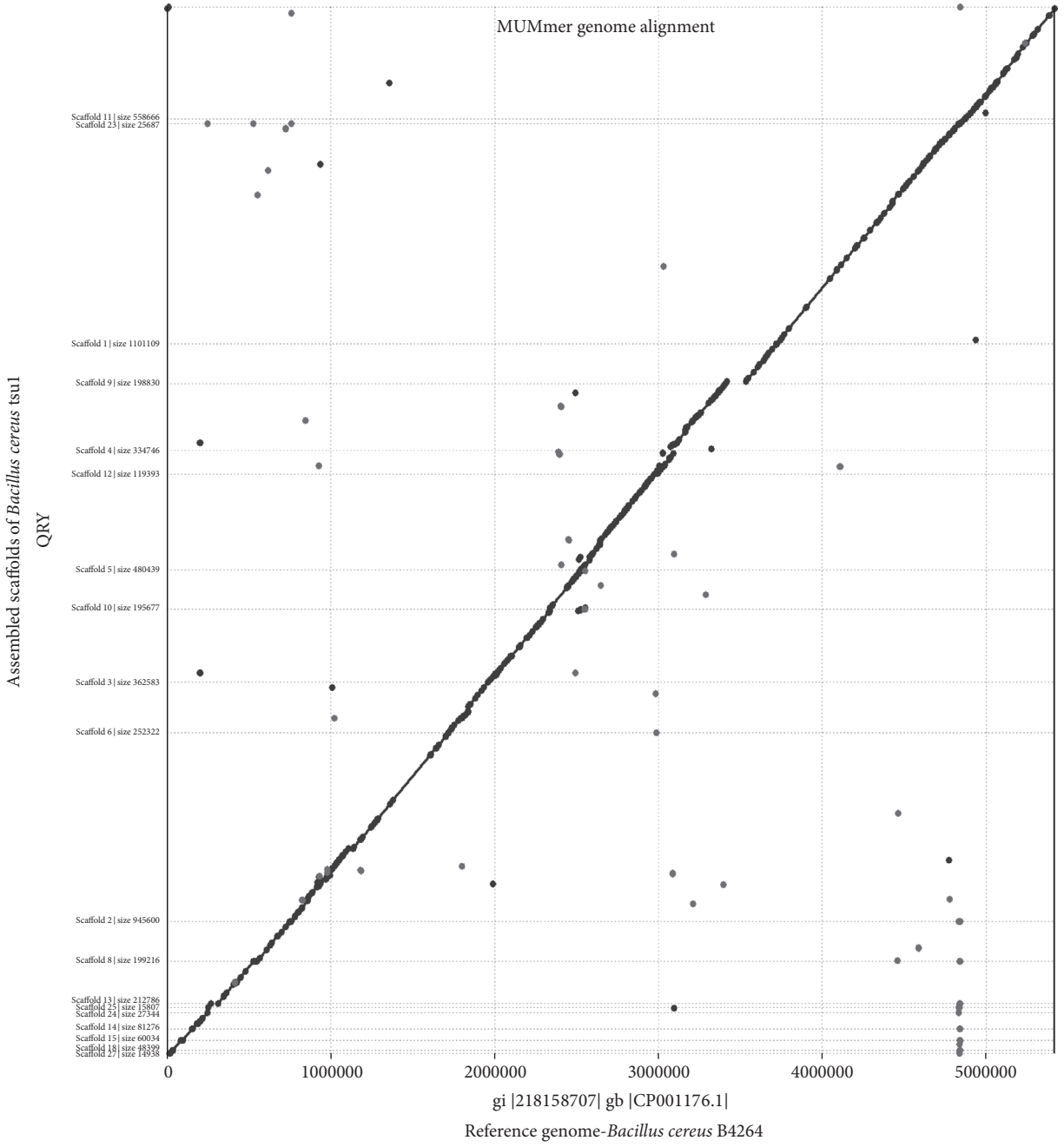

Figure 1: Alignment of assembled scaffolds from *Bacillus cereus* tsu1 with the reference genome of *B. cereus* B4262 using MUMmer on biou.psc.edu/galaxy.

After overnight batch culture, the cell dry weight reached 540–575 mg/L, which produced a 13-14% PHB content per cell biomass (Table 1).

3.5. Physical Structural Properties of PHB. PHB extracts from tsu1 cultures in RCS were compared to poly-(R)-3-hydroxybutyric acid (Sigma, MO) as the standard. The spectroscopic data of Raman and FTIR were used to determine the physical properties of PHB polymers [8]. The Raman spectra from regions 300–2200 cm^{-1} and from regions 2200–3000 cm^{-1} showed that the tsu1 PHB and the standard were both crystalline. The presence of sharp and narrow peaks in the Raman spectra at the major positions 434 and 841 cm^{-1} also indicated the crystallinity of the tsu1 PHB. However, peaks corresponding to C=O stretching and to CH_3 stretching occur at 1731.2 and 2935.4 cm^{-1}, respectively, showing that there were some amorphous regions in the tsu1 PHB extracts (see Table S6 in the Supplementary Material). Both Raman and FTIR spectra of tsu1 PHB extracts matched those from the standard (Figure 5). The mean square deviation is 3.7

Table 1: *Bacillus cereus* tsu1 cell propagation and PHB production on RCS substrate[†].

Items	Batch 1	Batch 2	Average
Cell biomass (mg/L culture)	575.17 ± 56.02	540.89 ± 18.43	558.03 ± 28.58
PHB mixture extract (mg/L)[a]	139.44 ± 14.18	112.78 ± 12.54	126.11 ± 9.88
Pure PHB content (mg/L)[b]	74.66 ± 8.54	80.61 ± 10.32	77.64 ± 6.45
PHB content in cell biomass (%)[c]	13%	14.9%	13.95%
PHB conversion efficiency of rape seed cake (g/kg)	2.99	3.22	3.10

[†]*Bacillus cereus* tsu1 was batch cultured for 24 hours in one-liter bottle containing (25 g/L) aqueous extracts of RCS. Two independent experiments each containing six replicates were conducted; [a]PHB was extracted from dried bacterial cells. Six replicates were conducted; [b]PHB content in crude extracts was determined by spectrophotometry analysis; [c]PHB content measured using the spectrometric method is similar to the HPLC method (37).

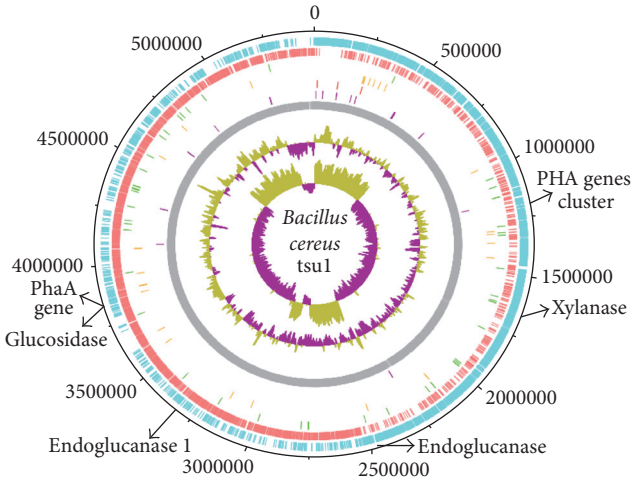

Figure 2: Circular genome map of *Bacillus cereus* tsu1. The map was generated using DNAPlotter (version 10.2) based on annotation data of the assembled scaffolds of *B. cereus* tsu1 (NCBI accession KN321896-KN321931). The draft genome sequence is 5.81 Mb, and 5.4 Mb was aligned to create the circular genome map. Genes in PHB biosynthesis pathway phaA, phaR, phaB, phaC, phaQ, phaP, and phaJ and cellulase genes for endoglucanase, glucosidase, and hemicellulase gene xylanase were indicated on the genome map. Locations of genes on the assembled scaffolds and their linkage to the circular map were provided in Supplementary Table S1.

to 7.1 cm^{-1}, which is within the range of discrepancy between Raman and FTIR spectra of PHB reported in previous studies [44–46].

4. Discussions

In this paper, we are reporting the characterization of *B. cereus* tsu1, a bacterium that has the ability to produce PHB polymer and degrade cellulose. In order to understand the molecular basis for these biochemical activities and evaluate the biotechnological potential of this bacterial strain, we proceeded to analyze its genome structure and test its extracellular cellulase and PHB producing ability. Analysis of cellulose degradation activity using GPC and Congo red staining methods suggests that the bacteria can degrade cellulose into smaller molecular products, but the end-products of degradation were not identified [47–49]. Cellulose has been used as a low-cost substrate in PHAs fermentation studies. Gao et al. reported that the successful transformation of cellulase and PHB synthesis pathway genes into *E. coli* resulted in the production of PHB directly from cellulose; however, the conversion efficiency and PHB yield were very low [50, 51]. In our study, the annotated *B. cereus* tsu1 genome contained cellulase (GenBank ID: KGT42715.1; KGT43479.1) and xylanase (GenBank ID: KGT44235.1) genes. A cellulase was also identified in secreted proteomes in CMC liquid culture. In addition, genes in each step of PHB biosynthesis pathway were identified in *B. cereus* tsu1 genome including several *phaA* genes and a gene cluster with six PHA genes: *phaR* (PHB synthase subunit), *phaB* (acetoacetyl-coA reductase), *phaC* (PHB synthase), and a *phaJ,* the downstream *phaP* (Phasin protein), and the *padR* (PhaQ transcription regulator) (see Table S7 in the Supplementary Material).

Based on the PHB gene cluster, *B. cereus* tsu1 should express class IV PHA synthase, which is composed of subunits PhaC and PhaR. PhaC is the key enzyme involved in the polymerization process; it determines the types of monomers (R-hydroxyacyl-CoAs) incorporated into the PHA polymer chain based on the enzyme's substrate specificity, as well as controlling PHA chain length and polydispersity. Previous researches consistently indicate that class IV synthases favor short-chain-length monomers such as 3-hydroxybutyrate (C4) and 3-hydroxyvalerate (C5) for polymerization, but it can also polymerize some unusual monomers as minor components [52–54]. There is an increasing interest in class IV PHA synthase, due to the possible alcoholysis activity as an inherent feature among these enzymes [55]. This alcoholysis reaction is useful not only for the regulation of PHA molecular weight but also for the modification of the PHA carboxy terminus, which can be manipulated to produce more promising PHA materials with more beneficial properties [56, 57]. The discovery of these genes has increased our understanding of the PHB synthesis pathway because they have a specific role that would affect the efficiency and the types of PHB polymers being synthesized. These genes found in *B. cereus* tsu1 genome related to PHB synthesis and cellulose degradation will contribute in building a library of information for constructing more efficient PHB fermenter hosts in future work.

The high cost associated with the production of PHAs remains a major barrier for large scale use of bioplastics [58]. In order to produce PHAs economically, a reliable and economical supply of raw material is essential; meanwhile, new bacterial strains and genes need to be discovered in order

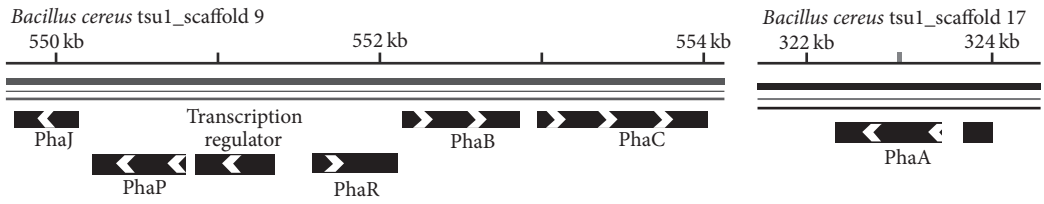

(a) Loci of genes in PHB biosynthesis pathways

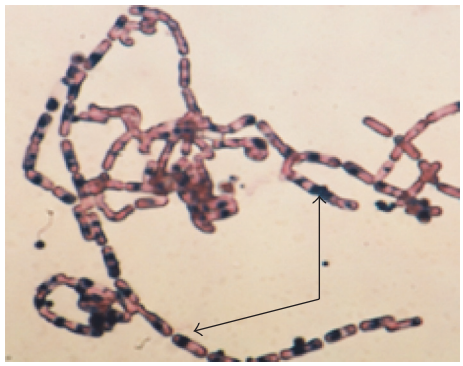

(b) Accumulation of PHB granules (indicated by arrows) in *Bacillus cereus* tsu1

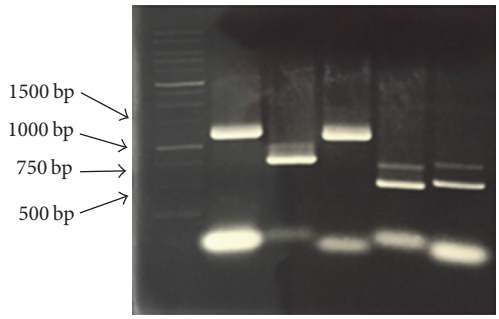

(c) PCR cloning of PHB genes

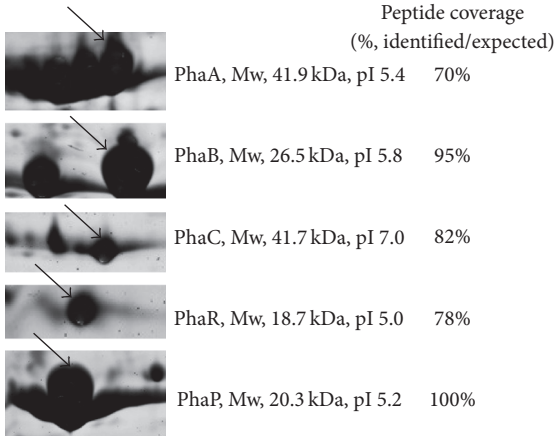

(d) Recombinant PHB proteins (indicated by arrows) on 2D gels and confirmation using peptide mapping

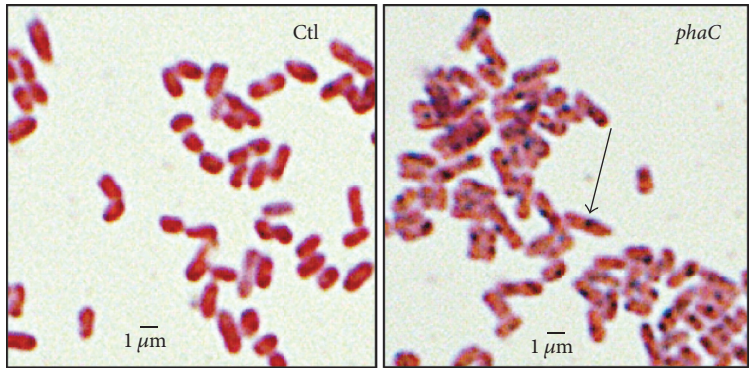

(e) *E. coli* with *phaC* genes displayed PHB producing activity

Figure 3: Characterization of genes in the poly-3-hydroxybutyrate (PHB) biosynthesis pathways in *Bacillus cereus* tsu1. (a) Genes in the PHB biosynthesis pathways: *phaR*, *phaB*, and *phaC* on the same operon, *phaJ*, *phaP*, and *phaQ* on reverse direction, and *phaA* located on a separate locus. (b) Sudan Black staining of *B. cereus* tsu1 showing accumulation of PHB granules in the bacterial cells. (c) The PHB gene fragments amplified from the genomic DNA of *Bacillus cereus* tsu1 using polymerase chain reaction (PCR) and separated on a 0.7% agarose gel. (d) Two-dimensional gel electrophoresis of recombinant proteins of PhaA, PhaB, PhaC, PhaR, and PhaP. The PCR amplified gene fragments showing identical sequence matches with the PHB synthesis genes were cloned into TOPO pET101 vector (Invitrogen, CA); recombinant proteins were expressed in DE3 cells. Recombinant proteins were separated on 2D gels. Protein spot with matching molecular size and isoelectric point (pI) of each predicted protein was picked from the gel. Protein identity was confirmed using the peptide fingerprinting (70–100% coverage with identical predicated peptides) using mass spectrometry analysis of tryptic digests of these proteins. (e) Sudan Black staining of the recombinant *E. coli* (over)expressing phaC gene showing intracellular PHB granules; *E. coli* transformed with the empty vector had no PHB accumulation. The arrow refers to the black spots inside of the bacterial cell, which is the PHB accumulation stained with Sudan Black.

to use a wider variety of substrates [59, 60]. The aqueous extract of rapeseed cake (RCS) can be a promising raw material for PHB production. In this study, PHB content was 13-14% per cell dry weight in overnight batch culture in RCS. Taking into consideration that no other nutrients were added in RCS, the bacterial growth performance and PHB content are relatively lower than other well-developed nutrient substrates. Meanwhile, in this batch culture for PHB production, no pH buffer solution was added, which may limit the biomass production, and further limit the PHB production

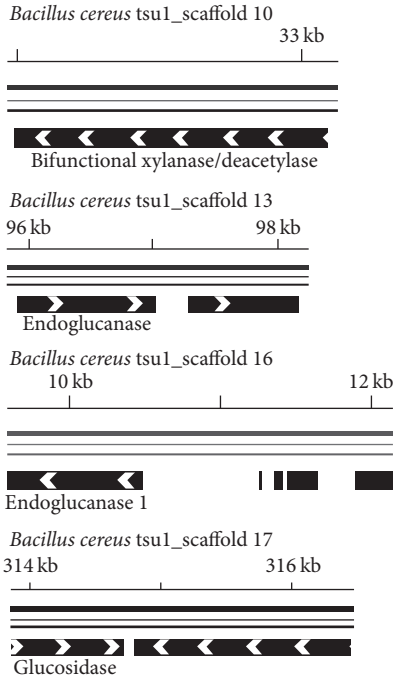

(a) Gene sequences

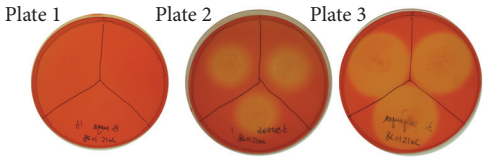

(b) Congo Red staining assay on CMC plates. Plate 1, *Escherichia coli (negative control)*; Plate 2, *Bacillus cereus* tsu1; Plate 3, *Paenibacillus polymyxa (positive control)*

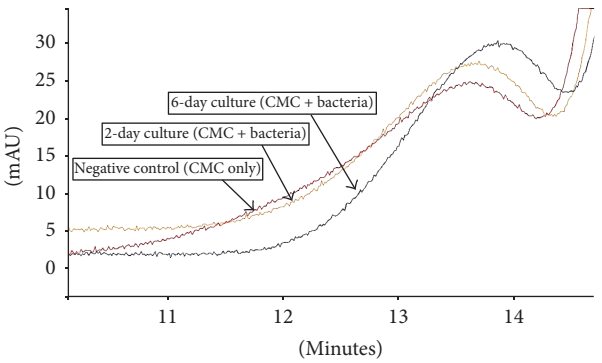

(c) Gel permeation chromatography assay of products derived from CMC cultured with *Bacillus cereus* tsu1

FIGURE 4: Characterization of cellulase gene and enzymatic activity of *Bacillus cereus* tsu1. (a) Cellulase genes annotated in the *Bacillus cereus* tsu1 genome. (b) Congo red plate assay of cellulase activity. Bacteria were cultured on the double-layered carboxymethylcellulose sodium salt- (CMC-Na-) containing plates of which the bottom M9 minimal salt (11%; wt/vol) agar medium was overlaid with soft-agar containing 1% (wt/vol) CMC-Na (Sigma, St. Louis, MO). Plates from two-day incubation at 37°C were stained with 0.1% Congo red. The yellowish halo around the bacterial colony indicates degradation of CMC. Plate 1, *E. coli* showing no CMC degradation activity (negative control); Plate 2, *B. cereus* tsu1; Plate 3, *Paenibacillus polymyxa* 25A2^T with CMC degradation activity (a positive control of cellulolytic bacterial strain from the Bacillus Genetic Stock Center, Columbus, OH). (c) Gel permeation assay of CMC derived products after incubation with *B. cereus* tsu1 for 2 days and 6 days. The right shifts of the peaks indicate that the CMC derived molecules after the digestion with *B. cereus* tsu1 were smaller in size and therefore they were eluted at a delayed time-frame than the original CMC. These results confirmed the extracellular cellulase activity of the bacterial strain.

[61]. RCS was estimated to have 8.98 g/L crude proteins, and it also contained all the essential amino acids for bacterial growth, and some α- and γ-amino-butyric acid (AIB, GABA) (see Figure S3 in Supplementary Material). Some of these amino acids can potentially be converted into PHB through various alternative pathways (see Figure S4 in Supplementary Material). In a previous study [62], GABA was reported as an alternative route of catabolism in *Saccharomyces cerevisiae*. It is involved in the conversion of GABA into succinate-semialdehyde (SSA) by 4-aminobutyrate aminotransferase; meanwhile, glutamate can be converted into GABA by glutamate decarboxylase. In 2007, Valappil et al. reported that *B. cereus* 14579 genome contained all the alternative pathway genes involved for the conversion of succinyl-CoA from

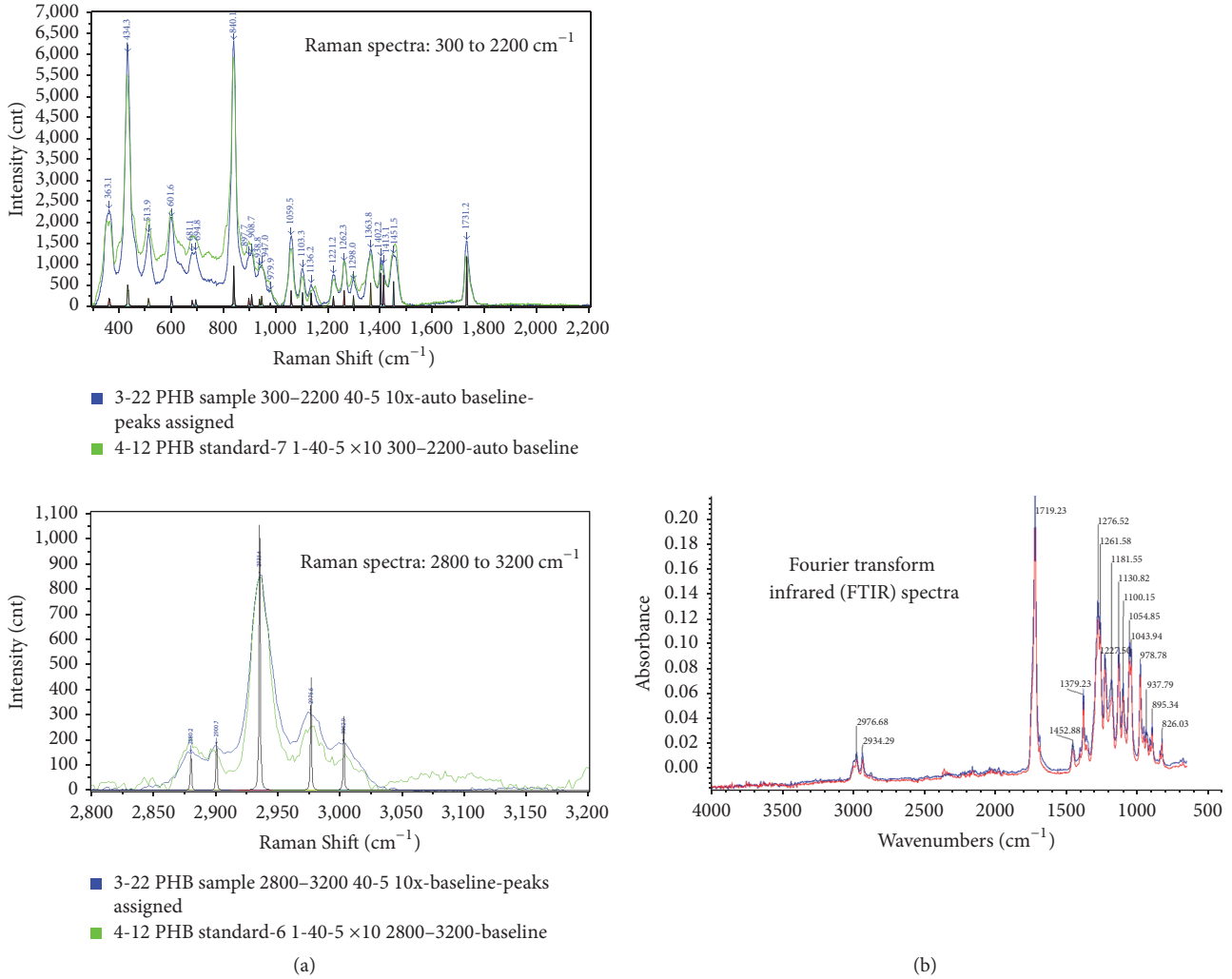

FIGURE 5: Physical properties of polyhydroxybutyrate PHB produced by *Bacillus cereus* tsu1 on rapeseed cake substrate (RCS). The PHB standard (Sigma) was used as the reference for these analyses. Raman spectra of PHB produced by *B. cereus* tsu1 and standard (a). FTIR spectra of PHB produced by *B. cereus* tsu1 and standard (b).

TCA cycle into P4HB/PH3B/P(3HB-co-4HB) [63]. P(3HB-co-4HB)-like copolymer was found in *B. cereus* SPV. In this alternative pathway, succinyl-CoA is first converted to SSA by SSA dehydrogenase followed by reduction of SSA into GABA by 4-hydroxybutyrate dehydrogenase. GABA is activated to 4-hydroxybutyryl-CoA by a Co-A transferase enzyme. The R-4-hydroxybutyryl-CoA and/or R-3-hydroxybutyryl-CoA are then to be polymerized to form P4HB/PH3B/P(3HB-co-4HB) by PHB synthase.

The (R)-specific enoyl-CoA hydratase/MaoC-like protein (PhaJ) is a monomer supplying enzyme from fatty acid β-oxidation. Tajima et al. demonstrated that PhaJ may make a channeling route from β-oxidation to PHA biosynthesis and PhaC synthases from *B. cereus* and its relatives have the ability to incorporate both scl and mcl PHAs [64]. This alternative metabolic pathway was confirmed [65] in a recombinant *E. coli* strain which utilizes two substrate-specific enoyl-CoA hydratases, R-hydratase (PhaJ) and S-hydratase (FadB). In these bacterial strains, the PhaJ works in coordination with S-specific hydratases to provide (R)-3HB-CoA for PHA synthesis from crotonyl-CoA. In 2012, Cai reported that *B. cereus* may be another example harboring *phaJ* in the pha locus [66]. In *B. cereus* tsu1, the *phaJ* gene encoding R-specific enoyl-CoA hydratase (GenBank ID: KGT44860.1) may function coordinately with an acyl-CoA dehydrogenase to form (R)-3HB-CoA via crotonyl-CoA intermediate which is derived from fatty acid β-oxidation (see Figure S4 in Supplementary Material). Genes in this pathway were found in the genome of *B. cereus* tsu1. The production of PHB from RCS may support this alternative catabolism, which may shed new light on the PHB biosynthesis pathway and open up new opportunities for its industrial applications.

Disclosure

Mention of trade names or commercial products in this publication is solely for the purpose of providing specific information and does not imply recommendation or

endorsement by the U.S. Department of Agriculture. The funders of the project had no role in study design, data collection and interpretation, or the decision to submit the work for publication.

Conflicts of Interest

The authors declare that they have no conflicts of interest.

Acknowledgments

The authors wish to thank Dr. Charles Lee at USDA/ARS for his advice on gene cloning strategies, Dr. Peter A. Schweitzer at Cornell University Institute of Biotechnology for sequencing the bacterial genome, Dr. Roger Sauve for reviewing this manuscript, Dr. Korsi Dumenyo for suggestions of bacterial cellulase activity assay, Dr. Fur-Chi Chen, Kevin Howe, and Tara Fish for protein analysis, and Dr. Jason P. de Koff for kindly providing canola seed cake materials and Mrs. Sarabjit Bhatti for assisting in the experiments. Amino acid analysis of rapeseed cake was conducted by Dr. John Schulze, Molecular Structure Facility at University of California at Davis. PHB analysis using HPLC was conducted by Dr. Allison Pieja at Mango Materials Co., California, USA.

References

[1] J. Hammer, M. H. S. Kraak, and J. R. Parsons, "Plastics in the marine environment: the dark side of a modern gift," *Reviews of Environmental Contamination and Toxicology*, vol. 220, pp. 1–44, 2012.

[2] M. Claessens, L. Van Cauwenberghe, M. B. Vandegehuchte, and C. R. Janssen, "New techniques for the detection of microplastics in sediments and field collected organisms," *Marine Pollution Bulletin*, vol. 70, no. 1-2, pp. 227–233, 2013.

[3] L. Van Cauwenberghe, A. Vanreusel, J. Mees, and C. R. Janssen, "Microplastic pollution in deep-sea sediments," *Environmental Pollution*, vol. 182, pp. 495–499, 2013.

[4] A. L. Lusher, A. Burke, I. O'Connor, and R. Officer, "Microplastic pollution in the Northeast Atlantic Ocean: validated and opportunistic sampling," *Marine Pollution Bulletin*, vol. 88, no. 1-2, pp. 325–333, 2014.

[5] L. C. Woodall, A. Sanchez-Vidal, M. Canals et al., "The deep sea is a major sink for microplastic debris," *Royal Society Open Science*, vol. 1, no. 4, Article ID 140317, 2014.

[6] D. Eerkes-Medrano, R. C. Thompson, and D. C. Aldridge, "Microplastics in freshwater systems: a review of the emerging threats, identification of knowledge gaps and prioritisation of research needs," *Water Research*, vol. 75, pp. 63–82, 2015.

[7] R. Jain and A. Tiwari, "Biosynthesis of planet friendly bioplastics using renewable carbon source," *Journal of Environmental Health Science and Engineering*, vol. 13, no. 1, article 11, 2015.

[8] S. Muhammadi, M. Afzal, and S. Hameed, "Bacterial polyhydroxyalkanoates-eco-friendly next generation plastic: production, biocompatibility, biodegradation, physical properties and applications," *Green Chemistry Letters and Reviews*, vol. 8, no. 3-4, pp. 56–77, 2015.

[9] S. J. Park, S. Y. Lee, and Y. Lee, "Biosynthesis of R-3-hydroxyalkanoic acids by metabolically engineered *Escherichia coli*," *Applied Biochemistry and Biotechnology*, vol. 113-116, pp. 373–379, 2004.

[10] G.-Q. Chen, "A microbial polyhydroxyalkanoates (PHA) based bio- and materials industry," *Chemical Society Reviews*, vol. 38, no. 8, pp. 2434–2446, 2009.

[11] J. Zhang, N. Hao, and G.-Q. Chen, "Effect of expressing polyhydroxybutyrate synthesis genes (*phbCAB*) in *Streptococcus zooepidemicus* on production of lactic acid and hyaluronic acid," *Applied Microbiology and Biotechnology*, vol. 71, no. 2, pp. 222–227, 2006.

[12] P. Gu, J. Kang, F. Yang, Q. Wang, Q. Liang, and Q. Qi, "The improved L-tryptophan production in recombinant *Escherichia coli* by expressing the polyhydroxybutyrate synthesis pathway," *Applied Microbiology and Biotechnology*, vol. 97, no. 9, pp. 4121–4127, 2013.

[13] B. S. Saharan, A. Grewal, and P. Kumar, "Biotechnological production of polyhydroxyalkanoates: a review on trends and latest developments," *Chinese Journal of Biology*, vol. 2014, Article ID 802984, 18 pages, 2014.

[14] C.-S. Ha and W.-J. Cho, "Miscibility, properties, and biodegradability of microbial polyester containing blends," *Progress in Polymer Science*, vol. 27, no. 4, pp. 759–809, 2002.

[15] Y. K. Leong, P. L. Show, C. W. Ooi, T. C. Ling, and J. C.-W. Lan, "Current trends in polyhydroxyalkanoates (PHAs) biosynthesis: insights from the recombinant *Escherichia coli*," *Journal of Biotechnology*, vol. 180, pp. 52–65, 2014.

[16] V. Urtuvia, P. Villegas, M. González, and M. Seeger, "Bacterial production of the biodegradable plastics polyhydroxyalkanoates," *International Journal of Biological Macromolecules*, vol. 70, pp. 208–213, 2014.

[17] P. Kumar, S. Ray, S. K. S. Patel, J.-K. Lee, and V. C. Kalia, "Bioconversion of crude glycerol to polyhydroxyalkanoate by *Bacillus thuringiensis* under non-limiting nitrogen conditions," *International Journal of Biological Macromolecules*, vol. 78, pp. 9–16, 2015.

[18] B. H. A. Rehm, "Polyester synthases: natural catalysts for plastics," *Biochemical Journal*, vol. 376, no. 1, pp. 15–33, 2003.

[19] C. Yang, W. Zhang, R. Liu et al., "Analysis of polyhydroxyalkanoate (PHA) synthase gene and PHA-producing bacteria in activated sludge that produces PHA containing 3-hydroxydodecanoate," *FEMS Microbiology Letters*, vol. 346, no. 1, pp. 56–64, 2013.

[20] K. Ushimaru, Y. Motoda, K. Numata, and T. Tsuge, "Phasin proteins activate aeromonas caviae polyhydroxyalkanoate (PHA) synthase but not *Ralstonia eutropha* PHA synthase," *Applied and Environmental Microbiology*, vol. 80, no. 9, pp. 2867–2873, 2014.

[21] P. I. Nikel, A. De Almeida, E. C. Melillo, M. A. Galvagno, and M. J. Pettinari, "New recombinant *Escherichia coli* strain tailored for the production of poly(3-hydroxybutyrate) from agroindustrial by-products," *Applied and Environmental Microbiology*, vol. 72, no. 6, pp. 3949–3954, 2006.

[22] Z. Lin, Y. Zhang, Q. Yuan et al., "Metabolic engineering of *Escherichia coli* for poly(3-hydroxybutyrate) production via threonine bypass," *Microbial Cell Factories*, vol. 14, no. 185, 2015.

[23] F. C. Oliveira, M. L. Dias, L. R. Castilho, and D. M. G. Freire, "Characterization of poly(3-hydroxybutyrate) produced by *Cupriavidus necator* in solid-state fermentation," *Bioresource Technology*, vol. 98, no. 3, pp. 633–638, 2007.

[24] C. S. Criddle, S. L. Billington, and C. W. Frank, "Renewable Bioplastics and Biocomposites from Biogas Methane and Waste-Derived Feedstock: Development of Enabling Technology, Life

Cycle Assessment, and Analysis of Costs," Tech. Rep., California Department of Resources Recycling and Recovery, Sacramento, Claif, USA, 2014.

[25] S. L. Riedel, J. Bader, C. J. Brigham et al., "Production of poly(3-hydroxybutyrate-co-3-hydroxyhexanoate) by *Ralstonia eutropha* in high cell density palm oil fermentations," *Biotechnology and Bioengineering*, vol. 109, no. 1, pp. 74–83, 2012.

[26] M. Frier and G. Roth, *Canola or Rapeseed Production in Pennsylvania*, Department of Crop and Soil Sciences, Pennsylvania, Pa, USA, 2006.

[27] H. Li, S. Zhou, T. Johnson, K. Vercruysse, A. J. Ropelewski, and T. W. Thannhauser, "Draft genome sequence of new *Bacillus cereus* strain tsu1," *Genome Announcements*, vol. 2, no. 6, article 2014, 2014.

[28] E. Afgan, D. Baker, M. van den Beek et al., "The Galaxy platform for accessible, reproducible and collaborative biomedical analyses: 2016 update," *Nucleic Acids Research*, vol. 44, no. W1, pp. W3–W10, 2016.

[29] R. L. Tatusov, D. A. Natale, I. V. Garkavtsev et al., "The COG database: new developments in phylogenetic classification of proteins from complete genomes," *Nucleic Acids Research*, vol. 29, no. 1, pp. 22–28, 2001.

[30] T. Carver, N. Thomson, A. Bleasby, M. Berriman, and J. Parkhill, "DNAPlotter: circular and linear interactive genome visualization," *Bioinformatics*, vol. 25, no. 1, pp. 119-120, 2009.

[31] D.-H. Lee, H. R. Kim, H. Y. Chung et al., "Complete genome sequence of *Bacillus cereus* FORC_005, a food-borne pathogen from the soy sauce braised fish-cake with quail-egg," *Standards in Genomic Sciences*, vol. 10, no. 1, article 97, 2015.

[32] S. Zhou, R. Sauvé, and T. W. Thannhauser, "Proteome changes induced by aluminium stress in tomato roots," *Journal of Experimental Botany*, vol. 60, no. 6, pp. 1849–1857, 2009.

[33] M. I. Alshelmani, T. C. Loh, H. L. Foo, W. H. Lau, and A. Q. Sazili, "Characterization of cellulolytic bacterial cultures grown in different substrates," *The Scientific World Journal*, vol. 2013, Article ID 689235, 6 pages, 2013.

[34] E. B. Górska, U. Jankiewicz, J. Dobrzyński, S. Russel, S. Pietkiewicz et al., "Degradation and colonization of cellulose by Diazotrophic Strains of *Paenibacillus polymyxa* isolated from soil," *Journal of Bioremediation & Biodegradation*, vol. 6, no. 2, 2015.

[35] R. López-Mondéjar, D. Zühlke, T. Větrovský, D. Becher, K. Riedel, and P. Baldrian, "Decoding the complete arsenal for cellulose and hemicellulose deconstruction in the highly efficient cellulose decomposer *Paenibacillus* O199," *Biotechnology for Biofuels*, vol. 9, no. 1, article 104, 2016.

[36] R. M. Teather and P. J. Wood, "Use of Congo red-polysaccharide interactions in enumeration and characterization of cellulolytic bacteria from the bovine rumen," *Applied and Environmental Microbiology*, vol. 43, no. 4, pp. 777–780, 1982.

[37] A. Sazci, K. Erenler, and A. Radford, "Detection of cellulolytic fungi by using Congo red as an indicator: a comparative study with the dinitrosalicyclic acid reagent method," *Journal of Applied Bacteriology*, vol. 61, no. 6, pp. 559–562, 1986.

[38] Y.-H. Wei, W.-C. Chen, C.-K. Huang et al., "Screening and evaluation of polyhydroxybutyrate-producing strains from indigenous isolate *Cupriavidus taiwanensis* strains," *International Journal of Molecular Sciences*, vol. 12, no. 1, pp. 252–265, 2011.

[39] S. K. Hahn, Y. K. Chang, B. S. Kim, and H. N. Chang, "Optimization of microbial poly(3-hydroxybutyrate) recover using dispersions of sodium hypochlorite solution and chloroform," *Biotechnology and Bioengineering*, vol. 44, no. 2, pp. 256–261, 1994.

[40] B. Aslim, F. Çalişkan, Y. Beyatli, and U. Gündüz, "Poly-β-hydroxybutyrate production by lactic acid bacteria," *FEMS Microbiology Letters*, vol. 159, no. 2, pp. 293–297, 1998.

[41] P. Singh and N. Parma, "Isolation and characterization of two novel polyhydroxybutyrate (PHB)-producing bacteria," *African Journal of Biotechnology*, vol. 10, no. 24, pp. 4907–4919, 2011.

[42] D. B. Karr, J. K. Waters, and D. W. Emerich, "Analysis of poly-β-hydroxybutyrate in *Rhizobium japonicum* bacteroids by ion-exclusion high-pressure liquid chromatography," *Applied and Environmental Microbiology*, vol. 46, no. 6, pp. 1339–1344, 1983.

[43] J. H. Law and R. A. Slepecky, "Assay of poly-beta-hydroxybutyric acid," *Journal of bacteriology*, vol. 82, pp. 33–36, 1961.

[44] T. Furukawa, H. Sato, R. Murakami et al., "Raman microspectroscopy study of structure, dispersibility, and crystallinity of poly(hydroxybutyrate)/poly(L-lactic acid) blends," *Polymer*, vol. 47, no. 9, pp. 3132–3140, 2006.

[45] J. De Gelder, D. Willemse-Erix, M. J. Scholtes et al., "Monitoring poly(3-hydroxybutyrate) production in *Cupriavidus necator* DSM 428 (H16) with Raman spectroscopy," *Analytical Chemistry*, vol. 80, no. 6, pp. 2155–2160, 2008.

[46] M. Ramezani, M. A. Amoozegar, and A. Ventosa, "Screening and comparative assay of poly-hydroxyalkanoates produced by bacteria isolated from the Gavkhooni Wetland in Iran and evaluation of poly-β-hydroxybutyrate production by halotolerant bacterium *Oceanimonas* sp. GK1," *Annals of Microbiology*, vol. 65, no. 1, pp. 517–526, 2015.

[47] B. Saake, S. Horner, T. Kruse, J. Puls, T. Liebert, and T. Heinze, "Detailed investigation on the molecular structure of carboxymethyl cellulose with unusual substitution pattern by means of an enzyme-supported analysis," *Macromolecular Chemistry and Physics*, vol. 201, no. 15, pp. 1996–2002, 2000.

[48] M. Melander and T. Vuorinen, "Determination of the degree of polymerisation of carboxymethyl cellulose by size exclusion chromatography," *Carbohydrate Polymers*, vol. 46, no. 3, pp. 227–233, 2001.

[49] A. Cohen, H. Schagerlöf, C. Nilsson, C. Melander, F. Tjerneld, and L. Gorton, "Liquid chromatography-mass spectrometry analysis of enzyme-hydrolysed carboxymethylcellulose for investigation of enzyme selectivity and substituent pattern," *Journal of Chromatography A*, vol. 1029, no. 1-2, pp. 87–95, 2004.

[50] C. Du, J. Sabirova, W. Soetaert, and S. K. Carol Lin, "Polyhydroxyalkanoates production from low-cost sustainable raw materials," *Current Chemical Biology*, vol. 6, no. 1, pp. 14–25, 2012.

[51] D. Gao, Y. Luan, Q. Wang, Q. Liang, and Q. Qi, "Construction of cellulose-utilizing *Escherichia coli* based on a secretable cellulase," *Microbial Cell Factories*, vol. 14, no. 1, article 159, 2015.

[52] G. J. McCool and M. C. Cannon, "PhaC and PhaR are required for polyhydroxyalkanoic acid synthase activity in *Bacillus megaterium*," *Journal of Bacteriology*, vol. 183, no. 14, pp. 4235–4243, 2001.

[53] S. Tomizawa, M. Hyakutake, Y. Saito et al., "Molecular weight change of polyhydroxyalkanoate (PHA) caused by the PhaC subunit of PHA synthase from *Bacillus cereus* YB-4 in recombinant *Escherichia coli*," *Biomacromolecules*, vol. 12, no. 7, pp. 2660–2666, 2011.

[54] T. Tsuge, M. Hyakutake, and K. Mizuno, "Class IV polyhydroxyalkanoate (PHA) synthases and PHA-producing *Bacillus*," *Applied Microbiology and Biotechnology*, vol. 99, no. 15, pp. 6231–6240, 2015.

[55] M. Hyakutake, Y. Saito, S. Tomizawa, K. Mizuno, and T. Tsuge, "Polyhydroxyalkanoate (PHA) synthesis by class IV PHA synthases employing *Ralstonia eutropha* PHB^{-}4 as host strain," *Bioscience, Biotechnology and Biochemistry*, vol. 75, no. 8, pp. 1615–1617, 2011.

[56] M. Hyakutake, S. Tomizawa, K. Mizuno, H. Abe, and T. Tsuge, "Alcoholytic cleavage of polyhydroxyalkanoate chains by Class IV synthases induced by Endogenous and exogenous ethanol," *Applied and Environmental Microbiology*, vol. 80, no. 4, pp. 1421–1429, 2014.

[57] M. Hyakutake, S. Tomizawa, K. Mizuno, T. Hisano, H. Abe, and T. Tsuge, "A common active site of polyhydroxyalkanoate synthase from *Bacillus cereus* YB-4 is involved in polymerization and alcoholysis reactions," *Applied Microbiology and Biotechnology*, vol. 99, no. 11, pp. 4701–4711, 2014.

[58] H. Yue, C. Ling, T. Yang et al., "A seawater-based open and continuous process for polyhydroxyalkanoates production by recombinant *Halomonas campaniensis* LS21 grown in mixed substrates," *Biotechnology for Biofuels*, vol. 7, no. 1, article 108, 2014.

[59] H. Chua and P. H. F. Yu, "Production of biodegradable plastics from chemical wastewater—a novel method to reduce excess activated sludge generated from industrial wastewater treatment," *Water Science and Technology*, vol. 39, no. 10-11, pp. 273–280, 1999.

[60] C. F. Budde, S. L. Riedel, L. B. Willis, C. Rha, and A. J. Sinskey, "Production of poly(3-hydroxybutyrate-co-3-hydroxyhexanoate) from plant oil by engineered *Ralstonia eutropha* strains," *Applied and Environmental Microbiology*, vol. 77, no. 9, pp. 2847–2854, 2011.

[61] X. Zhang, T. Bao, Z. Rao et al., "Two-stage pH control strategy based on the pH preference of acetoin reductase regulates acetoin and 2,3-butanediol distribution in *Bacillus subtilis*," *PLoS ONE*, vol. 9, no. 3, Article ID e91187, 2014.

[62] B. Bach, E. Meudec, J.-P. Lepoutre et al., "New insights into γ-aminobutyric acid catabolism: evidence for γ-hydroxybutyric acid and polyhydroxybutyrate synthesis in *Saccharomyces cerevisiae*," *Applied and Environmental Microbiology*, vol. 75, no. 13, pp. 4231–4239, 2009.

[63] S. P. Valappil, A. R. Boccaccini, C. Bucke, and I. Roy, "Polyhydroxyalkanoates in Gram-positive bacteria: insights from the genera *Bacillus* and *Streptomyces*," *International Journal of General and Molecular Microbiology*, vol. 91, no. 1, pp. 1–17, 2007.

[64] K. Tajima, T. Igari, D. Nishimura, M. Nakamura, Y. Satoh, and M. Munekata, "Isolation and characterization of *Bacillus* sp. INT005 accumulating polyhydroxyalkanoate (PHA) from gas field soil," *Journal of Bioscience and Bioengineering*, vol. 95, no. 1, pp. 77–81, 2003.

[65] S. Sato, C. T. Nomura, H. Abe, Y. Doi, and T. Tsuge, "Poly[(R)-3-hydroxybutyrate] formation in *Escherichia coli* from glucose through an enoyl-CoA hydratase-mediated pathway," *Journal of Bioscience and Bioengineering*, vol. 103, no. 1, pp. 38–44, 2007.

[66] S. Cai, L. Cai, H. Liu et al., "Identification of the haloarchaeal phasin (PhaP) that functions in polyhydroxyalkanoate accumulation and granule formation in *Haloferax mediterranei*," *Applied and Environmental Microbiology*, vol. 78, no. 6, pp. 1946–1952, 2012.

Hindawi
International Journal of Polymer Science
Volume 2017, Article ID 6942950, 10 pages
https://doi.org/10.1155/2017/6942950

Research Article

Synthesis of Poly-(R-hydroxyalkanoates) by *Cupriavidus necator* ATCC 17699 Using Mexican Avocado *(Persea americana)* Oil as a Carbon Source

Araceli Flores-Sánchez,[1] Ma. del Rocío López-Cuellar,[2] Fermín Pérez-Guevara,[3] Ulises Figueroa López,[1] José Mauricio Martín-Bufájer,[1] and Berenice Vergara-Porras[1]

[1]*Escuela de Ingeniería y Ciencias, Tecnológico de Monterrey, Campus Estado de México, Carretera Lago de Guadalupe Km 3.5, Margarita Maza de Juárez, Atizapán de Zaragoza, MEX, Mexico*
[2]*Cuerpo Academico de Biotecnología Agroalimentaria, Instituto de Ciencias Agropecuarias, Universidad Autónoma del Estado de Hidalgo, Pachuca, HGO, Mexico*
[3]*Departamento de Biotecnología y Bioingeniería, Centro de Investigación y Estudios Avanzados (CINVESTAV), Avenida IPN 2508, Zacatenco, Gustavo A. Madero, Ciudad de México, Mexico*

Correspondence should be addressed to Berenice Vergara-Porras; vergarabp@itesm.mx

Received 20 April 2017; Accepted 14 June 2017; Published 21 August 2017

Academic Editor: Raffaele Cucciniello

Poly-R-hydroxyalkanoates (PHAs) are polymers produced by a vast number of bacterial species under stress conditions. PHAs exhibit different thermal and mechanical properties that depend on their molecular structure. In this work, PHAs were produced using avocado oil as the carbon source. *Cupriavidus necator* H16 was cultured in three-stage fermentation using fructose during the cell growth stages and avocado oil during the PHA synthesis stage. Different concentrations of avocado oil were used during the third stage to test the incorporation of various monomeric units into the PHAs. Biomass and PHA production were measured during the fermentation. DSC, FTIR, and gas chromatography analysis aided the PHA characterization. Different proportions of 3-hydroxyvalerate were present in the 3-hydroxybutyrate main chain depending on the concentration of avocado oil. The results suggest that avocado oil is a viable new substrate for PHA production.

1. Introduction

Poly-R-hydroxyalkanoates (PHAs) are polymers synthesized by a large number of bacterial species as a response to unbalanced nutritional conditions [1]. PHAs are thermoplastic polyesters of R-hydroxy alkanoic acids and accumulate intracellularly as granules that exhibit different properties depending on their chemical composition [2, 3]. A single monomer that forms the chain of PHAs typically contains from 3 to 15 carbon atoms [4], but the final chemical composition of PHAs is related to the synthesizer microorganism, the carbon source, the culture conditions, and the specificity of the PHA-synthase enzyme [5–7]. Homopolymers, copolymers, or terpolymers of PHAs can be obtained; for example, PHA copolymers can be synthesized from a combination of different substrates [8]. The thermal properties of PHAs, such as melting temperature and degree of crystallinity, depend on the length of the PHA monomeric units. Monomers containing more than five carbon atoms significantly decrease the polymer melting temperature, as well as the degree of crystallinity [9].

Many PHAs have main chains formed from monomers with different numbers of carbon atoms. Short-length-chain PHAs (PHA_{slc}) consist of monomers ranging from 3 to 5 carbons, whereas medium-length-chain PHAs (PHA_{mlc}) are formed from monomers containing 6 to 14 carbon atoms [4, 8]. One PHA_{slc}, poly(3-hydroxybutyrate) (PHB), is the most common PHA and was first identified by Maurice Lemoigne in 1926 [1, 4]. PHB biodegradability and biocompatibility make it an attractive material; however, its

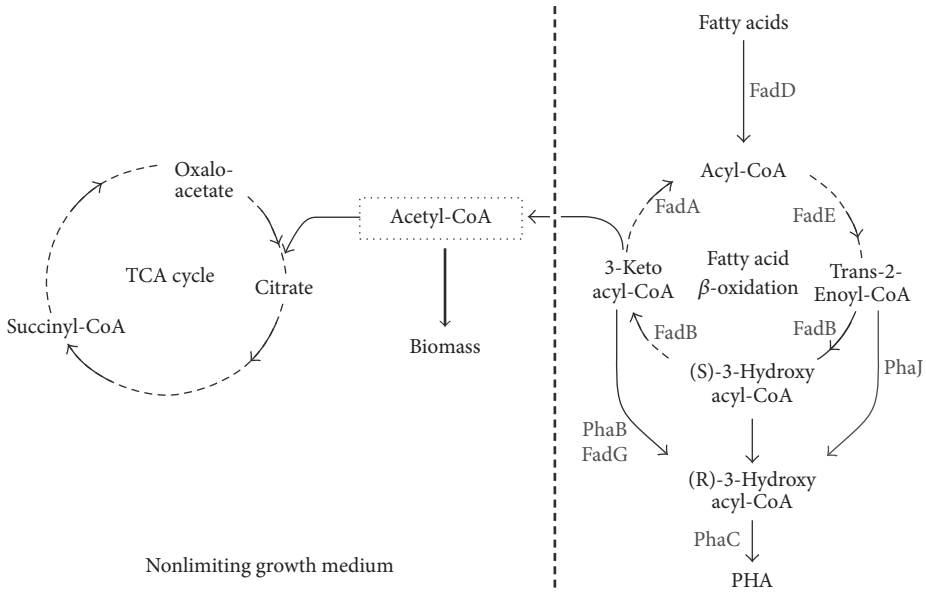

Figure 1: A simplified representation of fatty acid metabolism in *Cupriavidus necator*. In a nonlimiting growth media (left side), the tricarboxylic acid (TCA) cycle is active and the main product is biomass itself. Under unbalanced conditions (right side), caused by a noncarbon nutrient deficiency, C-source via fatty acid β-oxidation flows towards the poly-R-hydroxyalkanoate (PHA) biosynthesis pathway.

brittleness and limited degree of crystallinity have restricted its possible applications. The melting point of PHB (≈175°C) is also very close to its decomposition temperature (≈180°C), which creates challenges for thermal processing due to a narrow processing window [10]. Copolymers such as poly-(hydroxybutyrate-co-hydroxyvalerate) (PHBV) that contain (3)-hydroxybutyrate (3HB) and (3)-hydroxyvalerate (3HV) units in the chain show lower molecular weights and lower melting temperatures when compared to a PHB homopolymer. Babel and Steinbüchel [11] reported melting temperatures of 170, 162, 150, 145, and 137 when 3HV was in a 3, 9, 14, 20, and 25 mol% content, respectively.

Renewable carbon sources, such as sucrose, cellulose, and triacylglycerol, have served as substrates for PHA synthesis. Extensive studies have been conducted on the use of inexpensive substrates, including starch, glycerol, soybean oil, sugar cane bagasse, molasses, and activated sludge, to reduce the production cost of PHB [5, 12–14]. Similarly, byproducts from the food and the agroalimentary industry, methane, mineral oil, and lignite have been used to synthesize PHBV copolymers [1, 4, 15, 16]. Therefore, the carbon source and the microorganism consumption affinity are of great importance for the production of specific PHAs.

One organism that has been extensively used in the synthesis of PHAs is *Cupriavidus necator* (formerly *Ralstonia eutropha*), due to its versatility to accumulate polymer in amounts as high as 90% of its dry cell weight (DCW) [6]. The ability of *C. necator* to synthesize PHB and PHBV, as well as other PHAs, has been previously reported [6, 20, 21]. The limiting productions costs had led to proposals for the use of cheaper carbon sources, such as organic debris, wastewater, or even vegetable oils [22]. The use of complex carbon sources could also extend the incorporation of 3HV units to the main chain or even the synthesis of PHA_{mlc} [8].

The use of fatty acids, such as those present in vegetable oils, as a carbon source drives the β- fatty acid oxidation metabolic pathway in *C. necator*. The PHA synthesis in *C. necator* is highly associated with growth conditions and is mediated by the acetyl-CoA precursor [23, 24]. In balanced nutritional environments, fatty acids provide precursors, free energy, and cofactors for cell growth and maintenance and for macromolecular synthesis. By contrast, noncarbon nutrient limitation leads to inhibition of the central enzymes of the tricarboxylic cycle (TCA cycle). Consequently, the acetyl-CoA is channelled towards the PHA synthesis [23–25], as depicted in Figure 1.

Mexican avocado *(Persea americana)* is a lipid-rich fruit that occupies a prominent place in the market [26]. In 2015, 51.4% of the globally commercialized avocado was produced in Mexico [26]. During its cultivation, a high amount of waste material is produced. For example, in Mexico, nearly 54% of the annual avocado production is considered as waste. Moreover, the farming, packing, transportation, and commercialization stages are also important sources of avocado wastes [27]. Furthermore, fruit peel and seed, representing 12 to 15% and 20 to 27% of fruit weight, respectively, are currently discarded. Only the fruit pulp is destined for human consumption [28].

The fatty acids composition in Mexican avocado mainly includes palmitic, stearic, oleic, linoleic, heptanoic, nonanoic, and heptadecanoic acids [26]. The high content of fatty acid and the amount of waste generated from its cultivation identify avocado as a possible and sustainable carbon source for the biosynthesis of PHAs. As a first attempt, and to

standardize the chemical composition of the substrate, the viability of PHA biosynthesis from avocado oil by *C. necator* was tested. The biopolymers synthesized from different oil contents were thermally and chemically characterized to demonstrate the feasibility of using this oil as an alternative substrate for PHA production.

2. Materials and Methods

2.1. Strain, Media, and Materials. C. necator H16 (ATCC 17699) was grown in mineral medium supplemented with fructose for 24 h, at 30°C and 200 rpm, for seed culture preparation. The medium contained, per litre of water, 10 g fructose, 3.70 g $(NH_4)_2SO_4$, 0.40 g $MgSO_4$, 6.36 g $Na_2HPO_4{\cdot}7H_2O$, 2.70 g KH_2PO_4, and 1.0 g nutrient broth.

The growth medium contained, per litre of water, 10 g fructose, 1.57 g NH_4SO_4, 5.66 g $NaH_2PO_4{\cdot}12H_2O$, 1.5 g KH_2PO_4, 0.2 g $MgSO_4{\cdot}7H_2O$, 10 mg $CaCl_2{\cdot}2H_2O$, 20 mg $FeSO_4{\cdot}7H_2O$, and 1 mL of trace element solution (0.3 g H_3BO_3, 0.2 g $CoCl_2{\cdot}6H_2O$, 0.1 g $ZnSO_4{\cdot}7H_2O$, 30 mg $MnCl_2{\cdot}4H_2O$, 30 mg $Na_2MoO4{\cdot}2H_2O$, 20 mg $NiCl_2{\cdot}6H_2O$, and 10 mg $CuSO_4{\cdot}5H_2O$, in HCl 0.1 N solution); the pH was adjusted to 7.

Commercial Mexican avocado oil for PHA synthesis was obtained from a single batch (the same production number) (Ahuacatlán, Mexico) to ensure a homogeneous chemical composition of the substrate.

2.2. Fermentation Studies

2.2.1. Inoculum Preparation. Experiments were conducted in duplicate using 200 mL of growth media in 500 mL flasks at 30°C, pH 7.0, in an incubator with rotational agitation at 200 rpm (New Brunswick Innova 4300, USA). A 10% v/v of the seed culture was used to inoculate the growth medium to obtain 0.13 g L^{-1} (±0.1) of initial biomass (X) in the growth medium.

2.2.2. Fermentation. A fermentation procedure consisting of three different stages was carried out as follows.

Stage 1. Batch cultivation at an initial carbon/nitrogen (C/N) ratio of 14 using the growth medium: carbon depletion in the medium (3 g L^{-1} of fructose) determined the length of the stage.

Stage 2. A fed-batch stage to increase biomass density at C/N ratio of 6.5: two additions of fructose and ammonium were made. The time of addition was determined as the point when the fructose remaining in the media reached approximately 3 g L^{-1}.

Stage 3. PHA production under nitrogen limitation: avocado oil was added to the culture at the beginning of the stage, at 30 h. Different concentrations were tested: 5, 10, 15, 20, and 25% (v/v).

Control experiments consisted of additional flasks prepared using fructose as the carbon source for the three-stage fermentation.

2.2.3. Analytical Procedures. Fermentation samples were taken every two hours and immediately centrifuged at 10000 rpm for 10 min at 4°C. Fructose and ammonium were analysed in the supernatant, and the bottom pellet (biomass) was washed thoroughly with distilled water before lyophilizing for gravimetric estimation of the dry cell weights (DCW).

Fructose consumption in the fermentation media was quantified using a 3,5-dinitrosalicylic acid (DNS) method [29]. Ammonium consumption was analysed according to the protocol of Weatherburn [30].

The intracellular polymer was extracted from the lyophilized biomass using chloroform (1 g of biomass per 50 mL of solvent) at 60°C for 30 min with constant stirring. After incubation, PHA dissolved in the chloroform phase was filtered to eliminate cellular debris and then precipitated with hexane. The residual solvent in the polymer was removed by evaporation [31, 32].

Dimensionless biomass yield ($Y_{x/s}$) was estimated as the ratio of the amount of biomass produced to the amount of total substrate consumed. This was calculated at the end of Stages 1 and 2. Productivity was estimated at the end of the fermentation as the final PHA concentration achieved divided by the total cultivation time required to attain that concentration. Residual biomass was also calculated at the end of fermentation as final produced biomass (CDW) minus PHA concentration.

2.3. PHA Characterization

2.3.1. Gas Chromatography. Fatty acid methyl esters were derived from acid methanolysis of PHA at 100°C for 4 h by incubating 100 mg of PHA, 2 mL of chloroform, 2 mL of methanol (20% of HCl), and benzoic acid (as an internal standard) in borosilicate glass tubes with screw caps at 100°C for 4 h. After cooling, distilled water was added (1 mL), the tubes were vortexed for 60 s, and the lower phase containing the resulting methyl esters was recovered for analysis [33]. Fatty acid methyl esters (1 μL) were analysed on a gas chromatograph (SRI Instruments, Model 310, USA) equipped with a flame ionization detector (FID) and a 6 ft. × 1/8 in. silica gel column. Nitrogen at 30 mL min^{-1} was used as carrier gas and the injector and detector were set at 220 and 170°C, respectively. Reference standards were poly(hydroxybutyrate) and the copolymer poly(hydroxybutyrate-co-hydroxyvalerate) [12 mol% hydroxyvalerate] (Goodfellow, UK).

2.3.2. Fourier Transform Infrared (FTIR) Spectroscopy. FTIR was performed within wavenumber ranges from 600 to 4000 cm^{-1} (BUCK Scientific, model 530, USA). PHA was dissolved in chloroform before pouring the solution onto KBr plates to form the polymer films.

2.3.3. Differential Scanning Calorimetry (DSC). DSC curves were obtained using a differential scanning calorimeter

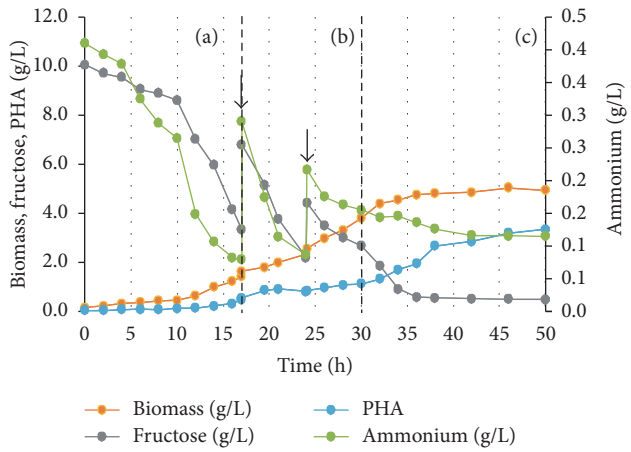

FIGURE 2: Profiles of fructose (grey circles), ammonium (green circles), biomass (orange circles), and poly-R-hydroxyalkanoate (PHA) (blue circles) production during the cultivation of *Cupriavidus necator* on fructose and avocado oil (20% v/v) in three-stage fermentation. Stage 1: batch cultivation (a), Stage 2: fed-batch stage (additions indicated by black arrows) (b), and Stage 3: PHA accumulation (c). Oil addition occurs at 30 h.

(Mettler Toledo DSC 823) according to López-Cuellar et al. [6]. Approximately 4 mg of the specimens was crimped in aluminium pans. The samples were evaluated under the following conditions: dynamic nitrogen atmosphere of 50 mL min^{-1}, a heating rate of 10°C min^{-1}, and an extended temperature range (−40 to 200°C). Two runs under same conditions were carried out; the first run erased the thermal history of sample. Thermograms obtained during the second run were analysed to determine the melting temperature (T_m) and melting enthalpy (ΔH_m) of the PHAs. Pure PHB (Goodfellow, UK) served as reference standard.

3. Results

3.1. Fermentation Studies. The representative profiles of the PHAs synthesized by *C. necator* H16 using fructose and avocado oil as carbon sources are depicted in Figure 2.

Stage 1 (Figure 2(a)), conducted as a batch cultivation, lasted 17 h and was initiated by adding 10 g L^{-1} of fructose and 0.42 g L^{-1} of ammonium to the medium. A lag phase of 10 h occurred. The concentration of substrate (i.e., fructose during Stage 1) decreased from 10 to 3.3 g L^{-1} (±0.10), whereas the biomass density, measured gravimetrically as DCW, increased from 0.13 to 1.44 g L^{-1} (±0.06) to achieve a growth yield ($Y_{x/s}$) of 0.19.

Stage 2 (Figure 2(b)), conducted as a fed-batch cultivation to increase cellular density, lasted about 12.5 h. Fructose as substrate was added on two different occasions: at 17.5 h and 24 h (Figure 2, black arrows). The first addition consisted of 3 g L^{-1} of fructose and 0.21 g L^{-1} of ammonium. For the second addition, the medium was supplemented with 2 g L^{-1} of fructose and 0.12 g L^{-1} of ammonium. During Stage 2, the biomass density increased from 1.44 (±0.06) to 3.79 g L^{-1} (±0.09), consuming about 5.63 g L^{-1} (±0.03) of fructose. At the end of Stage 2, an average $Y_{x/s}$ of 0.42 was achieved, matching the theoretical yield when simple sugars are used as carbon sources ($Y_{x/s}$ of 0.30–0.40) [8]. In addition, a slight accumulation of PHA was observed, but this only represented less than 30% of the DCW, in agreement with the balanced nutrient conditions.

Synthesis of PHAs (Stage 3) was first observed at 30 h (Figure 2(c)). The fructose remaining in the medium was about 1.9 g L^{-1} at the beginning of this stage. Avocado oil was added to the flasks in a single addition at the beginning of the stage to induce polymer synthesis. The avocado oil concentrations tested were 0 (used as a control), 5, 10, 15, 20, and 25% (v/v). Stage 3 lasted 20 h. During this time, nitrogen levels remained around 0.1 g L^{-1} to generate cellular stress and to promote polymer accumulation [6]. A rapid consumption of fructose was observed at the beginning of the stage and, by the end of the stage, fructose was barely detectable in the medium (<0.5 g L^{-1}).

The results of the 50 h, three-stage fermentation are summarized in Table 1. A significant amount of PHA accumulation was observed, ranging from 59 to 70% of the DCW. From the results, a positive trend for PHA accumulation was observed in flasks with avocado oil concentrations of 5, 10, 15, and 20% v/v. The highest PHA concentration was reached when the oil in the media was 20% (v/v), with PHA values of 3.48 g L^{-1} (±0.04) achieved, which represented 70.8% of the accumulated PHA in terms of DCW. However, flasks with and oil concentration of 25% (v/v) showed a decrease in PHA accumulation efficiency, reaching about 3.07 g L^{-1} (±0.02). The overall productivity of the experiments fluctuated between 0.053 and 0.070 g L^{-1} h^{-1}.

Conversely, control experiments (0% fed oil) produced 77% of the polymer, almost reaching the typical 80–85% PHA accumulation reported for the strain [34].

3.2. PHAs Composition Analysis through Gas Chromatography. From gas chromatography, the chemical composition of the PHAs was determined using benzoic acid (internal standard) as evaluation base. Representative chromatograms of the evaluated methyl esters are presented in Figure 3. The retention times for the reference standards and the samples were consistent (5.516 min for 3-hydroxybutyrate [3HB], 7.150 min for 3-hydroxyvalerate [3HV]).

The most abundant monomer detected in all samples was 3HB monomer ranging from 92.8 to 98.94% for samples fed with avocado oil, as summarized in Table 2. In all cases, 3HV monomeric units was also recognized, ranging from 1 to 7 mol%. The highest hydroxyvalerate amounts were found in the PHA synthesized from 20% (v/v) of oil, matching the biomass profiles. An unusual pattern was observed, wherein the accumulation of 3HV units was highly dependent on the avocado oil concentration, reaching a maximum value of 7% (Figure 2(c)). Other 3-hydroxy-acids containing more than five carbons were also identified in some PHAs, but in minimal quantities (i.e., less than 0.16 mol%). Thus, avocado oil could promote the synthesis of PHAs containing 3HB and significant fractions of 3HV monomers.

3.3. Functional Group Identification by Infrared Spectroscopy (FTIR). The spectra recorded from the PHAs, depicted in

Table 1: Final yields of poly-R-hydroxyalkanoates obtained from a three-stage fermentation of *Cupriavidus necator*.

Substrate	[a]Av. oil (% v/v)	[b]Biomass ($g\,L^{-1}$)	PHA ($g\,L^{-1}$)	[c]Residual biomass ($g\,L^{-1}$)	PHA (%)	Productivity ($g\,L^{-1}\,h^{-1}$)
Fructose	—	5.25 (±0.01)	4.04 (±0.02)	1.21 (±0.009)	76.87 (±1.03)	0.081
Fructose, avocado oil	5	4.45 (±0.02)	2.64 (±0.03)	1.82 (±0.012)	59.21 (±1.12)	0.053
	10	4.63 (±0.05)	3.14 (±0.04)	1.49 (±0.017)	67.69 (±1.38)	0.063
	15	4.74 (±0.04)	3.27 (±0.03)	1.47 (±0.013)	69.04 (±1.43)	0.065
	20	4.91 (±0.04)	3.48 (±0.04)	1.43 (±0.015)	70.83 (±1.31)	0.070
	25	4.61 (±0.03)	3.07 (±0.06)	1.54 (±0.011)	66.63 (±1.29)	0.061

[a]Av. oil: avocado oil concentrations (% v/v). [b]Biomass: measured gravimetrically. [c]Residual biomass: biomass concentration after PHA extraction.

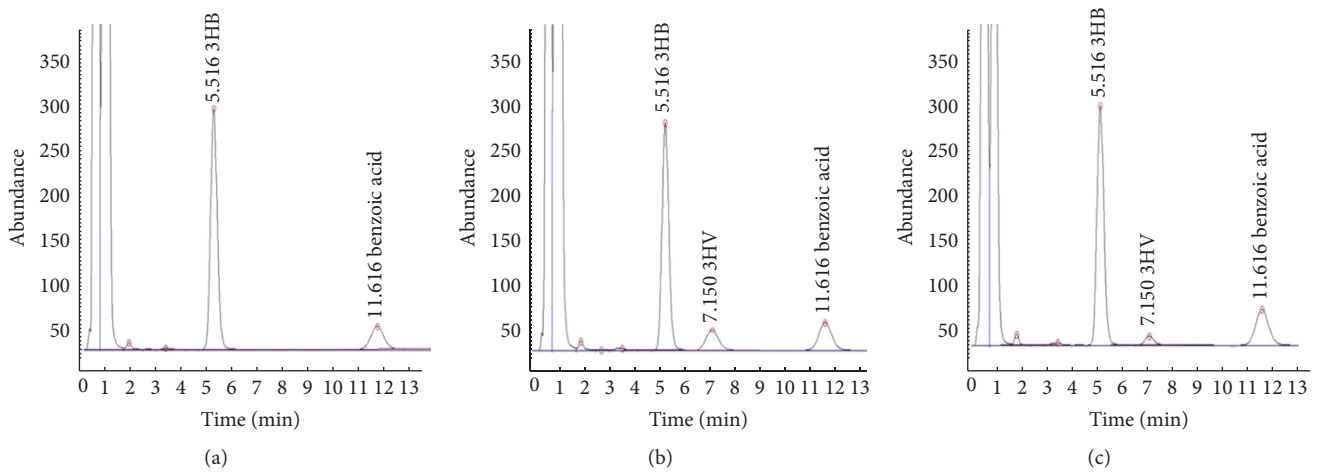

Figure 3: Chromatogram obtained from gas chromatography (GC) of (a) poly(3-hydroxybutyrate) (PHB) standard, (b) poly(hydroxybutyrate-co-hydroxyvalerate) (PHBV) standard with 12 mol% HV content, and (c) polymer produced from 20% v/v of avocado oil (7 mol% of HV). Benzoic acid was used as internal standard.

Figure 4, were similar to the PHBV spectra reported in previous studies [35]. The PHAs exhibited the particular chemical bonds of PHAs and replicated the absorption spectra among the samples.

The most prominent peak, located around 1720 cm^{-1}, was related to the ester carbonyl group (C=O). The bands located in the region of 2800 to 3000 cm^{-1} corresponded to the methyl-methylene groups. The presence of these peaks was due to the symmetric and asymmetric stretching of the CH_3 and CH_2 groups and these peaks were related to the monomeric units in the lateral chain. Besides the C=O group, an asymmetrical C-H bending vibration in CH_3 group shows an absorption band at 1453 cm^{-1}, whereas C-O-H bond shows a peak at 1378 [36]. Other peaks were recorded in the 1100 to 1290 cm^{-1} region; bands found around 1176, 1221, and 1270 cm^{-1} were attributed to polymer crystalline structures, and their presence was related to the C-O-C functional group [24].

3.4. Thermal Properties by DSC. The recorded thermograms obtained during the second run of the DSC analysis of the PHAs are shown in Figure 5. The melting points of the synthesized PHAs ranged from 159 to 173°C, whereas the measured ΔH_m was between 51 and 57 $J\,g^{-1}$ (Table 2). A decreasing trend was observed for the T_m value with increasing oil concentration. The lowest T_m and ΔH_m values were reached at 20% v/v, at 159°C and 51.81 $J\,g^{-1}$, respectively. An oil concentration above 20% v/v caused an increase in T_m of the synthesized PHA. Traces of monomers with a higher number of carbons were detected in some fed oil samples; however, these monomers were not identified, as mentioned in Table 2.

The thermal properties of the control experiment (0% fed oil) were also estimated and compared against a PHB reference standard. T_m of the sample fed with 0% oil was 175.16°C and ΔH_m value was 67.05 $J\,g^{-1}$. T_m of the PHB reference standard was 176.3°C and ΔH_m value was 75.48 $J\,g^{-1}$, in agreement with previous reports [37, 38] and confirming the production of pure PHB in the controls.

4. Discussion

Different PHAs were synthesized by *C. necator* H16 in a flask system using fructose and avocado oil as substrates. Fermentation was conducted using a three-stage process in order to increase biomass densities and polymer accumulation, without triggering the substrate inhibition reported to occur at levels of fructose higher than 10 $g\,L^{-1}$ [39]. Different oil

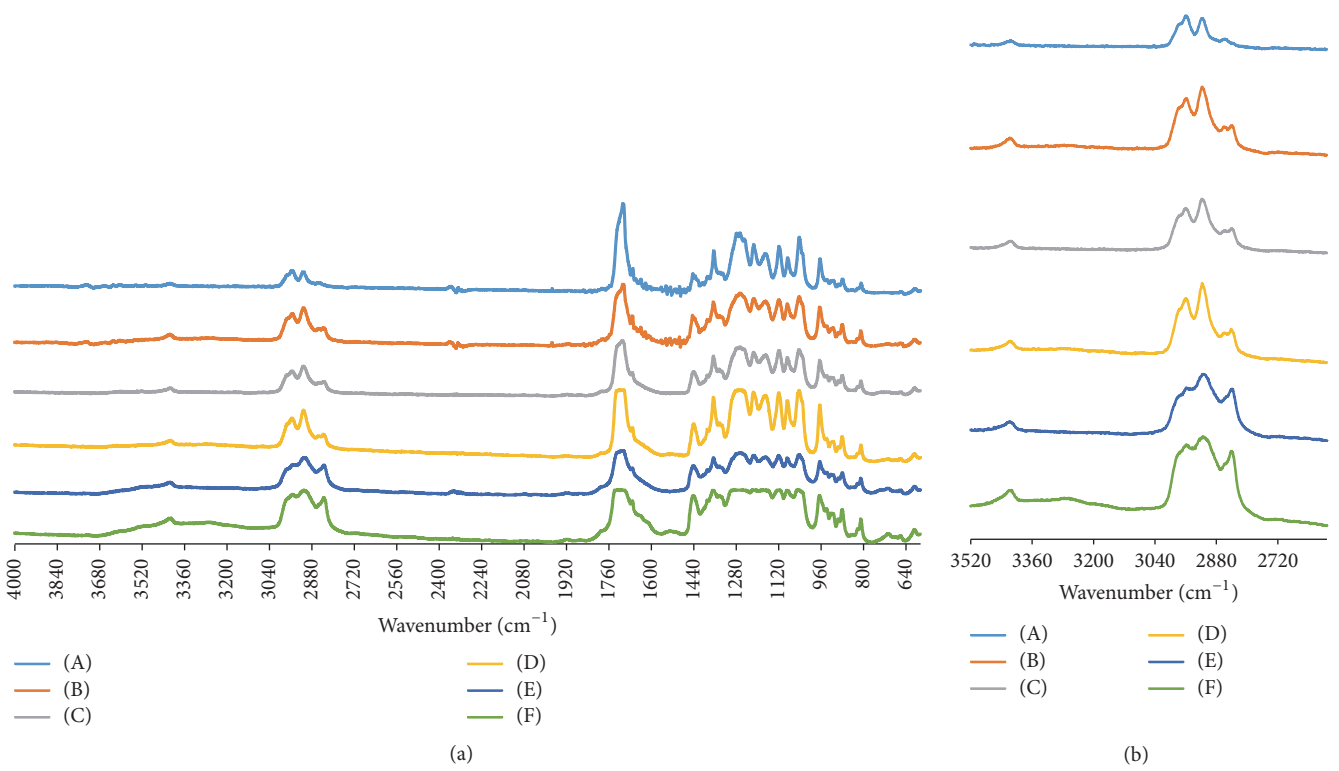

Figure 4: Fourier transform infrared spectroscopy (FTIR) spectra of the poly-R-hydroxyalkanoates (PHAs) produced by the addition of avocado oil: (A) 0 (control); (B) 5, (C) 10, (D) 15, (E) 20, and (F) 25 percent [v/v]. (a) 600 to 4000 cm^{-1}, (b) 2500 to 4000 cm^{-1}.

Table 2: Thermal properties and chemical composition of the poly-R-hydroxyalkanoates (PHAs) produced in *Cupriavidus necator*.

Substrate	[a]Av. oil (% v/v)	T_m (°C)	ΔH_m (J/g)	Monomeric composition of PHAs[b] (mol%)		
				3HB	3HV	3HA
Fructose	—	175.15	67.05	100.00	—	—
Fructose, avocado oil	5	173.22	56.68	98.94	1.06	
	10	169.71	55.32	97.15	2.77	0.08
	15	168.22	54.29	96.64	3.27	0.09
	20	159.57	51.81	92.83	7.01	0.16
	25	164.31	53.26	95.14	4.75	0.11

[a]Av. oil, avocado oil tested concentrations; [b]3HB, 3-hydroxybutyrate; 3HV, 3-hydroxyvalerate; 3HA, unidentified hydroxyl acid monomeric unit with more than 5 carbons.

concentrations (5, 10, 15, 20, and 25% v/v) were evaluated for PHA synthesis during Stage 3. The control experiments, using fructose as the carbon source during the overall process, complemented the studies.

Previous flask studies have typically been conducted in batch mode [12, 17–20], with overall productivities ranging from 0.025 to 0.08 $g\,L^{-1}\,h^{-1}$ (Table 3). In the current study, remarkable productivity was obtained, ranging from 0.05 to 0.07 $g\,L^{-1}\,h^{-1}$, for the evaluated oil concentrations (% v/v). Similar studies have achieved productivities between 0.025 and 0.05 $g\,L^{-1}\,h^{-1}$ [17, 19]. The highest productivity previously reported was reached using simple sugar as a carbon source [12] and resembled the productivity reported here for control samples (0.081 $g\,L^{-1}\,h^{-1}$). Hence, the feasibility of the three-stage fermentation was confirmed and suggested an interconnection with the operational mode of the system and the strain's affinity for the substrates [34].

A maximum biomass yield was reached with 20% v/v oil in the medium. Flasks with 25% v/v oil showed a decrease in cellular density and polymer accumulation. This yield decrease could be related to oxygen transfer limitations or a substrate inhibition [40]. Possibly, large oil amounts reduce

Table 3: Comparison of studies reporting PHAs production in *Cupriavidus necator*.

Strain	Substrate	Scale	Control strategy	PHA[1] produced	Biomass ($g\,L^{-1}$)	PHA ($g\,L^{-1}$)	PHA (%)	Productivity ($g\,L^{-1}\,h^{-1}$)	Reference
C. necator	Plant oils[2]	Flask	Batch	P(3HB)	3.6–4.3	2.9–3.4	79–81	0.04–0.05	Fukui and Doi [17]
C. necator (recombinant, *Aeromonas caviae*)	Plant oils[2]			P(3HB-co-3HHX)	3.5–3.6	2.7–2.9	76–81	0.04	
C. necator DSM 541	Fructose	Flask	Batch	P(3HB)	3.4	n.a	55	n.a	Dennis et al. [18]
	Palmitate			P(3HB-co-3HV-co-3HHX)	0.51	n.a	58	n.a	
	Oleate			P(3HB-co-3HHX)	1.44	n.a	57	n.a	
C. necator	Centrifuged fermented organic waste	Flask	Batch	P(3HB-co-3HV)	2.77	1.13	40.0	0.025	Ganzeveld et al., [19]
C. necator	Bagasse hydrolysate	Flask	Batch	n.a	6	3.9	65	0.08	Yu and Stahl [12]
C. necator	Palm oil	Flask	Batch	P(3HB-co-3HV)	3.6	2.66	74	n.a	Liu et al. [20]
C. necator	Fructose[3]	Flask	Fed batch	P(3PHB)	5,25	4.04	76.87	0.081	This study
	Fructose, avocado oil			P(3HB-co-3HV)	4.45–4.91	2.64–3.48	59–70	0.053–0.07	

[1]3PHB, 3 hydroxybutyrate; 3HV, 3 hydroxyvalerate; 3HHX, 3-hydroxyhexanoate. [2]Olive oil, corn oil and palm oil tested once at a time. [3]Control experiments. n.a: Not available.

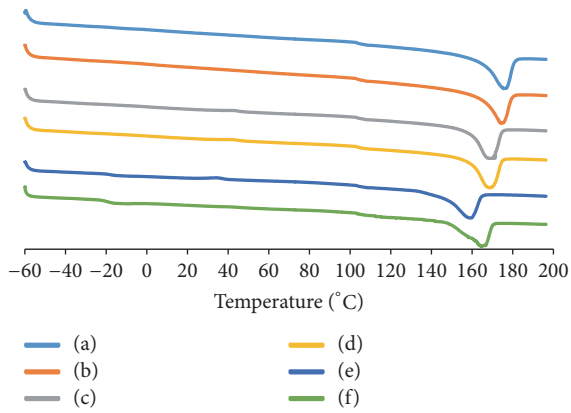

Figure 5: Thermograms obtained during the second run of differential scanning calorimetry (DSC) of the poly-R-hydroxyalkanoates (PHAs) produced by the addition of avocado oil at (a) 0 (control), (b) 5, (c) 10, (d) 15, (e) 20, and (f) 25 percent [v/v].

oxygen transfer to the cells, thereby delaying synthesis and accumulation of polymers. However, further studies on larger scales are required to analyse the oxygen transfer dynamics.

C. necator H16 is well known to exhibit a preference for synthesizing PHAs containing 3HB units as the most abundant monomer regardless of the carbon source, even from vegetable oils. Some studies have confirmed the synthesis of pure PHB when *C. necator* is grown in vegetable oils [41]. Conversely, Du et al. [42] achieved the production of PHBV using fatty acids from food scraps, whereas Dennis et al. [18] demonstrated that the *C. necator* synthase could accept C6 substrates (Table 3). A few studies have also identified larger monomeric units when using vegetable oils as carbon sources [6, 21].

In the present study, PHAs were composed mainly of 3HB monomers, followed by 3HV ranging from 1 to 7 mol%, and small quantities of 3HA (more than 5 carbons). Interestingly, all samples fed with avocado oil contained identifiable 3HV monomers and the presence of these monomers was highly correlated with the oil concentration in the medium. In some manner, the particular fatty acid composition of the avocado oil seems to promote the formation of 3HV precursors. Although Ganzeveld et al. [19] used centrifuged fermented organic waste and Liu et al. [20] employed palm oil to produce the same copolymer reported in this work (PHBV), the incorporation of 3HV monomers has not been sufficiently investigated when vegetable oils are used as the substrate (Table 3).

The thermal properties of the PHAs were enhanced by the presence of 3HV monomers in the polymer. As reported by Babel and Steinbüchel [11], T_m depends on the percentage of 3HV incorporated into the polymer. The melting temperature of the synthesized PHAs ranged from 159 to 173°C, in accordance with the 3HV mol% content (1 to 7 mol%). The presence of 3HV units in the polymer and even the small quantities of other 3HA improved the general thermal properties of PHA. Consequently, avocado oil as the substrate for PHA synthesis promoted the production of a more versatile material than what was obtained with pure PHB [43, 44], as demonstrated by DSC, FTIR, and GC analysis.

5. Conclusions

C. necator H16 is capable of incorporating small quantities of 3HV units into a PHA copolymer when avocado oil is used as substrate for PHA synthesis. The PHAs exhibited different monomeric compositions and properties, depending on the concentration of added oil. However, the highest yield, with a greater incorporation of larger monomer units (HV and more), was obtained when 20% (v/v) oil was added. Incorporation ranging from 1 to 7 mol% of 3HV monomeric units into the polymeric main chain was demonstrated. The results confirmed the feasibility of using avocado oil as a renewable carbon source for PHA production processes.

Disclosure

Partial results of this manuscript were presented as an abstract at the 9th Congress of FEBiotec (Annual Congress of Biotechnology).

Conflicts of Interest

The authors declare that they have no conflicts of interest.

Acknowledgments

Araceli Flores-Sánchez received grant-aided support from CONACyT (no. 417745). This research was partially funded by CONACyT (CONACyT-INFR-2015-254437 and CONACyT-CB-2014-239553). The authors acknowledge Alba-Flores Joel's (CINVESTAV) technical assistance during experimental development. Support of Piliado-Hernández D.M. (ITESM) and González-Bret K. during the writing of this manuscript was also appreciated.

References

[1] C. S. K. Reddy, R. Ghai, Rashmi, and V. C. Kalia, "Polyhydroxyalkanoates: an overview," *Bioresource Technology*, vol. 87, no. 2, pp. 137–146, 2003.

[2] M. V. Arcos-Hernández, B. Laycock, B. C. Donose et al., "Physicochemical and mechanical properties of mixed culture polyhydroxyalkanoate (PHBV)," *European Polymer Journal*, vol. 49, no. 4, pp. 904–913, 2013.

[3] J. Yu and Y. Si, "Metabolic carbon fluxes and biosynthesis of polyhydroxyalkanoates in Ralstonia eutropha on short chain fatty acids," *Biotechnology Progress*, vol. 20, no. 4, pp. 1015–1024, 2004.

[4] N.-S. Lau, D. H.-E. Ch'ng, K.-H. Chia, Y.-M. Wong, and K. Sudesh, "Advances in polyhydroxyalkanoate (PHA): Unraveling the development and new perspectives," *Journal of Biobased Materials and Bioenergy*, vol. 8, no. 2, pp. 118–129, 2014.

[5] E. Gasser, P. Ballmann, S. Dröge, J. Bohn, and H. König, "Microbial production of biopolymers from the renewable resource wheat straw," *Journal of Applied Microbiology*, vol. 117, no. 4, pp. 1035–1044, 2014.

[6] M. R. López-Cuellar, J. Alba-Flores, J. N. G. Rodríguez, and F. Pérez-Guevara, "Production of polyhydroxyalkanoates (PHAs) with canola oil as carbon source," *International Journal of Biological Macromolecules*, vol. 48, no. 1, pp. 74–80, 2011.

[7] R. Moita Fidalgo, J. Ortigueira, A. Freches et al., "Bio-oil upgrading strategies to improve PHA production from selected aerobic mixed cultures," *New Biotechnology*, vol. 31, no. 4, pp. 297–307, 2014.

[8] K. Sudesh, H. Abe, and Y. Doi, "Synthesis, structure and properties of polyhydroxyalkanoates: biological polyesters," *Progress in Polymer Science*, vol. 25, no. 10, pp. 1503–1555, 2000.

[9] B. Laycock, P. Halley, S. Pratt, A. Werker, and P. Lant, "The chemomechanical properties of microbial polyhydroxyalkanoates," *Progress in Polymer Science*, vol. 39, no. 2, pp. 397–442, 2014.

[10] L. M. W. K. Gunaratne, R. A. Shanks, and G. Amarasinghe, "Thermal history effects on crystallisation and melting of poly(3-hydroxybutyrate)," *Thermochimica Acta*, vol. 423, no. 1-2, pp. 127–135, 2004.

[11] W. Babel and A. Steinbüchel, *Biopolyesters. Special issue of advances in Biochem. Eng. Biotechnology*, Springer-Verlag, Berlin, Germany, 2001.

[12] J. Yu and H. Stahl, "Microbial utilization and biopolyester synthesis of bagasse hydrolysates," *Bioresource Technology*, vol. 99, no. 17, pp. 8042–8048, 2008.

[13] F. Fang, H. Jiang, J. Wang, and H.-Q. Yu, "Identifying the influential priority of the factors governing PHB production by activated sludge with integration of uniform design and grey relational analysis," *Separation and Purification Technology*, vol. 136, pp. 111–114, 2014.

[14] S. Anterrieu, L. Quadri, B. Geurkink et al., "Integration of biopolymer production with process water treatment at a sugar factory," *New Biotechnology*, vol. 31, no. 4, pp. 308–323, 2014.

[15] M. Venkateswar Reddy, Y. Yajima, Y. Mawatari, T. Hoshino, and Y.-C. Chang, "Degradation and conversion of toxic compounds into useful bioplastics by Cupriavidus sp. CY-1: relative expression of the PhaC gene under phenol and nitrogen stress," *Green Chemistry*, vol. 17, no. 9, pp. 4560–4569, 2015.

[16] A. F. Mohidin Batcha, D. M. R. Prasad, M. R. Khan, and H. Abdullah, "Biosynthesis of poly(3-hydroxybutyrate) (PHB) by Cupriavidus necator H16 from jatropha oil as carbon source," *Bioprocess and Biosystems Engineering*, vol. 37, no. 5, pp. 943–951, 2014.

[17] T. Fukui and Y. Doi, "Efficient production of polyhydroxyalkanoates from plant oils by Alcaligenes eutrophus and its recombinant strain," *Applied Microbiology and Biotechnology*, vol. 49, no. 3, pp. 333–336, 1998.

[18] D. Dennis, M. McCoy, A. Stangl, H. E. Valentin, and Z. Wu, "Formation of poly(3-hydroxybutyrate-co-3-hydroxyhexanoate) by PHA synthase from Ralstonia eutropha," *Journal of Biotechnology*, vol. 64, no. 2-3, pp. 177–186, 1998.

[19] K. J. Ganzeveld, A. Van Hagen, M. H. Van Agteren, W. De Koning, and A. J. M. S. Uiterkamp, "Upgrading of organic waste: production of the copolymer poly-3-hydroxybutyrate-co-valerate by Ralstonia eutrophus withorganic waste as sole carbon source," *Journal of Cleaner Production*, vol. 7, no. 6, pp. 413–419, 1999.

[20] Q. Liu, G. Luo, X. R. Zhou, and G.-Q. Chen, "Biosynthesis of poly(3-hydroxydecanoate) and 3-hydroxydodecanoate dominating polyhydroxyalkanoates by β-oxidation pathway inhibited Pseudomonas putida," *Metabolic Engineering*, vol. 13, no. 1, pp. 11–17, 2011.

[21] A. Rathinasabapathy, B. A. Ramsay, J. A. Ramsay, and F. Pérez-Guevara, "A feeding strategy for incorporation of canola derived medium-chain-length monomers into the PHA produced by wild-type Cupriavidus necator," *World Journal of Microbiology and Biotechnology*, vol. 30, no. 4, pp. 1409–1416, 2014.

[22] M. A. Hassan, L.-N. Yee, P. L. Yee et al., "Sustainable production of polyhydroxyalkanoates from renewable oil-palm biomass," *Biomass and Bioenergy*, vol. 50, pp. 1–9, 2013.

[23] S. Magdouli, S. K. Brar, J. F. Blais, and R. D. Tyagi, "How to direct the fatty acid biosynthesis towards polyhydroxyalkanoates production?" *Biomass and Bioenergy*, vol. 74, pp. 268–279, 2015.

[24] L. Shi and B. P. Tu, "Acetyl-CoA and the regulation of metabolism: mechanisms and consequences," *Current Opinion in Cell Biology*, vol. 33, pp. 125–131, 2015.

[25] R. A. J. Verlinden, D. J. Hill, M. A. Kenward, C. D. Williams, and I. Radecka, "Bacterial synthesis of biodegradable polyhydroxyalkanoates," *Journal of Applied Microbiology*, vol. 102, no. 6, pp. 1437–1449, 2007.

[26] M. d. Galvão, N. Narain, and N. Nigam, "Influence of different cultivars on oil quality and chemical characteristics of avocado fruit," *Food Science and Technology (Campinas)*, vol. 34, no. 3, pp. 539–546, 2014.

[27] L. González, *México es productor global montruo de aguacate:Grayeb*, The Economist, 2015.

[28] M. L. Dreher and A. J. Davenport, "Hass avocado composition and potential health effects," *Critical Reviews in Food Science and Nutrition*, vol. 53, no. 7, pp. 738–750, 2013.

[29] G. L. Miller, "Use of dinitrosalicylic acid reagent for determination of reducing sugar," *Analytical Chemistry*, vol. 31, no. 3, pp. 426–428, 1959.

[30] M. W. Weatherburn, "Phenol-hypochlorite reaction for determination of ammonia," *Analytical Chemistry*, vol. 39, no. 8, pp. 971–974, 1967.

[31] I. Chodak, "Polyhydroxyalkanoates: properties and modification for high volume applications," in *Degradable Polymers*, pp. 295–319, Springer, Dordrecht, 2002.

[32] M. Koller, A. Salerno, M. Dias, A. Reiterer, and G. Braunegg, "Modern biotechnological polymer synthesis: a review," *Food Technology and Biotechnology*, vol. 48, no. 3, pp. 255–269, 2010.

[33] K. Ichihara and Y. Fukubayashi, "Preparation of fatty acid methyl esters for gas-liquid chromatography," *Journal of Lipid Research*, vol. 51, no. 3, pp. 635–640, 2010.

[34] W. Babel and A. Steinbüchel, *Biopolyesters*, vol. 71, Springer, 2003.

[35] T. Mumtaz, S. Abd-Aziz, P. L. Yee, W. M. Z. W. Yunus, Y. Shirai, and M. A. Hassan, "Synthesis, characterization, and structural properties of intracellular copolyester poly(3-hydroxybutyrate-co-3-hydroxyvalerate) produced by comamonas sp. EB 172 from renewable resource," *International Journal of Polymer Analysis and Characterization*, vol. 15, no. 6, pp. 329–340, 2010.

[36] K. Hong, S. Sun, W. Tian, G. Q. Chen, and W. Huang, "A rapid method for detecting bacterial polyhydroxyalkanoates in intact cells by Fourier transform infrared spectroscopy," *Applied Microbiology and Biotechnology*, vol. 51, no. 4, pp. 523–526, 1999.

[37] T. Furukawa, H. Sato, R. Murakami et al., "Structure, dispersibility, and crystallinity of poly(hydroxybutyrate)/ poly(L-lactic acid) blends studied by FT-IR microspectroscopy and differential scanning calorimetry," *Macromolecules*, vol. 38, no. 15, pp. 6445–6454, 2005.

[38] C.-Y. Loo, W.-H. Lee, T. Tsuge, Y. Doi, and K. Sudesh, "Biosynthesis and characterization of poly(3-hydroxybutyrate-co-3- hydroxyhexanoate) from palm oil products in a Wautersia

eutropha mutant," *Biotechnology Letters*, vol. 27, no. 18, pp. 1405–1410, 2005.

[39] B. S. Kim, S. C. Lee, S. Y. Lee, H. N. Chang, Y. K. Chang, and S. I. Woo, "Production of poly(3-hydroxybutyric-co-3-hydroxyvaleric acid) by fed-batch culture of Alcaligenes eutrophus with substrate control using on-line glucose analyzer," *Enzyme and Microbial Technology*, vol. 16, no. 7, pp. 556–561, 1994.

[40] F. Garcia-Ochoa and E. Gomez, "Bioreactor scale-up and oxygen transfer rate in microbial processes: an overview," *Biotechnology Advances*, vol. 27, no. 2, pp. 153–176, 2009.

[41] F. C. Oliveira, D. M. G. Freire, and L. R. Castilho, "Production of poly(3-hydroxybutyrate) by solid-state fermentation with Ralstonia eutropha," *Biotechnology Letters*, vol. 26, no. 24, pp. 1851–1855, 2004.

[42] G. Du, L. X. L. Chen, and J. Yu, "High-efficiency production of bioplastics from biodegradable organic solids," *Journal of Polymers and the Environment*, vol. 12, no. 2, pp. 89–94, 2004.

[43] A. J. Anderson and E. A. Dawes, "Occurrence, metabolism, metabolic role, and industrial uses of bacterial polyhydroxyalkanoates," *Microbiological Reviews*, vol. 54, no. 4, pp. 450–472, 1990.

[44] S. Bengtsson, A. R. Pisco, M. A. M. Reis, and P. C. Lemos, "Production of polyhydroxyalkanoates from fermented sugar cane molasses by a mixed culture enriched in glycogen accumulating organisms," *Journal of Biotechnology*, vol. 145, no. 3, pp. 253–263, 2010.

Hindawi
International Journal of Polymer Science
Volume 2017, Article ID 1846031, 6 pages
https://doi.org/10.1155/2017/1846031

Research Article

UV Radiation Induced Cross-Linking of Whey Protein Isolate-Based Films

Markus Schmid,[1,2] Tobias Konrad Prinz,[1] Kerstin Müller,[1] and Andreas Haas[1]

[1]*Fraunhofer Institute for Process Engineering and Packaging IVV, Giggenhauser Strasse 35, 85354 Freising, Germany*
[2]*Chair for Food Packaging Technology, Technische Universität München, Weihenstephaner Steig 22, 85354 Freising, Germany*

Correspondence should be addressed to Markus Schmid; markus.schmid@ivv.fraunhofer.de

Received 11 April 2017; Accepted 9 May 2017; Published 4 June 2017

Academic Editor: Raffaele Cucciniello

Casted whey protein films exposed to ultraviolet irradiation were analyzed for their cross-linking properties and mechanical and barrier performance. Expected mechanical and barrier improvements are discussed with regard to quantification of the cross-linking in the UV-treated whey protein films. Swelling tests were used to determine the degree of swelling, degree of cross-linking, and cross-linking density. When the UV radiation dosage was raised, a significant increase of the tensile strength as well as an increase in Young's modulus was observed. No significant changes in water vapor and oxygen barrier properties between the UV-treated films and an untreated reference sample could be observed. The cross-linking density and the degree of cross-linking significantly increased due to UV radiation. Combined results indicate a disordered protein network in cast films showing locally free volume and therefore only minor mechanical and barrier improvements.

1. Introduction

Packaging materials are designed to enable long shelf life and maintain the quality of packaged products [1]. Due to the growing awareness of the consumers and the industry, the development of biopolymers increased in recent years. Those also include biodegradable packaging materials from renewable raw materials such as wheat gluten, soy protein, casein, or whey proteins [2]. Whey protein isolate- (WPI-) based films showed high barrier performance against oxygen, leading to suitable biomaterials for packaging applications [3]. WPI consists of different whey proteins, linked by thermal, chemical, biochemical, and/or physical treatments [4], such as ultraviolet (UV) irradiation. Double bonds, including aromatic rings of amino acids like tyrosine or phenylalanine, can absorb UV radiation, followed by the formation of free radicals and intermolecular covalent bonds [5, 6]. Films derived from soy protein, corn zein, wheat gluten, peanut protein, fish gelatin, egg albumin, sodium caseinate, and whey protein have been treated with UV radiation [5–12], mainly stating various changes in final film properties. However, there is very little information on the structural changes such as UV-light-induced cross-linking mechanisms in protein films. Therefore, the objective of this work was to evaluate cross-linking properties of whey protein-based cast films depending on applied UV radiation doses. Furthermore, this study offers a direct approach for the quantification of cross-linking in protein films. Besides the determined cross-linking parameters, structure dependent properties such as mechanical and barrier performance were analyzed and discussed.

2. Materials and Methods

2.1. Cast Films. A glycerol plasticized denatured whey protein standard solution (WPSS) containing 10% (w/w) WPI was prepared according to the procedure developed by Schmid et al. [3]. Films were casted into Petri dishes with a target thickness of 50 μm (final thicknesses were 39 ± 16.1 μm) and dried at ambient conditions in a climate chamber at 23°C and 50% RH until equilibrium was proved by constant weight.

2.2. Thickness Measurement. For density calculation, mechanical and barrier tests and thickness measurements were performed with a precision thickness gauge FT3 (Rhopoint

Table 1: List of the processed samples with indicated dose of UV-C (per side) and exposure time (per side).

Sample name	Dose of UV-C (per side) [J/cm^2]	Radiation time (per side) [min]
UV_0	0	0
UV_5	1,2 ± 0,3	5
UV_10	2,8 ± 0,2	10
UV_50	11,6 ± 0,3	50
UV_100	19,9 ± 0,1	100
UV_200	42 ± 3,3	200

Instruments, Bexhill-on-Sea, UK) using average values of five random positions around the film testing area of each specimen.

2.3. Ultraviolet Radiation Treatment. For UV radiation treatment, casted films were placed under a UV cartridge (Heraeus Noblelight GmbH, Hanau, Germany). The distance between the sample and the UV source was set to 70 mm. The experimental setup of the ultraviolet radiation was installed in a metal housing to protect the operator from the radiation following the configuration by Schmid et al. [12].

Films were radiated on both sides. In order to stabilize the intensity of the ultraviolet radiation, the lamp was switched on at least five minutes before the samples were inserted. The UV dose determined with a UV Power Puck (Electronic Instrumentation and Technology Inc., Sterling, USA) and the applied radiation times are listed in Table 1. According to own measurements, the UV-C radiation intensity at the center of the housing was 0.05 ± 0.01 [W/cm^2]. In addition, a temperature increase of up to 50°C was determined. The measurement was accomplished with an iButton (Maxim Integrated, San Jose, USA). After the radiation process, the films were stored at 23°C and 50% RH prior to further characterization.

2.4. Determination of the Degree of Swelling, Degree of Cross-Linking, and the Cross-Linking Density. To determine the degree of swelling (DoS), the degree of cross-linking (DoC), and the cross-linking density (CLD), swelling tests were performed according to the methods described by Schmid et al. [13] according to the DIN EN ISO 175:2000. The casted and dried films were cut to 50 mm × 50 mm and weighed. After the addition of 288 mL of distilled water (23°C), the samples were stored for 24 hours at 23°C and 50% RH. Adherent liquid was removed and films were dried at 65°C and high air circulation until constant weight. The DoS [%] was then calculated as follows [13]:

$$\mathrm{DoS} = \frac{m_2 - m_3}{m_3} \cdot 100, \tag{1}$$

where m_2 is the film mass after the swelling process [g] and m_3 is the film mass after the complete drying process [g]. CLD and DoC were determined using water vapor sorption isotherms measured with a SPS sorption test system SPS-1μ High Load (ProUmid GmbH, Ulm, Germany) at a temperature of 23°C with ascending and descending humidities from 0 to 90% RH and 90 to 0% RH, respectively, using steps of 10% RH. The DoC [%] was calculated using the following formula [13]:

$$\mathrm{DoC} = \frac{\overline{M_0}}{M_C}, \tag{2}$$

where $\overline{M_0}$ [g/mol] is the molecular weight of the average amino acids in WPI and M_C [g/mol] is the average molecular weight of the polymer between the cross-links. The applied $\overline{M_0}$ was 123.3 [g/mol] [13]. The CLD is defined as

$$\mathrm{CLD} = \frac{1}{M_C}, \tag{3}$$

where M_C is the average molecular weight of the polymer between the cross-links [g/mol].

M_C is determined with the help of swelling experiments and calculated with the equation of Flory-Rehner [14–16]:

$$M_c = -\frac{\rho_{\mathrm{WPI}} \cdot V_2 \cdot \left(\varphi_1{}^{1/3} - \varphi_1/2\right)}{\ln\left(1-\varphi_1\right) + \varphi_1 + \chi \cdot \varphi_1{}^2}, \tag{4}$$

where V_2 [cm^3 ∗ mol^{-1}] is the molar volume of the deionized water, ρ_{WPI} (1.40 ± 0.06 [g∗cm^{-3}]) is the film density (evaluated following [17]), φ_1 [−] is the volume fraction of the polymer in the swollen gel, and χ is the interaction parameter of the water and the WPI.

The volume fraction of the polymer in the swollen gel φ_1 is defined as

$$\varphi_1 = \frac{m_{\mathrm{WPI}}/\rho_{\mathrm{WPI}}}{m_{\mathrm{WPI}}/\rho_{\mathrm{WPI}} + m_s/\rho_s}, \tag{5}$$

where m_{WPI} [g] is the polymer mass in the swollen gel, ρ_{WPI} [g∗cm^{-3}] is the film density, m_s [g] is the mass of water in the swollen gel, and ρ_s [g∗cm^{-3}] is the water density.

The Flory-Huggins equation was fitted with the least squares method to the determined water vapor sorption isotherms with the help of the Excel solver tool (Microsoft Office Professional Plus 2010, Version 14.0.7177.5000). This is essential to determine the interaction parameter χ. The Flory-Huggins equation [18, 19] is

$$\frac{\Delta\mu^{\mathrm{mix}}}{RT} = \ln a_w = \ln\left(1-\varphi_1\right) + \varphi_1 + \chi \cdot \varphi_1{}^2, \tag{6}$$

where $\Delta\mu^{\mathrm{mix}}$ [J ∗ mol^{-1} ∗ K^{-1}] is the chemical potential difference of the WPI film and water, R is the ideal gas constant [J ∗ mol^{-1} ∗ K^{-1}], T is the temperature [K], φ_1 [−] is the volume fraction of the polymer in the swollen gel, and χ [−] is the interaction parameter.

2.5. Determination of Mechanical Properties. Tensile strength, elongation at break, and Young's modulus were determined using a tensile testing machine Z005 (Zwick GmbH & Co. KG, Ulm, Germany) according to DIN EN ISO 527-1.

For the measurement, ten sample strips of 15 mm width were cut out of the films and clamped into the testing machine at 23°C and 50% RH. The clamping length was set to 50 mm and the applied force was 50 N until breakage with a testing speed of 100 mm/min. Young's modulus was measured with a testing speed of 0.5 mm/min.

2.6. Determination of Barrier Properties. Water vapor transmission rate (WVTR) was measured at 23°C and a decreasing relative humidity from 50% to 0% with a gravimetric method according to DIN 53122-1 with a fourfold determination [20]. Specimens were weighed four times in 48 hours when constant weight was reached. The water vapor transmission rate was calculated with

$$\mathrm{WVP} = \frac{\mathrm{WVTR}}{\Delta p\left(\mathrm{H_2O}\right)} * d, \tag{7}$$

where WVP is the water vapor permeation coefficient [g μm m^{-2} d^{-1} bar^{-1}], WVTR is the water vapor transmission rate [g m^{-2} d^{-1}], $\Delta p(\mathrm{H_2O})$ is the partial pressure difference between the two chambers [bar], and d is the thickness of the film [μm].

Oxygen permeability (OP) was measured at 23°C and 50% RH according to DIN 53380-3 with an OX-Tran Twin Oxygen Permeation Measuring Machine (MOCON Inc. World Headquarters, Minneapolis, USA). An oxygen permeation coefficient (OP) [cm^3 m^{-2} d^{-1} bar^{-1}] was applied which is defined as the oxygen transmission rate (OTR) in relation to the partial pressure $\Delta p(\mathrm{O_2})$ [bar] between both sides of the film, multiplied by its thickness d [μm] [20]:

$$\mathrm{OP} = \frac{\mathrm{OTR}}{\Delta p\left(\mathrm{O_2}\right)} * d. \tag{8}$$

2.7. Statistical Evaluation. All statistical tests were performed with the software Visual-XSel® Version 12.1 (CRGRAPH GbR, Starnberg, Germany). Except for oxygen permeability measurements (twofold determination), all sample sets were checked on normal distribution. According to the number of repeated measurements, different normality tests were applied which were the Kolmogorov-Smirnov test (sample size ≤ 4) or the Anderson-Darling normality test (sample size ≥ 5). The tests were performed with a significance value (α) of 0.05 [21]. For sample comparison, a multi-t-test was performed with a significance value of 0.05. Significant differences between samples detected with the multi-t-test are marked by different letters within figures and tables.

3. Results and Discussion

3.1. Intermolecular Characteristics

3.1.1. Cross-Linking Density and Degree of Cross-Linking. Figure 1 shows CLD and DoC values depending on the applied UV dose as well as a nonradiated reference.

Except for samples with a radiation time of 5 and 50 min, radiated samples showed significantly higher CLD and DoC values compared to the reference sample. Due to high standard deviations, the other samples do not differ significantly among each other. High deviations probably resulted from difficult handling of the thin films. DoC and CLD increase with a rising radiation dose. The highest CLD and DoC were determined with a UV-C dose of 19.9 J/cm^2 with a CLD of about 110 $*$ 10^{-4} mol/cm^3. Up to now, only few comparable studies are known to the authors dealing with cross-linking properties of whey protein-based cast films. However, since natural rubber is also cross-linked via disulfide bridges and shows similar mechanical behavior, results described by Ahmed et al. [22] are chosen for comparison. The CLD of natural rubber of 2.0 $*$ 10^{-4} mol/cm^3 is significantly exceeded compared to the CLD of the whey protein standard formulation with 18 $*$ 10^{-4} mol/cm^3. Previous studies on whey protein films determined a cross-linking density of 1.7 $*$ 10^{-4} mol/cm^3 for the standard whey protein formulation [13]. The deviation of the measured values from the literature values is caused by several influencing factors. The most influencing factor is the volume fraction of the polymer in the swollen gel, which is determined by swelling experiments. It has a particularly high influence on the average molecular weight of the polymer between the cross-links (M_C), the degree of cross-linking, and the cross-linking density. It is stated that UV radiation significantly increases the cross-linking between the protein fractions at a radiation time of 10 min. Schmid et al. [12] concluded that a large proportion of the cross-linkages are already linked during the first 10 min of radiation. It is assumed that the required energy for the formation of radicals is already present at a dose of about 3 J/cm^2, resulting in protein cross-linking by a chain-growing process, which was qualitatively confirmed in this study with the methods described by Schmid et al. [12].

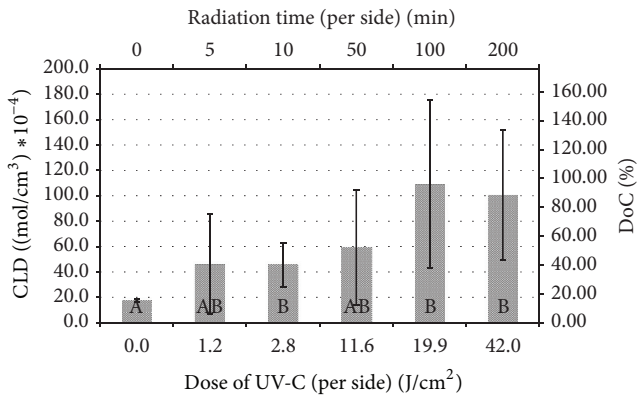

Figure 1: Influence of UV radiation dose and respective radiation time on DoC and CLD of WPI-based cast films. Bars with different letters are significantly different ($p < 0.05$).

3.1.2. Degree of Swelling. The DoS (see Figure 2) of the radiated samples behaves contrarily to the DoC and CLD. The reference sample has the highest DoS value with about 210%, while DoS tends to decrease with an increasing UV-C dose. This effect is consistent with the investigations

Table 2: Mechanical properties of UV-treated WPI-based films as a function of UV dose and radiation time; significant differences are indicated by different letters ($p < 0.05$).

UV-C dose (per side) [J/cm^2]	Radiation time (per side) [min]	Young's modulus [MPa]	Tensile strength [MPa]	Elongation at break* [%]
0.0	0	69.8 ± 52.4^{ab}	4.52 ± 0.75^{a}	23.7 ± 20.1^{ab}
1.2	5	65.1 ± 15.7^{a}	4.32 ± 0.25^{a}	43.2 ± 19.7^{a}
2.8	10	65.7 ± 31.7^{a}	6.38 ± 0.57^{b}	42.6 ± 30.6^{ab}
11.6	50	114.5 ± 44.3^{ab}	7.39 ± 0.67^{c}	25.5 ± 7.0^{ab}
19.9	100	112.8 ± 22.5^{b}	7.58 ± 0.51^{c}	30.7 ± 12.1^{a}
42.0	200	227.7 ± 149.5^{ab}	13.61 ± 3.64^{d}	14.1 ± 9.1^{b}

*Layer thicknesses in μm according to the increasing radiation time: 47.0 ± 8.2, 49.2 ± 9.3, 48.4 ± 8.0, 38.0 ± 5.7, 49.3 ± 9.9, and 37.5 ± 7.9.

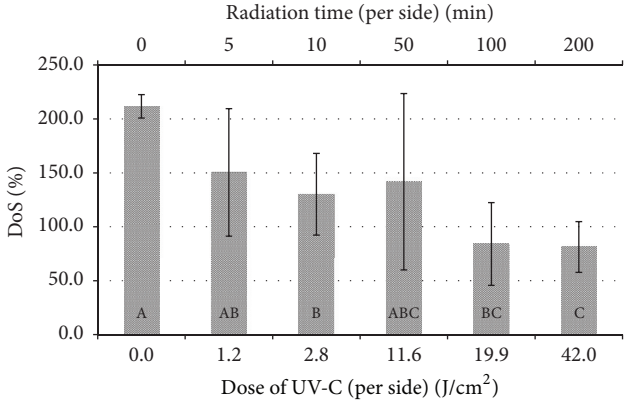

Figure 2: Degree of swelling as a function of the UV dose and the radiation time; bars with different letters are significantly different ($p < 0.05$).

of Schmidt et al. [23], who stated that an increasing proportion of cross-links within the polymer structure leads to a decreasing swelling capability. The behavior is attributed to the decreasing free volume with an increasing cross-linking density in the polymer network. Comparing the determined DoS of the WPI films with those of natural rubber (of about 370% according to Ahmed et al. [22]), the DoS of the standard whey protein formulation were reduced by half. The radiated samples have lower values, especially at a radiation time of 200 min with a degree of swelling of about 80%, indicating cross-linking reactions. It should be noted that, compared to the reference, the DoS of the film which was treated with a radiation time of 10 min is significantly lower.

3.2. Mechanical Properties. Mechanical data of all samples can be seen in Table 2. Young's modulus of the prepared films shows almost no significant differences between the samples, except for the sample with a radiation time of 100 min, at which Young's modulus is significantly higher than Young's modulus of the samples with radiation times of 5 or 10 min. Due to high standard deviations, only few statistical differences could be detected. However, a general increase of the mean Young's moduli with an increased UV-C dose can be observed. Ustunol and Mert [24] stated that UV radiation of the film-forming solution has no significant effect on Young's modulus. Young's modulus of the UV-treated cast films has been studied by Schmid et al. [12], who can partly confirm this effect. This means that a significant increase could be observed when measuring in the cross direction, but not in machine direction. During the coating process, protein molecules are oriented in machine direction. Therefore, cross-links between the protein chains rather occur in cross direction. An explanation of the polymer orientation effect is described in Figure 3.

Figure 3 shows that, in the extreme case, the cast film can only form cross-links between the ends of the polymer chains. The forming of cross-links along the polymer chains results in a high Young's modulus. Polymer orientation does not occur in cast films, but a disordered network is present. This is the reason why the film can be stressed equally in all directions. The polymer chains interfere with each other, resulting in a big distance between them. Then, the proteins are not able to form cross-links anymore and the free volume of the films increases. In addition, the films are about twice as thick as the coatings described by Schmid et al. [12]. The films were radiated on both sides to compensate for the higher layer thickness. Díaz et al. [7] radiated non-heat-treated whey protein concentrate cast films with a significantly higher layer thickness of 120–145 μm on only one film side with doses of up to 12 J/cm^2, without any significant effect on Young's modulus. This is probably caused by the low UV dose (2.8 J/cm^2; 25 μm; 0.0 J/cm^2).

The tensile strength of the UV cross-linked films increased significantly with an increasing radiation time and dose. The tensile strength of the sample which was treated with a UV-C dose of 1.2 J/cm^2 did not increase compared to the reference sample. These results confirm the investigations of Schmid et al. [12] about UV-radiated coatings, who tested their peeled-off coatings in machine direction. The usage of cast films (where the protein molecules are disordered in the film) leads to cross-linking at different positions. This creates a chaotic network where the tensile strength increases with an increasing degree of cross-linking. Díaz et al. [7] also observed an increase of the tensile strength at radiated cast films.

Due to high standard deviations, elongation at break measurements showed no significant differences between the films, except for the film with 200-minute treatment. The elongation at break of this sample is significantly lower than

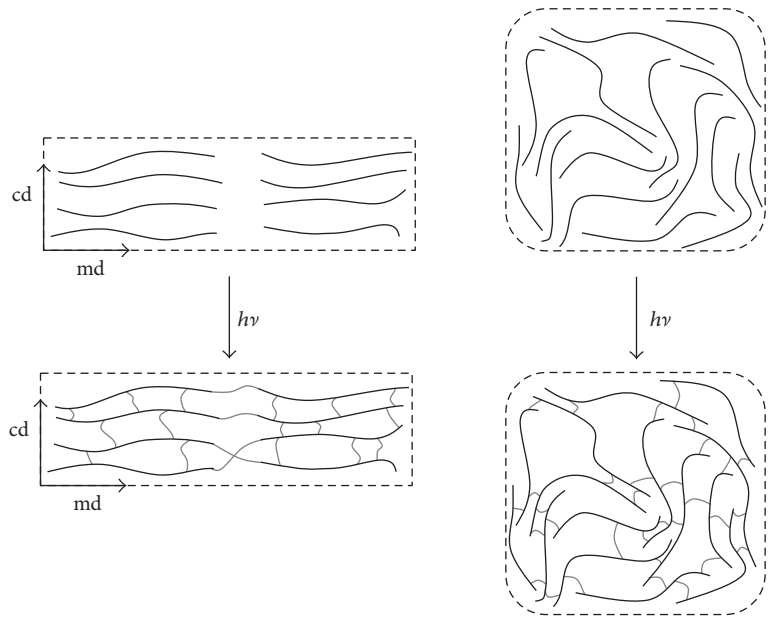

Figure 3: Film morphology of WPSS coatings (cd: cross direction; md: machine direction; adapted from Schmid et al. [12]) and cast films after UV radiation; the figure shows the additional covalent intermolecular interactions induced by UV radiation; disulfide bonds are not shown.

of the samples which were radiated for 5 or 100 min. The film thicknesses are not considered during the measurement of the elongation at break. Compared to the other samples, the films (radiated for 50 or 200 min) which have lower elongation at break are up to 20% thinner. These results are confirmed by Schmid et al. [12] as well as Díaz et al. [7], who showed that the UV radiation has no significant influence on the elongation at break.

3.3. Barrier Properties. Water vapor transmission rate and oxygen permeability of UV-radiated samples as well as the reference sample are shown in Table 3. There were no significant differences between the samples. No significant differences between the film samples were detectable, concluding that UV radiation has no significant effect on the water vapor transmission rate of whey protein cast films. Ustunol and Mert [24] stated the same conclusion, but they worked with a radiated film-forming solution and not with radiated dry whey protein films. Díaz et al. [7], who observed WPC cast films, did not detect any significant influence of the UV radiation on the water vapor transmission rate. This could also be explained by a disordered protein network where cross-links only occur at the end of the polymer chains (Figure 3). For the diffusion path of the water vapor molecules, these cross-links are negligible since the pathway is rather oriented at the free volume sections between the polymer chains.

The same could be applied for oxygen permeability, since results of the samples also differ minimally from each other; only the sample which was radiated for 5 min shows an increased OP. This would correspond to the results of Schmid et al. [12], who did not detect any significant change in the oxygen barrier by UV-radiated coatings.

Table 3: Water vapor transmission rate and oxygen permeability normalized to 100 μm film thickness as a function of the UV dose. Different letters indicate significant differences ($p < 0.05$).

UV-C dose (per side) [J/cm^2]	Radiation time (per side) [min]	Water vapor transmission rate Q_{100} [g/(m^2 d)]	Oxygen permeability* Q_{100} [cm^3/(m^2 d bar)]
0.0	0	92.7 ± 44.0[a]	11.4 ± 3.1
1.2	5	48.1 ± 11.7[a]	24.3 ± 8.5
2.8	10	48.0 ± 17.5[a]	16.5 ± 4.1
11.6	50	59.1 ± 22.4[a]	16.0 ± 2.1
19.9	100	61.8 ± 18.9[a]	17.0 ± 4.9
42.0	200	44.5 ± 8.2[a]	13.9 ± 2.0

*Twofold determination. Mean of minimum and maximum value.

4. Conclusion

The UV cross-linked films show a significant increase in the tensile strength from 4.52 MPa (reference sample) to 13.61 MPa after 200 min of radiation and to 6.38 MPa after 10 min of radiation. A trend increase is present in Young's modulus with an increasing radiation process. The film treatment with UV radiation did not lead to a significant change of the barrier properties. One possible reason for this occurrence is that the polymers in casting films are present in a disordered network, resulting in locally free volumes. These volumes offer a small diffusion barrier to oxygen and water molecules. The cross-linking density and degree of cross-linking increased significantly, while the degree of swelling was significantly reduced by UV radiation. The CLD increased from $17.7 * 10^{-4}$ (mol/cm^3) of the UV reference to

$108.9 * 10^{-4}$ (mol/cm^3) of the sample which was treated with a UV dose of 19.9 J/cm^2 on both sides. All in all, the developed methods can provide cross-linking quantification and can be further used to elucidate the morphology of protein network in whey protein films.

Conflicts of Interest

The authors declare no conflicts of interest regarding the publication of this paper.

Acknowledgments

This work was supported by the German Research Foundation (DFG) and the Technische Universität München within the funding programme Open Access Publishing. The authors wish to acknowledge the support of all involved colleagues in the Materials Development and Process Engineering Departments at Fraunhofer IVV. Special thanks are extended to Zuzana Scheuerer and Marius Jesdinszki for their outstanding support.

References

[1] J. Multon, "The role of packaging in preserving foodstuffs," Food Packaging Technology, 1, 3–23, 1996.

[2] M.-B. Coltelli, F. Wild, E. Bugnicourt et al., "State of the art in the development and properties of protein-based films and coatings and their applicability to cellulose based products: an extensive review," *Coatings*, vol. 6, no. 1, p. 1, 2016.

[3] M. Schmid, K. Dallmann, and E. Bugnicourt, "Properties of whey-protein-coated films and laminates as novel recyclable food packaging materials with excellent barrier properties," *International Journal of Polymer Science*, vol. 2012, Article ID 562381, 7 pages, 2012.

[4] M. Wihodo and C. I. Moraru, "Physical and chemical methods used to enhance the structure and mechanical properties of protein films: a review," *Journal of Food Engineering*, vol. 114, no. 3, pp. 292–302, 2013.

[5] A. Gennadios, J. W. Rhim, A. Handa, C. L. Weller, and M. A. Hanna, "Ultraviolet radiation affects physical and molecular properties of soy protein films," *Journal of Food Science*, vol. 63, no. 2, pp. 225–228, 1998.

[6] J. W. Rhim, A. Gennadios, D. Fu, C. L. Weller, and M. A. Hanna, "Properties of ultraviolet irradiated protein films," *LWT—Food Science and Technology*, vol. 32, no. 3, pp. 129–133, 1999.

[7] O. Díaz, D. Candia, and Á. Cobos, "Effects of ultraviolet radiation on properties of films from whey protein concentrate treated before or after film formation," *Food Hydrocolloids*, vol. 55, pp. 189–199, 2016.

[8] C.-C. Liu, A. M. Tellez-Garay, and M. E. Castell-Perez, "Physical and mechanical properties of peanut protein films," *LWT—Food Science and Technology*, vol. 37, no. 7, pp. 731–738, 2004.

[9] V. Micard, R. Belamri, M.-H. Morel, and S. Guilbert, "Properties of chemically and physically treated wheat gluten films," *Journal of Agricultural and Food Chemistry*, vol. 48, no. 7, pp. 2948–2953, 2000.

[10] C. G. Otoni, R. J. Avena-Bustillos, B.-S. Chiou, C. Bilbao-Sainz, P. J. Bechtel, and T. H. McHugh, "Ultraviolet-B radiation induced cross-linking improves physical properties of cold- and warm-water fish gelatin gels and films," *Journal of Food Science*, vol. 77, no. 9, pp. E215–E223, 2012.

[11] J. W. Rhim, A. Gennadios, A. Handa, C. L. Weller, and M. A. Hanna, "Solubility, tensile, and color properties of modified soy protein isolate films," *Journal of Agricultural and Food Chemistry*, vol. 48, no. 10, pp. 4937–4941, 2000.

[12] M. Schmid, J. Held, F. Hammann, D. Schlemmer, and K. Noller, "Effect of UV-radiation on the packaging-related properties of whey protein isolate based films and coatings," *Packaging Technology and Science*, vol. 28, no. 10, pp. 883–899, 2015.

[13] M. Schmid, S. Pröls, D. M. Kainz, F. Hammann, and A. Stäbler, "Impact of hydrolyzed whey protein on the molecular interactions and cross-linking density in whey protein isolate-based films," *International Journal of Polymer Science*, vol. 2016, 9 pages, 2016.

[14] B. Isik and M. Kis, "Preparation and determination of swelling behavior of poly(acrylamide-co-acrylic acid) hydrogels in water," *Journal of Applied Polymer Science*, vol. 94, no. 4, pp. 1526–1531, 2004.

[15] E. Favre, Q. T. Nguyen, P. Schaetzel, R. Clément, and J. Néel, "Sorption of organic solvents into dense silicone membranes. Part 1.—validity and limitations of Flory-Huggins and related theories," *Journal of the Chemical Society, Faraday Transactions*, vol. 89, no. 24, pp. 4339–4346, 1993.

[16] J. L. Valentín, J. Carretero-González, I. Mora-Barrantes, W. Chassé, and K. Saalwächter, "Uncertainties in the determination of cross-link density by equilibrium swelling experiments in natural rubber," *Macromolecules*, vol. 41, no. 13, pp. 4717–4729, 2008.

[17] M. Schmid, S. Sängerlaub, L. Wege, and A. Stäbler, "Properties of transglutaminase crosslinked whey protein isolate coatings and cast films," *Packaging Technology and Science*, vol. 27, no. 10, pp. 799–817, 2014.

[18] P. J. Flory, "Themodynamics of high polymer solutions," *The Journal of Chemical Physics*, vol. 10, no. 1, pp. 51–61, 1942.

[19] M. L. Huggins, "Solutions of long chain compounds," *Journal of Chemical Physics*, vol. 9, no. 5, p. 440, 1941.

[20] G. F. Mehyar and J. H. Han, "Physical and mechanical properties of high-amylose rice and pea starch films as affected by relative humidity and plasticizer," *Journal of Food Science*, vol. 69, no. 9, pp. E449–E454, 2004.

[21] H. Holland and K. Scharnbacher, *Grundlagen statistischer WahrscheinlichkeitenKombinationen, Wahrscheinlichkeiten, Binomial- und Normalverteilung, Konfidenzintervalle, Hypothesentests*, Springer Gabler, Wiesbaden, Germany, 2004.

[22] K. Ahmed, S. S. Nizami, N. Z. Raza, and K. Mahmood, "Mechanical, swelling, and thermal aging properties of marble sludge-natural rubber composites," *International Journal of Industrial Chemistry*, vol. 3, no. 1, pp. 1–12, 2012.

[23] M. Schmidt, N. Rodler, O. Miesbauer et al., "Adhesion and barrier performance of novel barrier adhesives used in multi-layered high-barrier laminates," *Journal of Adhesion Science and Technology*, vol. 26, no. 20-21, pp. 2405–2436, 2012.

[24] Z. Ustunol and B. Mert, "Water solubility, mechanical, barrier, and thermal properties of cross-linked whey protein isolate-based films," *Journal of Food Science*, vol. 69, no. 3, pp. FEP129–FEP133, 2004.

Hindawi
International Journal of Polymer Science
Volume 2017, Article ID 1249134, 9 pages
https://doi.org/10.1155/2017/1249134

Research Article

(1→3)-α-D-Glucan from Fruiting Body and Mycelium of *Cerrena unicolor* (Bull.) Murrill: Structural Characterization and Use as a Novel Inducer of Mutanase

Monika Osińska-Jaroszuk,[1] Adrian Wiater,[2] Adam Choma,[3] Małgorzata Pleszczyńska,[2] Magdalena Jaszek,[1] Grzegorz Janusz,[1] Marcin Skowronek,[4] and Janusz Szczodrak[2]

[1]*Department of Biochemistry, Maria Curie-Skłodowska University, Akademicka 19, 20-033 Lublin, Poland*
[2]*Department of Industrial Microbiology, Maria Curie-Skłodowska University, Akademicka 19, 20-033 Lublin, Poland*
[3]*Department of Genetics and Microbiology, Maria Curie-Skłodowska University, Akademicka 19, 20-033 Lublin, Poland*
[4]*Laboratory of Biocontrol, Application and Production of EPN, Department of Biotechnology and Environment Sciences, Centre for Interdisciplinary Research, John Paul II Catholic University of Lublin, Konstantynów 1 J, 20-708 Lublin, Poland*

Correspondence should be addressed to Monika Osińska-Jaroszuk; moniosi73@gmail.com

Received 1 December 2016; Accepted 24 January 2017; Published 16 February 2017

Academic Editor: Raffaele Cucciniello

Water-insoluble, alkali-soluble polysaccharide (marked as ASP) was extracted from the vegetative mycelium and fruiting body of *Cerrena unicolor* strain. Monosaccharide examination of ASP demonstrated that the isolated biopolymer was composed mainly of glucose, xylose, and mannose monomers. The methylation investigation of studied polymers indicated that (1→3)-linked α-D-Glc*p* is the major chain constituent (92.2% for glucans isolated from fruiting body and 90.1% from mycelium). ^{1}H NMR, FT-IR, and immunofluorescent labelling determinations confirmed that the polysaccharides isolated from both fruiting body and mycelium of *C. unicolor* are (1→3)-α-D-glucans. The obtained (1→3)-α-D-glucans showed differences in viscosity and similar characteristics in optical rotations. (1→3)-α-D-Glucans extracted from mycelium and fruiting body of *C. unicolor* were also used as potential and specific inducers of mutanase synthesis by *Trichoderma harzianum*. The highest mutanase activity (0.38 U/mL) was obtained after induction of enzyme by (1→3)-α-D-glucan isolated from the mycelium of *C. unicolor*, and this biopolymer has been suggested as a new alternative to streptococcal mutan for the mutanase induction in *T. harzianum*. (1→3)-α-D-Glucan-induced mutanase showed high hydrolysis potential in reaction with dextranase-pretreated mutan, where maximal degree of saccharification and solubilization of this bacterial homoglucan (83.1% and 78.4%, resp.) was reached in 3 h at 45°C.

1. Introduction

Cerrena unicolor is a white rot fungus belonging to the family of Polyporaceae which is able to degrade both polysaccharide and lignin compounds in wood [1]. A crucial role in this process is played by laccases and peroxidases. Fungal laccases are extensively studied for its use in industry, particularly in numerous detoxification processes and waste water regeneration [2]. Potential use in biotechnology of bioactive fractions, laccase, endopolysaccharides, and low molecular weight components with high prooxidant and antibacterial activity, isolated from *C. unicolor,* has also recently published [3].

The main structural components of fungal cell wall are glycoproteins and polysaccharides which determine its rigidity and necessary flexibility during cell growth. The individual elements form the layer structure, wherein the glycoprotein are the outer and polysaccharides (1→3)-β-D-glucans, (1→6)-β-D-glucans, (1→3)-α-D-glucans, and chitin are an interior layer [4]. Glucans are a very diverse group of sugar polymers, whose structure depends on the enzymes responsible for their synthesis. Glucose molecules in polysaccharides chains may be linked to each other by (1→3)-α-, (1→4)-α-, or (1→6)-α- bonds which determines their degree of branching and the spatial distribution in the side chains [5]. These

properties also affect the physical nature of α-D-glucans and their solubility. An important group of α-glucans are (1→3)-α-D-glucans, which are produced by both the bacterial and fungal cells [6]. (1→3)-α-D-Glucans that are components of the cell wall fulfill functions as a support cell wall, virulence factor in some pathogens, or reserve material [7, 8]. Some immunomodulating and antitumor activity of (1→3)-α-D-glucans have been reported [9, 10]. This kind of biopolymers has also been described as a source of effective and specific activators for the synthesis of mutanolytic enzymes [11].

Hydrolytic enzymes group α-(1→3)-glucanases are capable of acting on (1→3)-α-D-glucans. Within this group are enzymes which degrade streptococcal mutan, called mutanases [6]. Bacterial mutanases are produced mainly by soil microorganisms (*Streptomyces*, *Bacillus*, *Pseudomonas*, and *Flavobacterium*) whose glucanolytic activities are much lower than those detected in fungal cultures [12]. Currently, the main source of mutanase is filamentous fungi especially of the *Trichoderma* genus. It should be emphasized that the mutanolytic enzymes are important in the fight against tooth decay, because they degrade forming dental plaque sticky, water-insoluble mutans, produced by cariogenic bacteria *Streptococcus mutans* and *S. sobrinus*.

Mutanases are mainly extracellular and inducible enzymes that decompose compounds containing α-(1→3)-glucosidic linkages. Therefore, the effective biotechnological production of these catalysts can be carried out only in the culture media supplemented in (1→3)-α-D-glucans as specific stimulants of mutanase synthesis [12]. Until now, the main and most powerful stimulus of mutanase synthesis was streptococcal α-D-glucan known as mutan [6]. Besides the mutan, fungal pseudonigeran, cells of *Schizosaccharomyces pombe,* and alkali-soluble α-D-glucans isolated from *Polyporus tumulosus*, *Phytophthora infestans,* and *Piptoporus betulinus* are also used as mutanase synthesis inducers [13–15]. Additionally, Wiater et al. [11] showed that α-D-glucan isolated from *Laetiporus sulphureus* induced significantly mutanase activity derived from *T. harzianum* cultures.

The main aim of these investigations was isolation, identification, and structural characterization of a new (1→3)-α-D-glucan derived from laboratory cultured vegetative mycelium of *Cerrena unicolor* and harvested from the natural environment fruiting body of this fungus. Fungal polysaccharides, for example, isolated from laboratory cultivated *C. unicolor* mycelia may express many industrial and biomedical applications [3]. The study also focused on assessing the possibility of use the isolated (1→3)-α-D-glucan for induction of mutanase synthesis in *T. harzianum* strain. Hydrolytic potential of (1→3)-α-D-glucan-induced mutanase was evaluated in reaction with a dextranase-pretreated streptococcal mutan.

2. Materials and Methods

2.1. Microorganisms and Culture Conditions. The fruiting body of *Cerrena unicolor* (Bull.) Murrill was collected from deciduous tree *Salix caprea* grown in Drobin, Poland (Table 1). The specimen was identified by molecular biological assay of the internal transcribed region (ITS) of the 5.8S rDNA as described below. Voucher specimen (CU-1A) was stored in the Department of Industrial Microbiology, Maria Curie-Skłodowska University (Lublin, Poland). *Cerrena unicolor* strain C-139 was obtained from Culture Collection of the Regensburg University (Regensburg, Germany). Examined microorganism was stored on malt agar slants at 4°C. Mycelium of *C. unicolor* was cultured on earlier optimized medium in the growth conditions as described by Rola et al. [16]. *Trichoderma harzianum* strain designated as CCM F-340 (Czech Collection of Microorganisms, Brno, Czech Republic) was used as a culture for mutanase production induced by (1→3)-α-D-glucan from fruiting body and vegetative mycelium of *C. unicolor*. Stock cultures of *T. harzianum* stored on potato dextrose agar slants at 4°C were used for inoculations. Liquid Mandels medium A (pH 5.3) [17] modified by addition of 0.4% of (1→3)-α-D-glucan (from fruiting body or mycelium of *C. unicolor*), 0.1% Tween 80, and 0.05% proteose peptone was used for mutanase production. Shaken cultures of *T. harzianum* were performed in 500 mL flasks containing 100 mL of sterile medium. The flasks were seeded with fungal conidia to a final concentration of about 2×10^5 conidia/mL and placed on an orbital rotary shaker (Innova 44, New Brunswick, USA) at 300 rpm and 30°C for 3 days.

2.2. Genomic DNA Isolation and PCR Amplification of the ITS Region. The extraction procedure was performed according to the method described by Borges et al. [18] with our minor modifications. Approximately 20 mg of fruiting body was suspended in lysis buffer (10 mM EDTA, 10 mM β-mercaptoethanol, 4 mM spermidine, 0.1 M NaCl, 0.5% SDS, and 40 mM Tris-HCl, pH 8.0) and incubated at 65°C for 40 min. Prepared in this way fungal fruiting body suspension was extracted with chloroform and phenol, centrifuged for 20 min at 10,000 ×g, and precipitated with ice-cold ethanol. Next, precipitate was washed with 70% ethanol, dried, and redissolved in TE buffer (1 mM Tris-HCl, 0.1 M EDTA, pH 8). Degree of purification and concentration of the DNA sample were estimated using ND1000 spectrophotometer (Thermo Scientific, West Palm Beach, FL, USA). Polymerase chain reaction amplifications (PCR) with primers (ITS 1, ITS 2, ITS 3, and ITS 4) were carried out according to the protocol of White et al. [19]. Reactions were done in a TPersonal thermocycler (Biometra, Germany). Amplified PCR products were quantified by gel electrophoresis (1% agarose gel stained with ethidium bromide), GeneRuler 100 bp Plus DNA Ladder (Thermo Scientific), and purified by microfiltration using Clean-up kit (A&A Biotechnology, Poland). BigDye™ Terminator Cycle Sequencing Kit and ABI PRISM 3730 XL sequencer were used in automatic sequencing (Applied Biosystems, Carlsbad, CA, USA). The GenBank accession number HM357713 was assigned to the nucleotide sequence determined in this study (Table 1).

2.3. Immunofluorescent Labelling of Cell Wall (1→3)-α-D-Glucan. (1→3)-α-D-Glucan was localized within *C. unicolor* cell wall using fluorescently labelled antibodies [20]. The samples prepared from fresh mycelia of *C. unicolor* were placed on Lab-Tek II Chamber slides (Nunc, Rochester, USA)

Table 1: Characteristics of harvested fruiting body of *C. unicolor*.

GenBank accession number	Geographic origin	Host tree	Fruiting body size	Fruiting body maturity[a]	(1→3)-α-D-Glucan(%)[b]
HM357713	Drobin (52°44′N, 19°59′E)	*Salix caprea*	<20 cm	+++	46.1 ± 0.8

[a]Fruiting body maturity: +: immature fruiting body (lack of hymenophore); ++: mature fruiting body with immature spores; +++: mature fruiting body with mature spores. [b]Amount of (1→3)-α-D-glucan in fruiting body dry mass. Results are shown as mean ± SD of three independent experiments.

and fixed with a 3% (v/v) formaldehyde solution in distilled water at 65°C for 30 min. The next, fixed fungal cells were washed three times in PBS buffer (137 mM NaCl, 2.7 mM KCl, 8.1 mM Na_2HPO_4, and 1.5 mM KH_2PO_4, pH 7.4) before infiltration by 1% (v/v) Tween 20 in PBS buffer (PBS-T). The presence of the (1→3)-α-D-glucan was detected by use of 150 μL of solution of mouse IgM MOPC-104E (0.1 mg/mL in PBS buffer) (Sigma, St Louis, MO, USA) as the primary antibody and in the same amount of Alexa Fluor 488 goat anti-mouse IgM (μ-chain specific) (Sigma, St Louis, MO, USA) as the secondary antibody. The samples were incubated as follows: primary antibodies overnight at 4°C in a wet chamber and secondary antibodies by 2 h in dark at 37°C. (1→3)-α-D-Glucan was observed on fluorescence microscope (Olympus BX 51, Germany), at an emission wavelength of 525/550 nm and excitation wavelength of 470/500 nm.

2.4. Isolation of Alkali-Soluble Polysaccharides (ASPs). Vegetative mycelium and fresh fruiting body and of *C. unicolor* were lyophilized and milled, and the dried materials were used for the isolation of the alkali-soluble polysaccharides according to a method described by Wiater et al. [11]. Both the dried materials of mycelium (100 g) and fruiting body (100 g) were milling and treating the resulting powders with water at 121°C for 1 h (×3). Wall materials were removed by centrifugation (10,000 rpm for 30 min) and freeze-dried. To isolate the alkali-soluble fraction, freeze-dried materials were suspended in 1 M NaOH under constant stirring. After an overnight incubation at room temperature, the supernatants were neutralized with 1 M HCl. The insoluble fractions were collected by centrifugation, washed with water (×3), and lyophilized to give the white powders [ASPs, purified (1→3)-α-D-glucan preparations].

2.5. Carbohydrate Analysis. For sugar analysis, the polysaccharides were hydrolyzed with 2 M TFA (100°C, 4 h). For absolute configuration of monosaccharides, analysis of acetylated *R*-(-)2-butylglycosides was used [21]. The studied sugars were modified into alditol acetates form [22]. Glucans were methylated by the method of Hakomori [23] and purified on a Sep-Pak C_{18} cartridge according to the method of York et al. [24]. The resulting material was hydrolyzed in 2 M TFA (100°C, 4 h) and reduced with $NaBD_4$. The partially methylated alditols were transformed to acetate derivatives. Prepared alditol acetates and partially methylated alditol acetates were analyzed using GC-MS analyses on a Hewlett-Packard gas chromatograph (model HP5890A, Germany) equipped with a mass selective detector (MSD model HP5971). Separations were accomplished in a capillary column (HP-5MS, 30 m × 0.25 mm) with helium as the carrier gas. The temperature program was 150°C (5 initial min) and then raised to 310°C at a ramp rate of 3°C/min and final time 20 min. ^{1}H NMR spectra of the polysaccharide dissolved in 1 M NaOD in D_2O were recorded with a Bruker Avance (300 MHz) spectrometer. The ^{1}H chemical shift was obtained using acetone (δ_H – 2.225 ppm) as the internal standard. FT-IR spectroscopy was recorded with a Perkin Elmer FT-IR spectrophotometer (Model 1725X, Wellesley, MA, USA) in the wavelength range between 400 and 4000 cm^{-1}. A specimen was prepared by the KBr-disk method. Specific rotation $[\alpha]_D^{25}$ (*c* 1 M sodium hydroxide) was determined at 589 nm using a Perkin Elmer Automatic Polarimeter model 341 LC (Wellesley, MA, USA). The viscosity of polysaccharides (*c* 1 M sodium hydroxide) was measured with a Brookfield viscometer model DV 3 (Stoughton, MA, USA) at 20°C.

2.6. Mutanase Assay. Mutanase activity was estimated using the method described by Wiater et al. [11]. The reaction mixture contained 0.5 mL of 0.2% (w/v) dextranase-pretreated mutan (DTM) in 0.2 M sodium acetate buffer (pH 5.5) and 0.5 mL of the suitably diluted enzyme solution. The samples were incubated for 1 hour at 45°C, and next the reducing sugars released were quantified by the Somogyi-Nelson method [25, 26]. Appropriate substrate and enzyme blanks were included to correct any free reducing group not emanating from DTM. One unit of mutanase activity (U) was calculated as the amount of enzyme hydrolyzing dextranase-pretreated mutan (DTM) to yield reducing sugars equivalent to 1 μmol of glucose/min. Mutanase activity was expressed as units per mL of culture (U/mL).

2.7. Preparation of Dextranase-Pretreated Mutan (DTM). For the determination of the mutanase activity, dextranase-pretreated mutan (DTM) substrate (50 U of dextranase/mg of native mutan was incubated at pH 6.0, 37°C, 3 × 24 h) was prepared. Native mutan was synthesized according to the procedure described by Wiater et al. [12]. Dextranase of *Penicillium* sp. (enzyme activity of 12.9 U/mg preparation, Sigma-Aldrich (St. Louis, MO., USA)) was used in described method. As demonstrated using ^{1}H NMR method the linkage structure of the native and the dextranase-pretreated mutan have mixed-linkage (1→3)-α- and (1→6)-α-biopolymers but a greater proportion of (1→3)-α- than (1→6)-α- linkages was observed.

2.8. Protein Estimation. The protein content was measured at 595 nm by the method of Bradford [27], using bovine serum albumin as a reaction standard in the range of the concentrations from 40 μg/mL to 400 μg/mL.

2.9. Reducing Sugars Estimation. The reducing sugars concentration was determined by the Somogyi-Nelson colorimetric method [25, 26]. The test solution (0.5 mL) was mixed with 0.5 mL alkaline copper reagent and then boiled in water bath for 20 min. After cooling, with 0.5 mL of chromogenic reagent (arsenomolybdate) and 1.5 mL of distilled water, the absorbance was measured at a wavelength of 520 nm. Concentration of reducing sugars was calculated based on the calibration curve with glucose as a standard. The amount of reducing sugars was expressed in μg/mL.

2.10. Induction of T. Harzianum Mutanase by (1→3)-α-D-Glucan. The synthesis of *T. harzianum* mutanase was induced by (1→3)-α-D-glucans isolated from the mycelium and fruiting body of *C. unicolor* strains. Flask submerged cultures of the fungus *T. harzianum* were carried out by 3 days on Mandels medium, pH 5.3, containing (g/L) KH_2PO_4 2; $(NH_4)SO_4$ 1.4; urea 0.3; $MgSO_4\times 7H_2O$ 0.3; $CaCl_2$ 0.3; Bacto-peptone 0.5; Tween 1 mL/L; and microelements solution 1 mL/L with tested (1→3)-α-D-glucan (in an amount of 0.4 g in 100 mL of medium) as a mutanase inducer. After cultivation, the mutanase activity, protein concentration, and pH value were estimated.

2.11. Hydrolysis Experiments. Hydrolysis was performed in plugged Eppendorf tubes using 0.05% NaN_3 as a preservative. The reaction mixtures contained 1 mg of dextranase-pretreated mutan (DTM) and *T. harzianum* mutanase induced by (1→3)-α-D-glucan isolated from mycelium of *C. unicolor* (1 U/mL) in 1 mL of 0.2 M sodium acetate buffer (pH 5.5). The samples were incubated for 24 h at 45°C and agitated at 300 rpm. Next, mutan hydrolyzates were withdrawn at various intervals of up to 24 h and heated at about 100°C for 5 min to stop the reaction. Total reducing sugars were analyzed by the Somogyi-Nelson method [25, 26]. The calculation included enzyme and substrate blanks. The percentage of mutanolysis was calculated by the following formula: saccharification (%) = [reducing sugars formed (mg) × 0.9/mutan (mg)] × 100. Additionally, the turbidimetric analysis (at 560 nm) the residual insoluble glucan was determined. The degree of mutan solubilization was calculated and expressed as a percentage.

2.12. Statistical Analysis. Data were analyzed using one-way ANOVA followed by a post hoc Tukey test. All the results are expressed as mean ± SD from three experiments ($n = 3$). Values of $P \leq 0.05$ were only reported as statistically significant.

3. Results and Discussion

3.1. Morphological and Genetic Characteristics of C. unicolor Strains. The strain of *Cerrena* whose fruiting body was collected from *Salix caprea* was identified at the species level by analysis of their ITS region. One product (length 648 bp) was obtained from PCR with ITS1-ITS4 primers and subsequently by direct sequencing. The complete sequence of this product indicated 100% identity to the *Cerrena unicolor* ITS sequences. The obtained sequence was deposited in GenBank under HM357713 accession number (Table 1). For comparative testing of the mycelium, *C. unicolor* 139 (ITS sequence deposited in GenBank under accession number DQ056858) obtained from Culture Collection of the Regensburg University (Regensburg, Germany) was used [28]. Based on the available genome sequence of *C. unicolor* future analysis of genome sequences and their expression is much easier. This also applies to the enzymes, for example, laccase *C. unicolor* of biotechnological interest and bioactive fraction having antioxidant, antibacterial, antitumor, or immunostimulatory activity [3].

3.2. Isolation and Structural Analysis of Alkali-Soluble Polysaccharides. Analysis of composition of *C. unicolor* fruiting body showed the presence of water (50%), water-insoluble (1→3)-α-D-glucan (23.1%), and the remaining part composed of other structural ingredients of cell wall. The ASPs were obtained from the lyophilized fruiting body and mycelium of *C. unicolor* by alkaline solution extractions with the yield of 46.1% from fruiting body and 9.5% from mycelium. As it was described earlier, the α-glucans content in the fungal cell walls varies depending on the species [4]. Fruiting bodies of *Laetiporus sulphureus* are the richest source of (1→3)-α-D-glucan (56.3%) [11]. In the case of *Aspergillus niger* mycelium, this water-insoluble biopolymer constituted only 9% of its composition [29] whereas it was absent in the *Saccharomyces cerevisiae* and *Candida albicans* cell walls [4]. For the detection of (1→3)-α-D-glucan in the *C. unicolor* mycelium cell walls, the immunofluorescent labelling with specific antibodies was done. This method was previously used by Fujikawa et al. [20] to visualize the location of (1→3)-α-D-glucans in the phytopathogenic fungus *Magnaporthe grisea* where these polysaccharides including chitosan are the main component of cell integument. The presence of (1→3)-α-D-glucan in the cell wall of *C. unicolor* was highlighted by use of the fluorescent microscope (Figure 1). In the present report, a detailed structural analysis of (1→3)-α-D-glucans was conducted using ^{1}H NMR and FT-IR spectra technique. ^{1}H NMR analysis of ASPs isolated from fruiting body and mycelium of *C. unicolor* showed the presence of glucose molecules linked by (1→3)-α-glucosidic bonds (Figure 2). It may be clearly observed by the existence of singlets at 5.6408 and 5.6283. Both of these values corresponded to the region of 5.200 to 5.650 ppm which characterize glucose α-anomers. Similar results were obtained earlier in the study of glucans isolated from *L. sulphureus* where 5.33 ppm resonance signal was observed [11]. Structural analysis of ASPs by FT-IR spectra was made in the wavelength range of 4000 to 500 cm^{-1}. As shown in Figure 3, FT-IR spectrum of ASPs displays absorption bands at 3336.01 cm^{-1} and 3313.04 cm^{-1} (for glucans isolated from fruiting body and mycelium, resp.) which indicates the presence of -OH group, characteristic of polysaccharides chains [30]. The band between 1000 and 1100 cm^{-1} (i.e., 1012.32 cm^{-1} and 1009.26 cm^{-1}) indicated the presence of O-substituted glucose residues and β-linkages in the glucosidic chain [31]. Additionally, characteristic α-linked glycosyl residues at 847.72 cm^{-1} and 822.00 cm^{-1} were

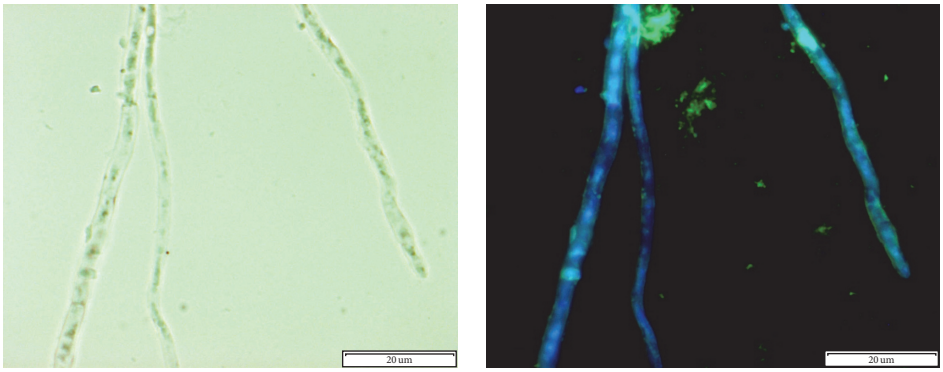

(a) (b)

Figure 1: Detection of (1→3)-α-D-glucan in the hyphae of *C. unicolor* strain C-139 by means of fluorophore-labelled antibodies (Clone IgM MOPC-104E). (a) Filaments in the light microscopy, (b) fluorescent image of the same filaments. Twenty samples were observed and typical images are presented. Scale bar = 20 μm.

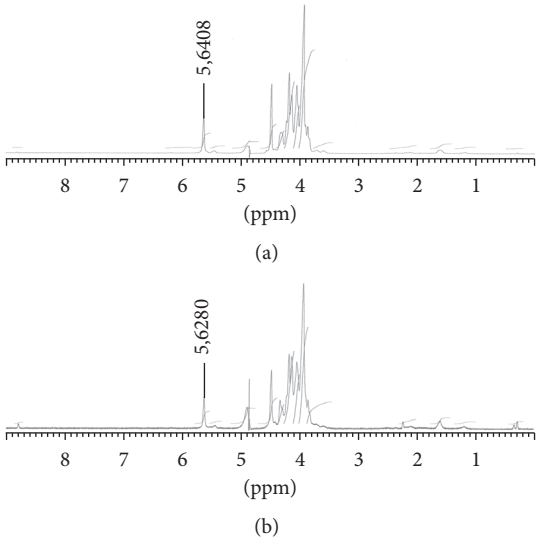

Figure 2: ^{1}H NMR spectra of alkali-soluble water-insoluble polysaccharides (ASPs) obtained from fruiting body (a) and vegetative mycelium (b) of *C. unicolor*.

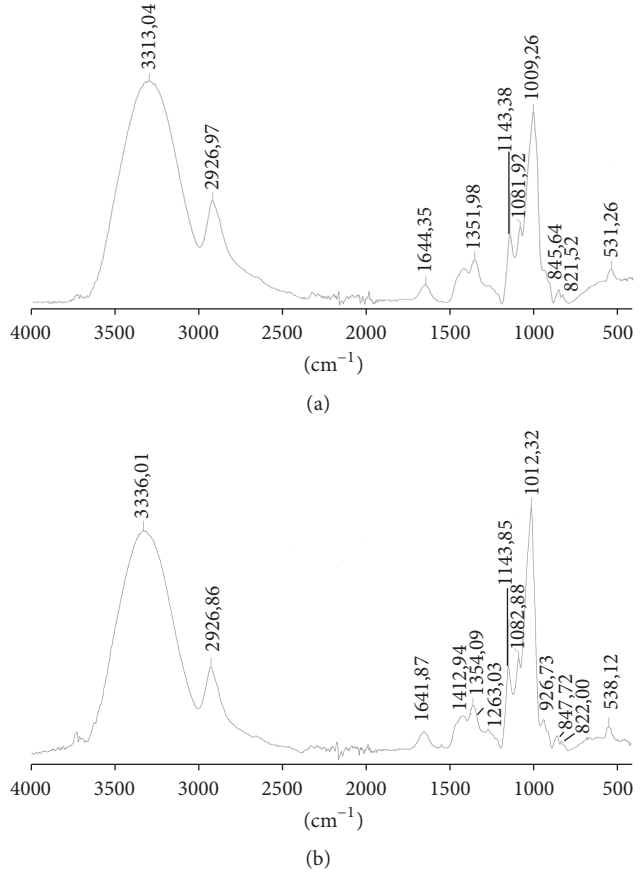

Figure 3: FT-IR spectra of alkali-soluble water-insoluble polysaccharides (ASPs) obtained from fruiting body (a) and vegetative mycelium (b) of *C. unicolor*.

obtained for ASPs isolated from mycelium of *C. unicolor*. In the case of biopolymer derived from fruiting body of *C. unicolor* we also showed, similarly to Kozarski et al. [32], two peaks at 845.64 cm^{-1} and 821.52 cm^{-1}, which indicate that the isolated material contained (1→3)-α-D-glucan. In the study of FT-IR spectra of glucans isolated from cell walls of *Piptoporus betulinus*, *Aspergillus nidulans,* and *L. sulphureus* the similar profile of the spectrum was observed [11, 33]. Monosaccharide analysis of ASPs isolated from fruiting body and mycelium of *C. unicolor* demonstrated that the basic monomer building these polysaccharides was glucose (93.5%, fruiting body, and 95.3%, mycelium) (Table 2). In addition, a small percentage of other monosaccharides, xylose (2.3 and 3.6%) and mannose (2.4 and 2.9%), were found. There was no significant differences in the percentage of the various monosaccharides isolated from the *C. unicolor* mycelium and fruiting body. A similar composition (with glucose, xylose, and mannose) of α-glucans isolated from the cell wall of

Table 2: Monosaccharide analysis (Glc: glucose; Xyl: xylose; Man: mannose) of ASP (alkali-soluble) preparations extracted from fruiting body and vegetative mycelium of *C. unicolor*.

Origin	Monosaccharide amounts (%)		
	Glc	Xyl	Man
Fruiting body	95.3 ± 1.0	2.3 ± 0.2	2.4 ± 0.1
Mycelium	93.5 ± 1.1	3.6 ± 0.3	2.9 ± 0.1

L. sulphureus was reported by Grün [4]. Methylation analysis of glucans extracted from fruiting body and vegetative mycelium of *C. unicolor* showed that (1→3)-linked *α*-D-Glc*p* is the major chain constituent (92.2% in fruiting body and 90.1% in mycelium) while (1→4)-linked *α*-D-Glc*p* (4.4% and 7.4%, resp.) is the minor one (Table 3). The obtained results proved that larger percentage of (1→4)-linked *α*-D-Glc*p* occurs in the glucan extracted from the mycelium which makes it even more branched. Furthermore, the structure of studied glucans contained one type of doubled substituted glucose residues (1→; →3, 4)-*α*-D-Glc*p*. The studied (1→3)-*α*-D-glucans preparations showed differences in viscosity and similar characteristics of their optical rotations (Table 4). The specific optical rotations of the *α*-glucans are in the range of +200° to +206°. The values of viscosity fluctuated between 2.12 and 7.55 mPa·s. Different viscosity of the tested *α*-glucans may indicate differences in their molecular mass. Based on the analysis of all the above data it can be concluded that the water-insoluble, alkali-soluble polysaccharides isolated both from fruiting body and mycelium of *C. unicolor* contained predominantly (1→3)-*α*-D-glucan.

3.3. Induction of T. harzianum Mutanase by (1→3)-α-D-Glucan. Mutanase is an inducible enzyme decomposing polymers containing in their structure (1→3)-*α*-glucoside bond. Therefore intensified production of this catalyst takes place only in a medium containing a specific inducer such as (1→3)-*α*-D-glucan [10]. In order to choose the best inducer for the mutanase synthesis by *T. harzianum* strain, shaken fungal cultures have been grown on the Mandels medium (pH 5.3) for 3 days. In the present work (1→3)-*α*-D-glucan from the mycelium and fruiting body of *C. unicolor* were used as a potential inducers of mutanase. The results obtained showed that the highest activity of mutanase by *T. harzianum* was detected in the cultures supplemented with (1→3)-*α*-D-glucan from the mycelium of *C. unicolor* (Table 5). The addition of this polysaccharide to the medium gave the maximal enzyme yield of 0.38 U/mL. Wiater et al. [11] obtained higher mutanase activity (0.82 U/mL) after induction of its synthesis by (1→3)-*α*-D-glucans obtained from the harvested fruiting bodies of *L. sulphureus*. On the other hand, the result achieved by us is slightly better than that (0.33 U/mL) given by Wiater et al. [34], who used a bacterial mutan to induce mutanase in *T. harzianum* F-470 strain. In turn, there were significantly lower levels of enzyme production by *T. harzianum* OMZ 779 (0.16 U/mL) shown by Guggenheim and Haller [35] in shaken flask cultures with 1% mutan. In the case of bacterial mutanases, Meyer and Phaff [14] reached

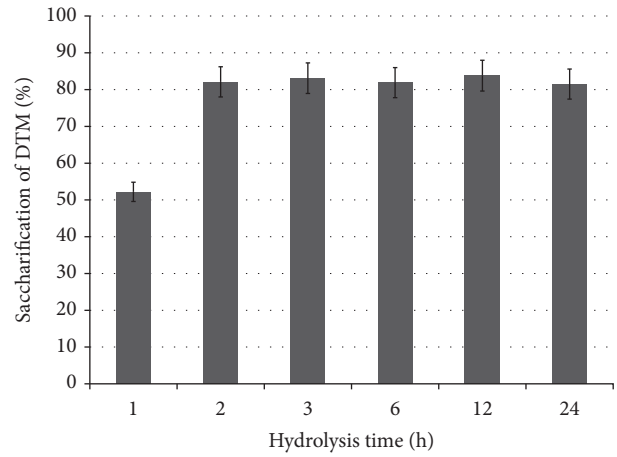

Figure 4: The kinetics of saccharification of dextranase-pretreated mutan (DTM) using *T. harzianum* mutanase induced by (1→3)-*α*-D-glucan isolated from mycelium of *C. unicolor*.

the maximal mutanase activity (0.31 U/mL) in cultures of *Bacillus circulans* WL-12 supplemented with whole cells of *Schizosaccharomyces pombe* or purified (1→3)-*α*-D-glucan from *A. niger*.

After using for the induction of mutanase the pure (1→3)-*α*-D-glucan isolated from the fruiting body of *C. unicolor*, a high enzyme productivity (0.26 U/mL) was also noted. Sanz et al. [36] showed intensified production of mutanase by *T. asperellum* after induction of this culture by *α*-D-glucans isolated from *Botrytis cinerea* mycelium and Ait-Lahsen et al. [37] used as a mutanase activator the mycelium from *A. niger*. In sum, the present study reveals that the (1→3)-*α*-D-glucan preparations, isolated from mycelium and fruiting body of *C. unicolor*, effectively induced mutanase in *T. harzianum* and fully substituted streptococcal mutan. In contrast to mutan, these new and powerful stimulants for inducible mutanase synthesis are inexpensive, easily available, and safe for humans. Therefore, they will be very useful to facilitate the mutanase production on a larger scale and at relatively low costs acceptable for oral applications. From the biotechnological point of view the use of *C. unicolor* mycelium as a source of (1→3)-*α*-D-glucan seems to be more efficient and promising for economic reasons. Additionally, the production of mutanase would become independent of the time for picking up fruiting bodies of this fungus from the environment.

3.4. Hydrolysis Experiments. Enzymatic hydrolysis of dextranase-pretreated streptococcal mutan (DTM) was carried out with the use of partially purified mutanase induced by (1→3)-*α*-D-glucan isolated from mycelium of *C. unicolor*. Experimental results were obtained by monitoring enzymatic saccharification of DTM and its solubilization (Figures 4 and 5). In both cases, hydrolysis reaction rates increased linearly in the initial phase of the process and later became almost constant. The maximum degree of mutan saccharification

Table 3: Summary of methylation analysis of glucans extracted from fruiting body and vegetative mycelium of *C. unicolor*.

Origin	Methylated sugar	Linkage type	Molar amounts (%)
Fruiting body	2,3,4,6-O-Me_4-D-glucose	α-D-Glc*p*-(1→	0.2
	2,4,6-*O*-Me_3-D-glucose	→3)-α-D-Glc*p*-(1→	92.2
	2,3,6-*O*-Me_3-D-glucose	→4)-α-D-Glc*p*-(1→	4.4
	2,6-*O*-Me_2-D-glucose	→3,4)-α-D-Glc*p*-(1→	3.2
Mycelium	2,4,6-*O*-Me_3-D-glucose	→3)-α-D-Glc*p*-(1→	90.1
	2,3,6-*O*-Me_3-D-glucose	→4)-α-D-Glc*p*-(1→	7.4
	2,6-*O*-Me_2-D-glucose	→3,4)-α-D-Glc*p*-(1→	2.5

The glucan preparation was methylated before being hydrolysed, reduced, and acetylated. Therefore, the methylated sugars mentioned refer to permethylated alditol acetates identified by GC–MS (e.g., 2,3,4,6-*O*-Me_4-D-glucose refers to 1,5-di-*O*-acetyl-2,3,4,6-tetra-*O*-methyl-D-glucitol).

Table 4: The data of viscosity and optical rotation analysis of (1→3)-α-D-glucans extracted from fruiting body and vegetative mycelium of *C. unicolor*.

Strain	Viscosity (mPa·s)	Optical rotation $[\alpha]_D^{25}$ (°)
Fruiting body	2.12 ± 0.1	206 ± 5
Mycelium	7.55 ± 0.3	200 ± 3

Results are shown as mean ± SD of three independent experiments.

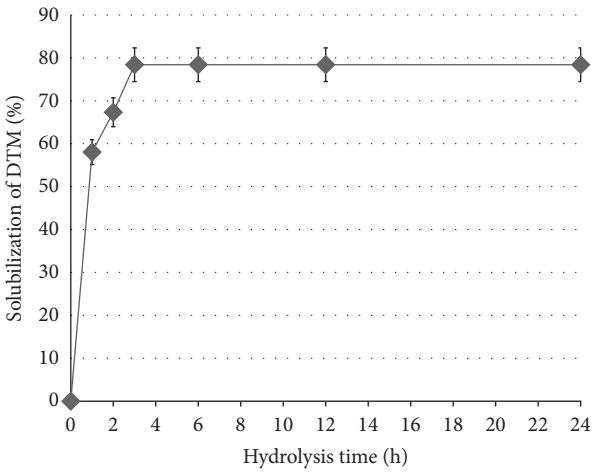

Figure 5: The kinetics of solubilization of dextranase-pretreated mutan (DTM) using *T. harzianum* mutanase induced by (1→3)-α-D-glucan isolated from mycelium of *C. unicolor*.

(83.1%) and its solubilization (78.4%) was reached after 3 h of hydrolysis. Having considered that dextranase-pretreated mutan, prepared in our laboratory, was a mixed-linkage glucan with 79.8 mol% of (1→3)-α-glucosidic linkages, it is possible to conclude that almost all of these glucosidic bonds were degraded during specific action of mutanase on this biopolymer. Wiater et al. [11] obtained similar results for *T. harzianum* mutanase induced by fruiting body of *L. sulphureus* where hydrolysis of substrate at a level of 80% was achieved after 3 h. In turn, Kopec and Vacca-Smith [38], during hydrolysis of insoluble mutan, obtained only 15.3% saccharification with mutan-induced mutanase of *T. harzianum* after 4 h of incubation at 30°C. Similar results (hydrolysis yield of up to 20% after 48–64 h at 37°C) were obtained for Dextranase 50 l (a commercial preparation containing several hydrolytic activities) and glucanohydrolase with dextranolytic and amylolytic activity from *Lipomyces starkeyi* [39, 40]. Thus, efficient solubilization of mutan in a short period of time gives a chance to use the *T. harzianum* mutanase induced by (1→3)-α-D-glucan of *C. unicolor* in preventive dentistry as a preparation in the fight against dental caries. High efficiency of mutan solubilization (83% after 6 hours) was also received by Pleszczyńska et al. [41] after using mutanase from *Paenibacillus* sp. MP-1-induced by *L. sulphureus* mycelium.

4. Conclusions

In this study, the new (1→3)-α-D-glucan preparations isolated from mycelium and fruiting body of *Cerrena unicolor* were exactly identified and characterized. Both tested glucans proved to be effective and easily accessible inducers of mutanase synthesis in *T. harzianum*. The simple culturing of *C. unicolor* mycelium and intensification the scale of its production are very interesting from technological point of view. In fact, obtaining large amounts of (1→3)-α-D-glucans from this source could significantly accelerate the production of mutanase which would increase the chance of getting the product that could be used in the prevention of dental caries. Mutanase could be used as an active additive to preparations intended for oral hygiene, such as mouthwashes, toothpastes, and dental gels, and also for washing and storage of prosthesis and prosthetic devices for removal of denture plaque located on their acrylic surfaces. As active ingredient, mutanase could become useful supplement to mechanical cleaning of teeth and dentures with a toothbrush, dental sticks, and dental floss.

Competing Interests

The authors declare that there is no conflict of interests.

Table 5: Effect of (1→3)-α-D-glucan inducers on mutanase production by *T. harzianum* strain cultivatedin shaken flask cultures.

Source of (1→3)-α-D-glucan	Activity of mutanase [U/mL]	Protein [μg/mL]	pH medium
Fruiting body	0.26 ± 0.004	103.2 ± 1.6	5.23
Mycelium	0.38 ± 0.007	120.6 ± 1.3	6.23

Results are shown as mean ± SD of three independent experiments.

Acknowledgments

This work was supported by the National Science Centre (Poland) based on the Decision no. DEC-2013/09/B/NZ9/01829 and the Research Program BS/UMCS.

References

[1] M. Mansur, M. E. Arias, J. L. Copa-Patiño, M. Flärdh, and A. E. González, "The white-rot fungus Pleurotus ostreatus secretes laccase isozymes with different substrate specificities," *Mycologia*, vol. 95, no. 6, pp. 1013–1020, 2003.

[2] A. Piscitelli, P. Giardina, V. Lettera, C. Pezzella, G. Sannia, and V. Faraco, "Induction and transcriptional regulation of laccases in fungi," *Current Genomics*, vol. 12, no. 2, pp. 104–112, 2011.

[3] M. Jaszek, M. Osińska-Jaroszuk, G. Janusz et al., "New bioactive fungal molecules with high antioxidant and antimicrobial capacity isolated from *Cerrena unicolor* idiophasic cultures," *BioMed Research International*, vol. 2013, Article ID 497492, 11 pages, 2013.

[4] C. H. Grün, *Structure and Biosynthesis of Fungal α-Glucans*, Universiteit Ultrecht, Utrecht, The Netherlands, 2003.

[5] A. Synytsya and M. Novak, "Structural analysis of glucans," *Annals of Translational Medicine*, vol. 2, no. 17, pp. 1–14, 2014.

[6] M. Pleszczyńska, A. Wiater, T. Bachanek, and J. Szczodrak, "Enzymes in therapy of biofilm-related oral diseases," *Biotechnology and Applied Biochemistry*, 2016.

[7] M. Kopecka, G. H. Fleet, and H. J. Phaff, "Ultrastructure of the cell wall of *schizosaccharomyces pombe* following treatment with various glucanases," *Journal of Structural Biology*, vol. 114, no. 2, pp. 140–152, 1995.

[8] L. H. Hogan and B. S. Klein, "Altered expression of surface alpha-1,3-glucan in genetically related strains of Blastomyces dermatitidis that differ in virulence," *Infection and Immunity*, vol. 62, no. 8, pp. 3543–3546, 1994.

[9] S. P. Wasser, "Medicinal mushrooms as a source of antitumor and immunomodulating polysaccharides," *Applied Microbiology and Biotechnology*, vol. 60, no. 3, pp. 258–274, 2002.

[10] A. Wiater, R. Paduch, A. Choma et al., "Biological study on carboxymethylated (1→3)-α-d-glucans from fruiting bodies of *Ganoderma lucidum*," *International Journal of Biological Macromolecules*, vol. 51, no. 5, pp. 1014–1023, 2012.

[11] A. Wiater, J. Szczodrak, and M. Pleszczyńska, "Mutanase induction in *Trichoderma harzianum* by cel wall of *Laetiporus sulphureus* and its application for mutan removal from oral biofilms," *Journal of Microbiology and Biotechnology*, vol. 18, no. 7, pp. 1335–1341, 2008.

[12] A. Wiater, J. Szczodrak, and M. Pleszczyńska, "Optimization of conditions for the efficient production of mutan in streptococcal cultures and post-culture liquids," *Acta Biologica Hungarica*, vol. 56, no. 1-2, pp. 137–150, 2005.

[13] M. Horisberger, B. A. Lewis, and F. Smith, "Structure of a (1→3)-α-d-glucan (pseudonigeran) of Aspergillus niger NNRL 326 cell wall," *Carbohydrate Research*, vol. 23, no. 2, pp. 165–330, 1972.

[14] M. T. Meyer and H. J. Phaff, "Purification and properties of (1→3)—glucanases from *Bacillus circulans* Wl-12," *Journal of General Microbiology*, vol. 118, pp. 197–208, 1980.

[15] E. T. Reese, A. Maguire, and F. W. Parrish, "1, 3, Glucanases of fungi and their relationships to mycodextranase," in *Fermentation Technology Today*, G. Terui, Ed., pp. 735–742, Fermentation Technology, Osaka, Japan, 1972.

[16] B. Rola, M. Karaśkiewicz, D. Majdecka et al., "Scale up of *Cerrena unicolor* laccase production," *Journal of the Faculty of Agriculture, Kyushu University*, vol. 58, no. 2, pp. 231–238, 2013.

[17] M. Mandels, F. W. Parrish, and E. T. Reese, "Sophorose as an inducer of cellulase in *Trichoderma viride*," *Journal of Bacteriology*, vol. 83, pp. 400–408, 1962.

[18] M. J. Borges, M. O. Azevedo, J. R. Bonatelli, M. S. S. Felipe, and S. Astolfi-Filho, "A practical method for the preparation of total DNA from filamentous fungi," *Fungal Genetics Newsletters*, vol. 37, article 10, 1990.

[19] T. J. White, T. Bruns, S. Lee, and J. Taylor, "Amplification and direct sequencing of fungal ribosomal RNA genes for phylogenetics," in *PCR Protocols: A Guide to Methods and Applications*, M. A. Innis, D. H. Gelfand, J. J. Sninsky, and T. J. White, Eds., pp. 315–322, Academic Press, New York, NY, USA, 1990.

[20] T. Fujikawa, Y. Kuga, S. Yano et al., "Dynamics of cell wall components of *Magnaporthe grisea* during infectious structure development," *Molecular Microbiology*, vol. 73, no. 4, pp. 553–570, 2009.

[21] G. J. Gerwig, J. P. Kamerling, and J. F. G. Vliegenthart, "Determination of the D and L configuration of neutral monosaccharides by high-resolution capillary GLC," *Carbohydrate Research*, vol. 62, no. 2, pp. 349–357, 1978.

[22] R. Russa, T. Urbanik-Sypniewska, K. Lindström, and H. Mayer, "Chemical characterization of two lipopolysaccharide species isolated from *Rhizobium loti* NZP2213," *Archives of Microbiology*, vol. 163, no. 5, pp. 345–351, 1995.

[23] S.-I. Hakomori, "A rapid permethylation of glycolipid, and polysaccharide catalyzed by methylsulfinyl carbanion in dimethyl sulfoxide," *Journal of Biochemistry*, vol. 55, no. 2, pp. 205–208, 1964.

[24] W. S. York, A. G. Darvill, M. McNeil, T. T. Stevenson, and P. Albersheim, "Isolation and characterization of plant cell walls and cell wall components," in *Methods in Enzymology*, A. Weissbach and H. Weissbach, Eds., pp. 3–40, Academic Press, London, UK, 1986.

[25] N. Nelson, "A photometric adaptation of the Somogyi method for the determination of glucose," *The Journal of Biological Chemistry*, vol. 153, pp. 375–380, 1944.

[26] M. Somogyi, "A new reagent for the determination of sugars," *The Journal of Biological Chemistry*, vol. 160, pp. 61–68, 1945.

[27] M. M. Bradford, "A rapid and sensitive method for the quantitation of microgram quantities of protein utilizing the principle of protein-dye binding," *Analytical Biochemistry*, vol. 72, no. 1-2, pp. 248–254, 1976.

[28] G. Janusz, A. Mazur, A. Checinska, W. Malek, J. Rogalski, and S. Ohga, "Cloning and characterization of a laccase gene from biotechnologically important basidiomycete *Cerrena unicolor*," *Journal of the Faculty of Agriculture, Kyushu University*, vol. 57, no. 1, pp. 41–49, 2012.

[29] T. F. Bobbitt, J. H. Nordin, M. Roux, J. F. Revol, and R. H. Marchessault, "Distribution and conformation of crystalline nigeran in hyphal walls of *Aspergillus niger* and *Aspergillus awamori*," *Journal of Bacteriology*, vol. 132, no. 2, pp. 691–703, 1977.

[30] P. R. Carey, *Biochemical Application of Raman and Resonance Raman Spectroscopies*, Academic Press, New York, NY, USA, 1992.

[31] B. Stone and A. Clarke, *Chemistry and Biology of (1, 3)-β-Glucans*, La Trobe University Press, 1992.

[32] M. Kozarski, A. Klaus, M. Niksic, D. Jakovljevic, J. P. F. G. Helsper, and L. J. L. D. Van Griensven, "Antioxidative and immunomodulating activities of polysaccharide extracts of the medicinal mushrooms *Agaricus bisporus*, *Agaricus brasiliensis*, *Ganoderma lucidum* and *Phellinus linteus*," *Food Chemistry*, vol. 129, no. 4, pp. 1667–1675, 2011.

[33] B. J. M. Zonneveld, "Morphogenesis in *Aspergillus nidulans*. The significance of α-1,3-glucan of the cell wall and α-1,3-glucanase for cleistothecium development," *Biochemica Biophysica Acta*, vol. 273, no. 1, pp. 174–187, 1972.

[34] A. Wiater, J. Szczodrak, and J. Rogalski, "Purification and characterization of an extracellular mutanase from *Trichoderma harzianum*," *Mycological Research*, vol. 105, no. 11, pp. 1357–1363, 2001.

[35] B. Guggenheim and R. Haller, "Purification and Properties of an α-(1 → 3) Glucanohydrolase from *Trichoderma harzianum*," *Journal of Dental Research*, vol. 51, no. 2, pp. 394–402, 1972.

[36] L. Sanz, M. Montero, J. Redondo, A. Llobell, and E. Monte, "Expression of an α-1,3-glucanase during mycoparasitic interaction of *Trichoderma asperellum*," *FEBS Journal*, vol. 272, no. 2, pp. 493–499, 2005.

[37] H. Ait-Lahsen, A. Soler, M. Rey, J. De La Cruz, E. Monte, and A. Llobell, "An Antifungal Exo-α-1,3-Glucanase (AGN13.1) from the Biocontrol Fungus *Trichoderma harzianum*," *Applied and Environmental Microbiology*, vol. 67, no. 12, pp. 5833–5839, 2001.

[38] L. K. Kopec and A. M. Vacca-Smith, "Structural aspects of glucans formed in solution and on the surface of hydroxyapatite," *Glycobiology*, vol. 7, no. 7, pp. 929–934, 1997.

[39] S.-J. Ryu, D. Kim, H.-J. Ryu, S. Chiba, A. Kimura, and D. F. Day, "Purification and partial characterization of a novel glucanhydrolase from *Lipomyces starkeyi* KSM 22 and its use for inhibition of insoluble glucan formation," *Bioscience, Biotechnology, and Biochemistry*, vol. 64, no. 2, pp. 223–228, 2000.

[40] M. Marotta, A. Martino, A. De Rosa, E. Farina, M. Cartenì, and M. De Rosa, "Degradation of dental plaque glucans and prevention of glucan formation using commercial enzymes," *Process Biochemistry*, vol. 38, no. 1, pp. 101–108, 2002.

[41] M. Pleszczyńska, A. Wiater, and J. Szczodrak, "Mutanase from *Paenibacillus* sp. MP-1 produced inductively by fungal α-1,3-glucan and its potential for the degradation of mutan and *Streptococcus mutans* biofilm," *Biotechnology Letters*, vol. 32, no. 11, pp. 1699–1704, 2010.